Photocatalytic [^{11}C]CO_2 Fixation for Synthesis of α-Hydroxy ^{11}C-Carboxylic Acids

Abhishek Praveenkumar Patel

Thesis submitted to the University of Ottawa in partial fulfilment of the requirements for Master of Science in Chemistry

Department of Chemistry and Biomolecular Sciences
University of Ottawa

Abstract

Rapid synthesis is essential for carbon-11, a routinely used radioactive isotope with a physical half-life of 20.4 minutes. Typically, cyclotron production delivers the isotope as $[^{11}C]CO_2$ or $[^{11}C]CH_4$, which can be converted to secondary carbon-11 precursors ($[^{11}C]CN$, $[^{11}C]CH_3I$, etc.), although the transformations lead to loss of activity yields. Hence, direct fixation of $[^{11}C]CO_2$ into complex molecules is appealing for operational simplicity and time efficiency.

Photocatalysis unlocks rapid reactivity under mild conditions. Our lab has developed photocatalytic methods to prepare ^{11}C-amino acids and ^{11}C-phenylacetic acids from $[^{11}C]CO_2$. These functional groups are found in biochemicals and drug molecules, opening synthetic routes to novel radiopharmaceuticals.

We have developed a photocatalytic method to prepare α-hydroxy ^{11}C-carboxylic acids, a functionality found in various metabolites and neuroactive drugs. This method leverages readily available ketone substrates as precursors for radiolabelling with $[^{11}C]CO_2$, assisted by an iridium-based photocatalyst. We have employed experimental design using Bayesian optimisation to improve the radiochemical yields of ^{11}C-α-hydroxy acids. Furthermore, we have developed conditions that efficiently extract $[^{11}C]CO_2$ into the reaction medium independent of the substrate structure, which overcomes a shortcoming of previously reported methods.

Subsequently, we have prepared a scope of ^{11}C-α-hydroxy acids to demonstrate the method's versatility. Since characterization of ^{11}C-α-hydroxy acids requires their non-radioactive standards, we developed a metal-free photocatalysed synthesis of α-hydroxy acids with stable CO_2. We were able to synthesize all requisite non-radioactive standards and, in the process, demonstrated the breadth of the metal-free method.

Contributions

The initial discovery of this work and all experiments described were carried out by me, unless otherwise stated. An undergraduate student in the lab, Ezana Ghedam, assisted with the project, preparing 2 non-radioactive compounds and obtained 7 high-field NMRs. This document is entirely my original work and has been prepared without the assistance of any text generation software such as LLMs.

This work has been presented at the following conferences –

1. Patel, A. P., Rotstein B. H. (2025, Nov 14-16) Lights, Carboxylation, Acid - Photocatalytic ^{11}C-carboxylation of ketones, Oral presentation, Quebec/Ontario Mini Symposium for Synthetic and Bio-organic Chemistry (QOMSBOC 2025), Quebec City, QC, Canada
2. Patel, A. P., Rotstein B. H. (2025, June 15-20) Lights, Carboxylation, Acid: ^{11}C-Carboxylation of Carbonyls Using Photocatalysis, Oral presentation, Canadian Chemistry Conference and Exhibition (CSC 2025), Ottawa, ON, Canada

Acknowledgements

The completion of this thesis is a sum-total of not only my own efforts, but also the support of many wonderful individuals. Firstly, this thesis was made possible by the opportunity afforded to me by my supervisor, Dr. Benjamin Rotstein. He has always been available to provide support for any aspect of my project. Furthermore, his mentorship has pushed me to pursue avenues that I did not believe were attainable, and I cannot thank him enough for his belief in my capabilities.

Next, I would like to thank the members of the Rotstein lab for providing a productive lab environment. To the graduate students Ariel, Braeden, Emily and Megan, and the undergraduate students Hala, Hunter, Ryan, Ezana and Puskar, I appreciate your kindness and support during my time in the lab. I would also like to thank the staff at the UOHI Radiochemistry facility Christian, Elmi, Hugo and Matt for enabling all my radiochemistry experiments to take place without any hiccups.

Finally, a mention to my friends Krushna, Khush and Sakshi who have always checked in on me and their calls have kept me going when I worked off-hours. Most importantly, I would like to thank my mother, her support could never be articulated into words, and my late father, who was the proudest man over every endeavour I undertook.

Table of Contents

List of Figures

List of Tables

List of Abbreviations

PET Positron Emission Tomography

RCC Radiochemical Conversion

TE Trapping Efficiency

RCY Radiochemical Yield

CIE Carbon Isotope Exchange

HAT Hydrogen atom transfer

SCE Standard Calomel Electrode

TEMPO 2,2,6,6-Tetramethylpiperidin-1-oxyl

mAChR Muscarinic Cholinergic Receptor

QNB Quinuclidinyl Benzilate

OVAT One Variable at a Time

DMBI 4-(2,3-dihydro-1,3-dimethyl-1*H*-benzimidazol-2-yl)-*N,N*-dimethylbenzenamine

EWG Electron Withdrawing Group

EDG Electron Donating Group

Chapter 1

Introduction

1.1 Radiochemistry for positron emission tomography

Molecular imaging is a non-invasive means to obtain functional information of cellular and biological processes. Positron emission tomography (PET) is a widely used molecular imaging modality used for research and diagnosis in the fields of oncology, cardiology and neurology, and in drug discovery.[1,2] PET relies on molecular probes, or tracers to generate the image.

1.1.1 The tracer principle

PET imaging begins with the preparation of a molecular imaging ligand, referred to as tracer. A tracer comprises of a positron emitting radionuclide attached to a targeting ligand. Generally, the targeting ligand is a bioactive molecule such as a drug, metabolite or their derivative.[2]

The tracer principle suggests that the radioactive tracer exhibits identical physical and chemical properties to its native counterpart and the administered dose of the tracer is a sub-pharmacological dose.[3] Dosage of the tracer is key, since PET images are primarily used for diagnosis, any pharmacological effects from tracer administration results in perturbation of the biological system and can lead to unreliable images. Adhering to these principles translates to preparation of a tracer that is chemically identical to its non-radioactive counterpart and is administered in trace amounts to the subject of interest.

The prepared tracer is then injected into the subject of interest, generally an animal (for pre-clinical studies) or a human patient. The radionuclide emits a positron, which annihilates with an electron in near proximity to produce two coincident ɣ-photons which are detected by the array of detectors in a PET scanner. The data collected is algorithmically reconstructed to produce an image of the spatial and temporal distribution of the tracer.[2,4]

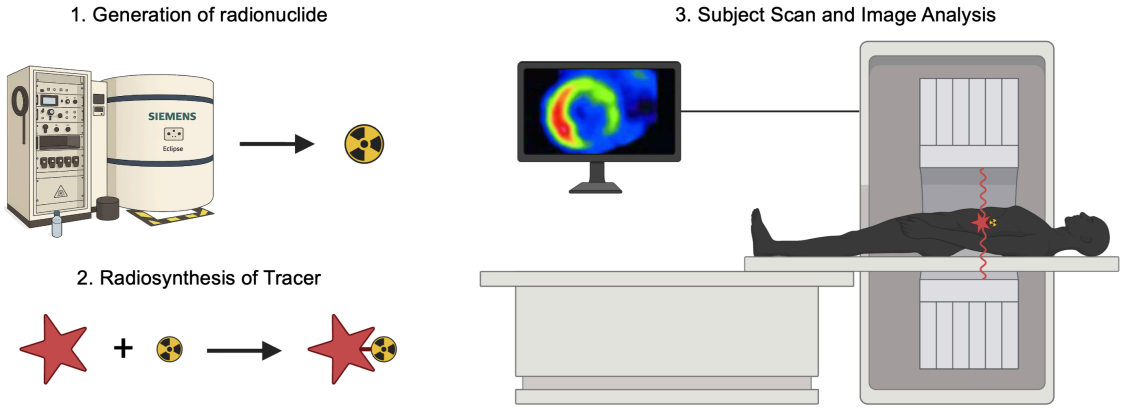

Figure 1 Radiochemistry is required for tracer development in diagnostic PET imaging

Figure created using BioRender

1.1.2 Radiochemistry for molecular imaging

The development of chemistries to incorporate a radionuclide into a tracer gave rise to the field of radiochemistry for molecular imaging. For diagnostic imaging, commonly employed radionuclides include positron emitting small atoms including ^{11}C, ^{18}F, ^{13}N and ^{15}O. Primarily, these nuclides are preferred in clinical settings for their short half-lives ($t_{1/2}$) which limits unnecessary exposure to radioactivity.[4,5]

Fluorine-18 ($t_{1/2}$ = 109.8 mins) is the most popular radioisotope for PET imaging due to the prevalence of 2-[^{18}F]fluoro-2-deoxy-D-glucose ([^{18}F]FDG) in clinical imaging, accounting for 95% of PET studies.[6] Since fluorine rarely occurs in natural biomolecules, tracers radiolabelled using fluorine-18 rely on being isosteric to a native ligand, as observed with [^{18}F]FDG. Hence, the tracers require experiments to validate their isosteric nature and the tracer can never perform identically to its native counterpart. Carbon forms the backbone of a very large spectrum of bioactive molecules. Hence, replacing an existing carbon-12 atom of a biomolecule with carbon-11 is an appealing radiolabelling strategy.

Carbon-11 ($t_{1/2}$ = 20.4 mins) is a widely used radioisotope for diagnostic PET imaging. The radionuclide is produced through the $^{14}N(p,\alpha)^{11}C$ nuclear reaction. The nuclear reaction takes place in a cyclotron, where a proton beam bombards a [^{14}N]N_2 target. Depending on the additive gas in the target, cyclotron generated carbon-11 affords two primary precursors. When H_2 is used as an additive, the

precursor yielded is [^{11}C]CH_4 while O_2 as an additive yields [^{11}C]CO_2. Since a no-carrier-added target is used, high enrichment of carbon-11 is observed in the target. However, external contamination of the gas target cannot be entirely eradicated. Either of the precursors are generated in trace quantities (up to 100 nmol) with a very significant (at least 99.9%) amount of non-radioactive precursors.[7,8]

From the primary carbon-11 precursors, [^{11}C]CH_4 and [^{11}C]CO_2, a multitude of secondary precursors can be prepared. Chiefly, secondary precursors such as [^{11}C]CO, [^{11}C]HCN and [^{11}C]CH_3I are routinely employed for tracer synthesis. While improving on reactivity, these precursors often require complex set ups for preparation from primary precursors and lead to loss of activity during the transformation.

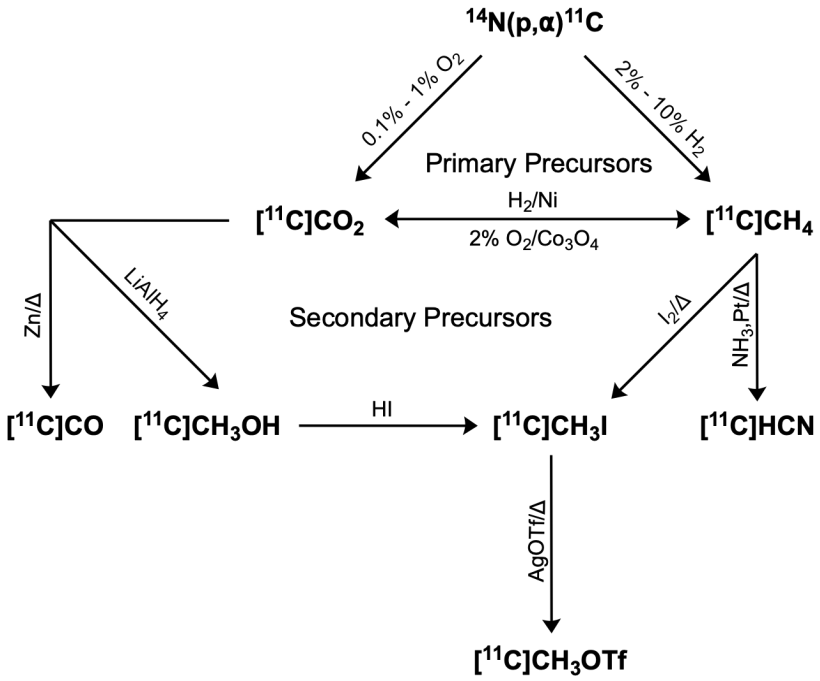

Figure 2 Reaction pathways for generation of ^{11}C-precursors

1.1.2.1 Terminology for Radiopharmaceutical sciences

The unique reaction conditions arising from radioactive decay and low concentrations demand that radiochemical reactions be measured using different set of performance parameters as agreed upon within the field of radiopharmaceutical sciences:[9]

Activity (*inf.* Radioactivity) measures

According to IUPAC, 'radioactivity' is the qualitative term to describe the spontaneous decomposition or rearrangement of a nuclei resulting in an emission of radiation. 'Activity' is the quantitative measurement of radioactivity, the number of decays of a given amount of material over a fixed time interval. (SI unit – 'Becquerel' (Bq), equal to one disintegration per second)

Specific Activity (A_s) and Molar Activity (A_m)

A_s – Measured activity per *gram* of compound (GBq/mg)

A_m – Measured activity per *mole* of compound (GBq/μmol)

Yield measures

Radiochemical conversion (RCC) is measured as the activity of the product, as a percentage (%) of the starting activity used, corrected for radioactive decay. This is identical to the concept of 'chemical yield' used in non-radioactive chemistry. Typically, RCC is determined using radioHPLC.

In the case of gaseous radionuclide precursors such as $[^{11}C]CO_2$ or $[^{11}C]CO$, the activity at the end of radionuclide production cannot be extracted into a radiochemical reaction with quantitative efficiency. Instead, activity is measured for the resultant reaction mixture to determine the 'trapping efficiency' (TE) of the gaseous radionuclide precursor. TE is measured as a percentage (%) of total activity produced. TE corrects RCC for the amount true activity that is available to react.

Together with the correction, we define the all-encompassing radiochemical yield (RCY), which is the percentage (%) of activity generated that converted to product.

$$\mathbf{RCY = TE \times RCC}$$

1.1.3 Radiochemistry with Carbon-11

Due to the very short half-life of carbon-11, the incorporation of the radionuclide occurs in the final or penultimate step of tracer synthesis. Referred to as late-stage functionalization, such strategies are common to both primary and secondary carbon-11 precursors. Popular radiochemical strategies to incorporate carbon-11 include:

- Methylation of nucleophilic centres using secondary precursors [^{11}C]CH_3I or [^{11}C]CH_3OTf
- C-C bond formation using secondary precursors ([^{11}C]CO, [^{11}C]CN^-, etc.) through transition metal mediated coupling/catalysis
- Carboxylic acids and their derivatives from [^{11}C]CO_2 carboxylation using organometallic reagents or copper catalysts

The simplicity afforded by ^{11}C-methylation has made it the most common strategy for carbon-11 radiolabelling. Generally, a nucleophilic heteroatomic centre is methylated using [^{11}C]CH_3I or [^{11}C]CH_3OTf, under mildly basic conditions in a single step (Figure 3.b). Occasionally, ^{11}C-methylation is employed at the cost of modifying the native ligand (Figure 3.c).

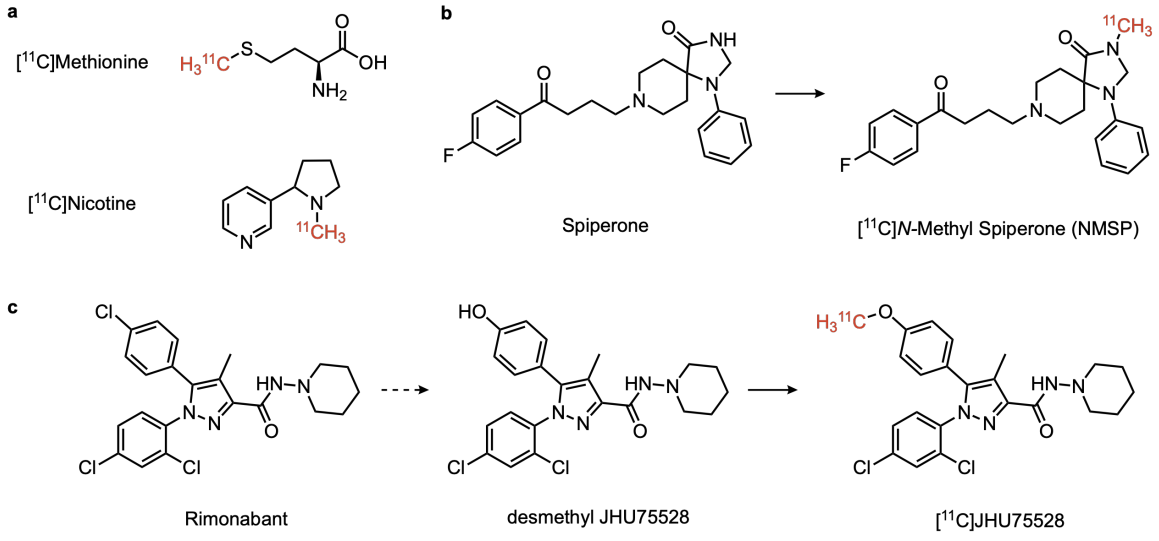

Figure 3 Tracers prepared using ^{11}C-methylation

(a) Tracers with identical structures to native ligands (b),(c) PET tracers for neuroimaging (b) Methylation of native ligand (Spiperone, antipsychotic drug) (c) Structural modification for methylation (Rimonabant, CB_1 targeting ligand)

[^{11}C]CO is a well-established precursor with a straightforward synthetic route and a variety of developed ^{11}C-carbonylations. However, it has poorly translated to clinical PET tracer synthesis due to the lack of automated synthesis units for [^{11}C]CO.[10] A similar case holds true for [^{11}C]HCN, a lack of widespread adoption of commercially available automated synthesis modules. Although, [^{11}C]HCN has been essential to generate different functionalities such as nitriles, hydantoins and (thio)cyanates. Through further steps, [^{11}C]HCN has been employed to prepare various carboxylic acid derivatives as well.[11]

As alluded to earlier, direct functionalization of the primary carbon-11 precursor [^{11}C]CO_2, is appealing due to activity not being lost to during the transformation to secondary precursors. Functionalization of [^{11}C]CO_2 is common using organometallic reagents (Grignard, organolithiums, etc.), providing access to carboxylic acids and a spectrum of carboxylic acid derivatives (Figure 4). Although these conditions are harsh, and require robust substrates, often with multiple protecting groups to prevent unfavourable reactivity. Furthermore, the reaction conditions must be rugged, requiring moisture-free conditions, which makes reproducibility difficult in a clinical production environment.

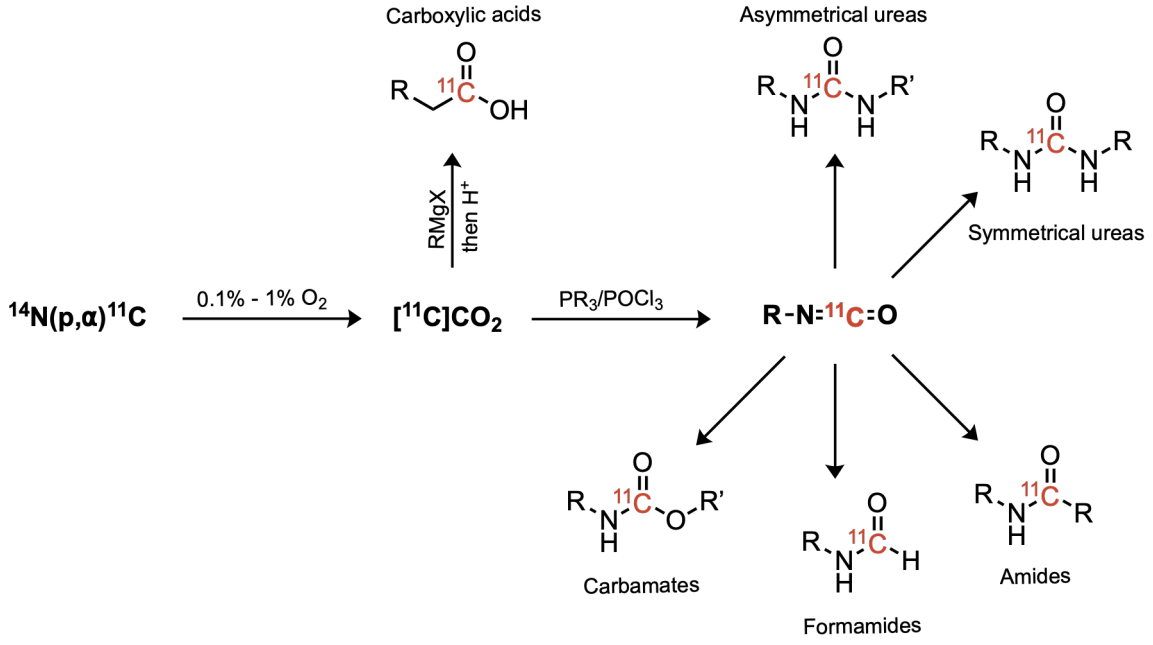

Figure 4 Preparation of ^{11}C-carboxylic acid derivatives

1.2 Photocatalysed methods for carbon-11 radiochemistry

Photochemistry has emerged as an exclusive route for certain organic transformations. Moreover, it has emerged as an important strategy for late stage functionalization in natural product synthesis, agrochemicals and active pharmaceutical ingredients.[12] Given the importance of late-stage functionalization in radiochemistry, photochemistry has been adapted to the constraints of radiochemistry. Photocatalysed methods for PET isotopes, namely ^{11}C and ^{18}F have emerged over the past decade.[13]

Photochemical methods for carbon-11 have emerged for various established precursors from the cyclotron-produced $[^{11}C]CO_2$ and secondary precursors emerging from transformations including $[^{11}C]CH_3I$, $[^{11}C]CO$ and $[^{11}C]CN^-$. In the subsequent sections, notable photochemical methods using various ^{11}C-precursors have been described. Alongside, the non-radioactive methods they were adopted from are compared to understand the key changes made for radiochemistry.

1.2.1 Photocatalysed coupling with $[^{11}C]CH_3I$

In 2021, Pipal and coworkers[14] disclosed a radiomethylation strategy to prepare ^{11}C and ^{3}H labelled tracers via a nickel mediated photoredox coupling (Figure 5) and the precursors used here are $[^{11}C]CH_3I$ and $[^{3}H]CH_3I$ respectively. The strategy employs a visible light activated photoredox catalyst to generate a silyl radical (tris(trimethylsilane)silane), which subsequently generates a $[^{11}C]CH_3^{\cdot}$ radical. Concurrently, the arylnickel halide intermediate is formed. An oxidative capture of $[^{11}C]CH_3^{\cdot}$ by the arylnickel halide intermediate converts it to a $[^{11}C]CH_3$-arylnickel intermediate which is reductively eliminated to yield the coupled product. A variety of radiotracers were synthesized from aryl-halide precursors while alkyl-halide precursors performed poorly, potentially due to poor reductive elimination from the nickel complex. The method is notable for being one of the initial methods published that provided a benchmark for reaction set up and scale for subsequent photocatalytic carbon-11 radiochemistry.

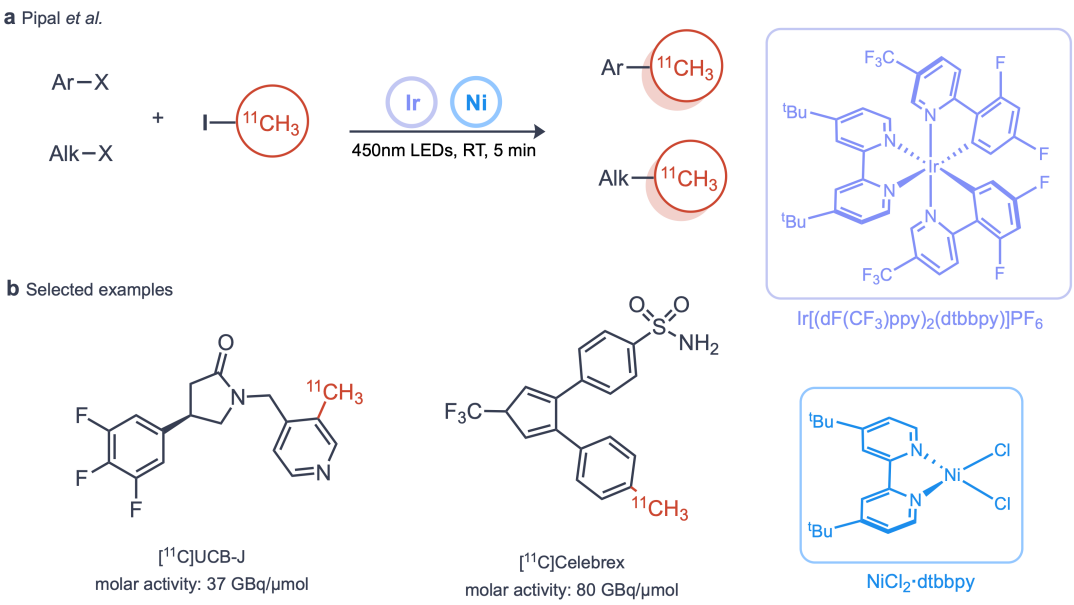

Figure 5 Metallophotoredox radiomethylation using [^{11}C]CH_3I

The method was adapted from the lab's previous work reported by Zhang *et al.*[15] which was an identical, but non-radioactive nickel mediated photoredox coupling. The changes made to adapt the non-radioactive method for radiochemistry were -

- Decrease in reaction time from 6 h → 5 min
- Decrease in total reaction volume from 2 mL → 300 μL
- Decrease in concentration of substrate from 0.25 M → 0.015 M

The above changes are generally expected in adaptation for radiochemistry. However, notable changes in the radiochemical method were the following:

- Increase in photocatalyst loading from 1 mol% [Ir] → 2 mol% [Ir]
- Increase in metal catalyst loading from 0.5 mol% [Ni] → 17 mol% [Ni]

The increased loading of catalysts enabled reducing reaction time from hours down to a few minutes. Short reaction times (<10 mins) are essential for carbon-11 methods given its physical half-life of 20.4 mins. For instance, if a reaction were run for 20 minutes, about 50% of the activity produced would be rendered useless regardless of reactivity.

1.2.2 Photocatalysed coupling with [^{11}C]CN^-

Li, Nicewicz and coworkers reported a photocatalytic method over multiple reports[16,17] for aryl C-H ^{11}C-radiocyanation and deoxy-^{11}C-radiocyanation (Figure 6.a). The former method suffered from poor site-selectivity on arene substrates (X = H) which the latter overcame through the installation of a methoxy directing group (X = OMe). Regardless, the proposed mechanism involves the acridinium based photocatalyst activating the substrate to form a radical cation, followed by nucleophilic radiocyanation to form a Meisenheimer-like radical intermediate. Finally, the intermediate is oxidised to yield the ^{11}C-cyanated product. Notably, the reports were limited to a scope of electron rich arenes, although tolerated nitrogenous heterocycles.

Similar to the radiomethylation method, this radiocyanation was adapted from the lab's previous work reported by McManus and Nicewicz.[18] General adaptations were made for radiochemistry by reducing the reaction volume and the substrate concentration, and the catalyst loading was increased. Furthermore, a more readily available source of CN^- was required due to carbon-11's inherently low concentrations. This led to the switch from trimethylsilyl cyanide (TMSCN) to tetrabutylammonium bicarbonate (TBAB, forming [^{11}C]TBACN) as a labile [^{11}C]CN^- trap, formed *in situ* or preformed).

These works paved the way for Li and Nicewicz[19] to report a decarboxylative radiocyanation strategy to yield ^{11}C-nitriles (Figure 6.b). The strategy shifts from a deoxy-cyanation to a decarboxylation-cyanation. The substrate compatibility of this method shifts from electron-rich arenes of previous reports to a spectrum of alkyl and benzyl positions on drug molecules that furnish a diverse library of carbon-11 labelled drug molecules, metabolites, amino acids and peptides.

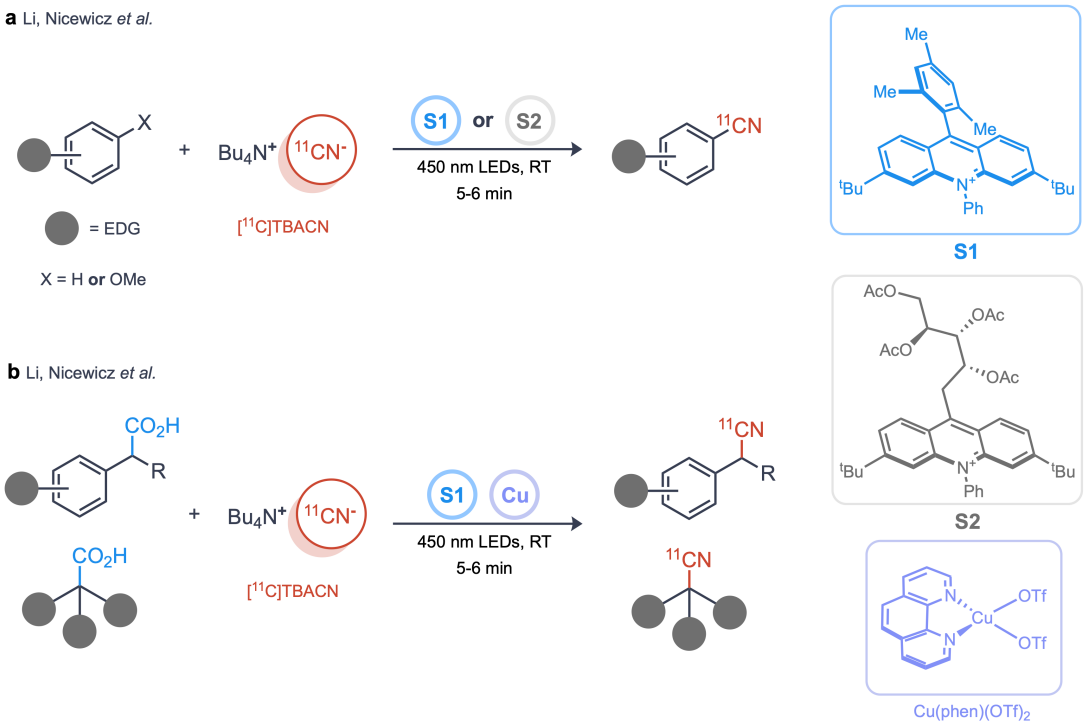

Figure 6 Photocatalysed radiocyanation using acridinium based photocatalysts

1.2.3 Photocatalysed carboxylation and isotopic exchange with [^{11}C]CO_2

Amidst the development of methods for secondary carbon-11 precursors, a myriad of strategies to label with [^{11}C]CO_2 were reported. Proximal to the radiomethylation strategy in 2021, Kong *et al.*[20] reported a mild metal-free approach to synthesize ^{11}C-carboxylic acids using carbon isotope exchange (CIE). No precursor synthesis is required as the native substrate acts as the precursor. It has been proposed that upon activation of the substrate using an organic phthalonitrile photocatalyst, a radical-polar crossover occurs causing the substrate to decarboxylate. The decarboxylation forms the anion **7(I)** which is labelled by [^{11}C]CO_2 to yield the corresponding acid (Figure 7.a).

The CIE method enables a one-step strategy for radiolabelling carboxylate groups with carbon-11 and is amenable to labelling a diverse range of radiotracers with phenylacetic acid moieties. However, since the precursor and final product are isotopologues, they exhibit identical physical and chemical properties. It is impossible to separate the radioactive product from the non-radioactive product (which, in this case is also the precursor). Due to the presence of non-radioactive product, the molar activity (A_m) of the

formulation is low for *in vivo* use (Figure 7.c). High molar activities are sought after to ensure the tracer dose is within pharmacological limits. Routinely used carbon-11 PET tracers are reported to have A_m values between ~1-200 GBq/µmol[21,22] to prepare a useful dose for PET imaging.

Nonetheless, this method was the first photocatalysed route for carbon-11 radiolabelling using [^{11}C]CO_2. The method is inspired by isotopic labelling methods reported for [$^{13/14}$C]CO_2 by Kong *et al.* (2020)[23] and Destro *et al.*[24] (Figure 7.b). Through a thermal metal-free CIE strategy, Destro *et al.* proposed that thermal decarboxylation of the amino acid salt leads to formation of the anion **7(I)** which reacts with [$^{13/14}$C]CO_2 to form isotopic phenylacetic acids. As described in subsequent sections, anions akin to **7(I)** are commonly proposed to be the reactive intermediate during photocatalysed carboxylation. Moreover, the formation of such anions is possible through multiple reductive pathways such as successive single electron transfer (SSET) or through radical-polar crossover. However, the method was limited to non-heteroatomic and sterically unhindered phenylacetic acids. Furthermore, the method performed poorly with [^{11}C]CO_2 and only one substrate was labelled with a reasonable yield.

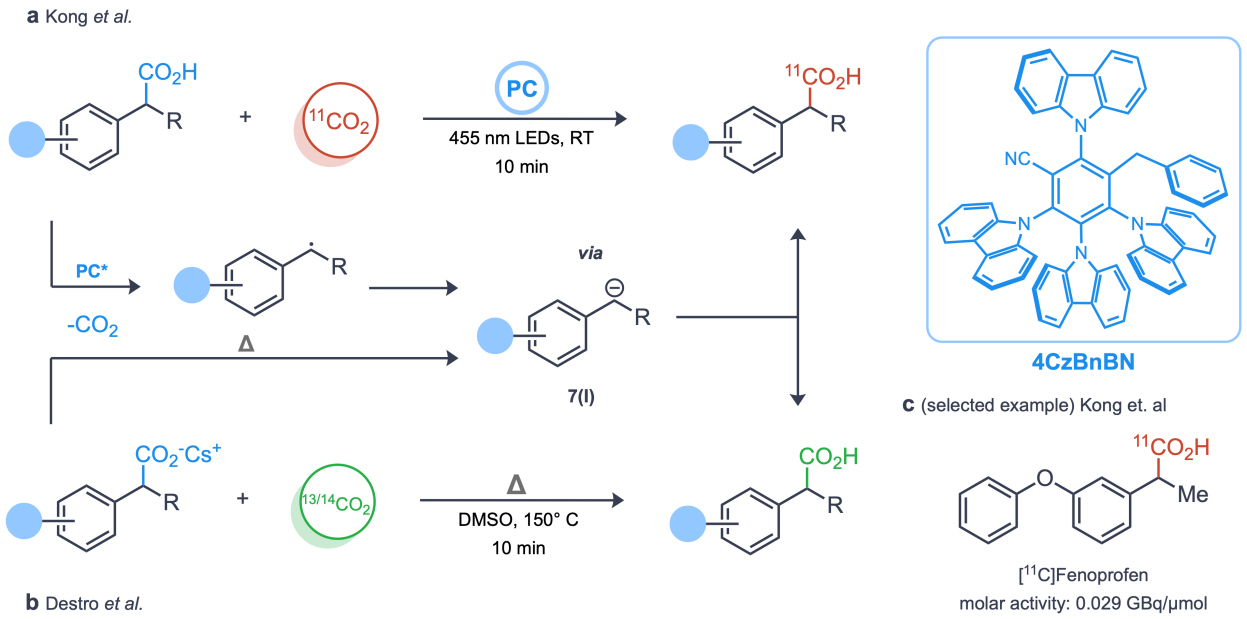

Figure 7 Carbon Isotope Exchange (CIE) for isotopic labelling

Obtaining low molar activity is an inherent flaw to CIE chemistry, to overcome this hurdle, Munch *et al.*[25] developed a direct photocatalysed carboxylation of benzylic positions to prepare ^{11}C-phenylacetic acids

(Figure 8.a). The absence of non-radioactive product improves molar activity as no inherent source of non-radioactive CO_2 exists beyond impurities from multiple sources. A similar scope of phenylacetic acids from the CIE method were labelled. More importantly, the molar activity was improved by an order of magnitude bringing it to a range for more usable for PET imaging (Figure 8.d).

The method was adopted from the photocarboxylation reported by Meng *et al.*[26], to install carboxylic acid groups on benzylic positions (Figure 8.b). The mechanism commences through a thiol-mediated hydrogen atom transfer to form the benzylic radical **8(I)** which is further reduced by a single electron transfer from the photocatalyst to form the anion **8(II)**, which reacts with CO_2 to yield the carboxylic acid. Such a mechanism reflects a classic radical polar crossover, given the formation of an anion from the reduction of a radical. The mechanism was partially verified though deuterium labelling experiments (Figure 8.c) where a kinetic isotopic effect (KIE) was observed in both intermolecular and intramolecular experiments. Primary KIE observed in the first experiment suggests the formation of the radical **8(I)** to be a potential rate determining step. The second experiment bolsters the role of **8(I)** being the rate determining intermediate. Since carboxylation through **8(II)** is understood to be a less reversible pathway, the reduction of **8(I)** should proceed given the high reduction potential of the photocatalyst. The carboxylation step to form the product from **8(II)** is generally a fast step. Experimental verification could be done by looking at isotopic effects with $[^{13}C]CO_2$.

Furthermore, during their experiments they detected the formation of alkylated photocatalysts. The photocatalyst 4CzIPN has one of its nitrile (CN) groups replaced by a benzyl group or phenylethyl group (Figure 8.e). Such alkylated photocatalysts have greater reduction potentials (Phenethylated catalyst, 4CzPEBN[P*/ P^-] = -1.69 V vs SCE) compared to the unmodified catalyst (4CzIPN[P*/ P^-] = -1.43 V vs SCE), and it has been proposed that the alkylated photocatalyst is the active photocatalyst in the reaction.[27] Hence, Munch *et al.* switched to preforming the alkylated photocatalyst to skip the induction period of the reaction where the photocatalyst is alkylated. Switching the photocatalyst shortens the reaction time and is the most critical change to adapt the method to radiochemistry.

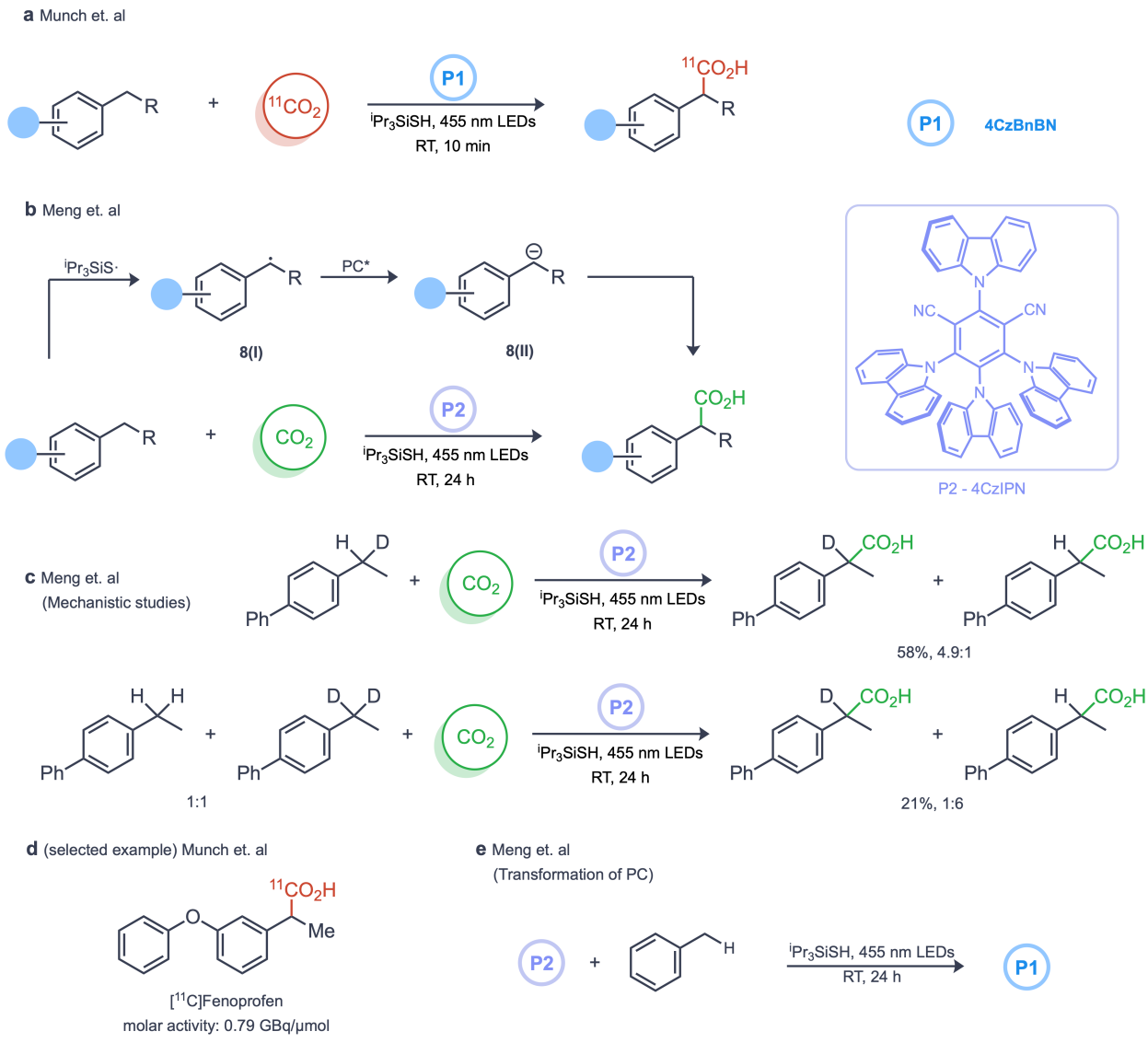

Figure 8 Direct photocatalysed carboxylation of benzylic positions

Most recently, Malandain *et al.*[28] reported a photocatalysed carboxylation with [^{11}C]CO_2 to prepare ^{11}C-carboxylic acids from activated styrenes and acrylamides using a formate salt mediated strategy (Figure 9.a). While the method was primarily developed for [$^{13/14}$C]CO_2, four substrates were labelled with carbon-11. The mechanism hinges on the formation of a radical anion species **9(I)** (Figure 9.d). Isotopic enrichment of sodium formate in the presence [^{13}C]CO_2 suggest an equilibrium between CO_2 and **9(I)**. The rest of the mechanism follows from the non-radioactive work the method has been adopted from.

This work has been developed from the report by Alektiar *et al.*[29] where carboxylation of styrenes is undertaken directly using formate (Figure 9.b). Here, they propose the formation of radical anion **9(I)** through a thiol-mediated hydrogen atom transfer. The radical anion reacts with the styrene to cause a homolytic fission. The more stable radical **9(II)** is formed due to stabilization of the radical from the phenyl group at the α-position. While a carboxylation at the α-position might occur, the radical formed would be less stable, making this route highly reversible. Next, the substrate is reduced through a hydrogen atom transfer from the thiol to yield the product. The mechanism is supported through an experiment using deuterated sodium formate and indicating the source of the proton (Figure 9.c).

Unlike methods described in earlier sections, which hinge on the formation of an anion species for carboxylation, this formate mediated method follows a radical-only mechanism. The method activates the carbon-11 precursor instead of the substrate molecule. Such an alternate path can create greater consistency in substrate compatibility as the conditions are tuned for the activation of a consistent moiety.

The carbon-11 formate carboxylation was employed to prepare four substrates with useful radiochemical yields. This method can carboxylate of β-benzylic positions and serves as complementary to the work by Munch *et al.* in preparing carboxylic acids at α-benzylic positions. Nevertheless, due to the presence of sodium formate in the reaction, the products have a low A_m (Figure 9.e), caused due to the introduction of non-radioactive CO_2 into the reaction from the ^{nat}C-sodium formate equilibrium with CO_2.

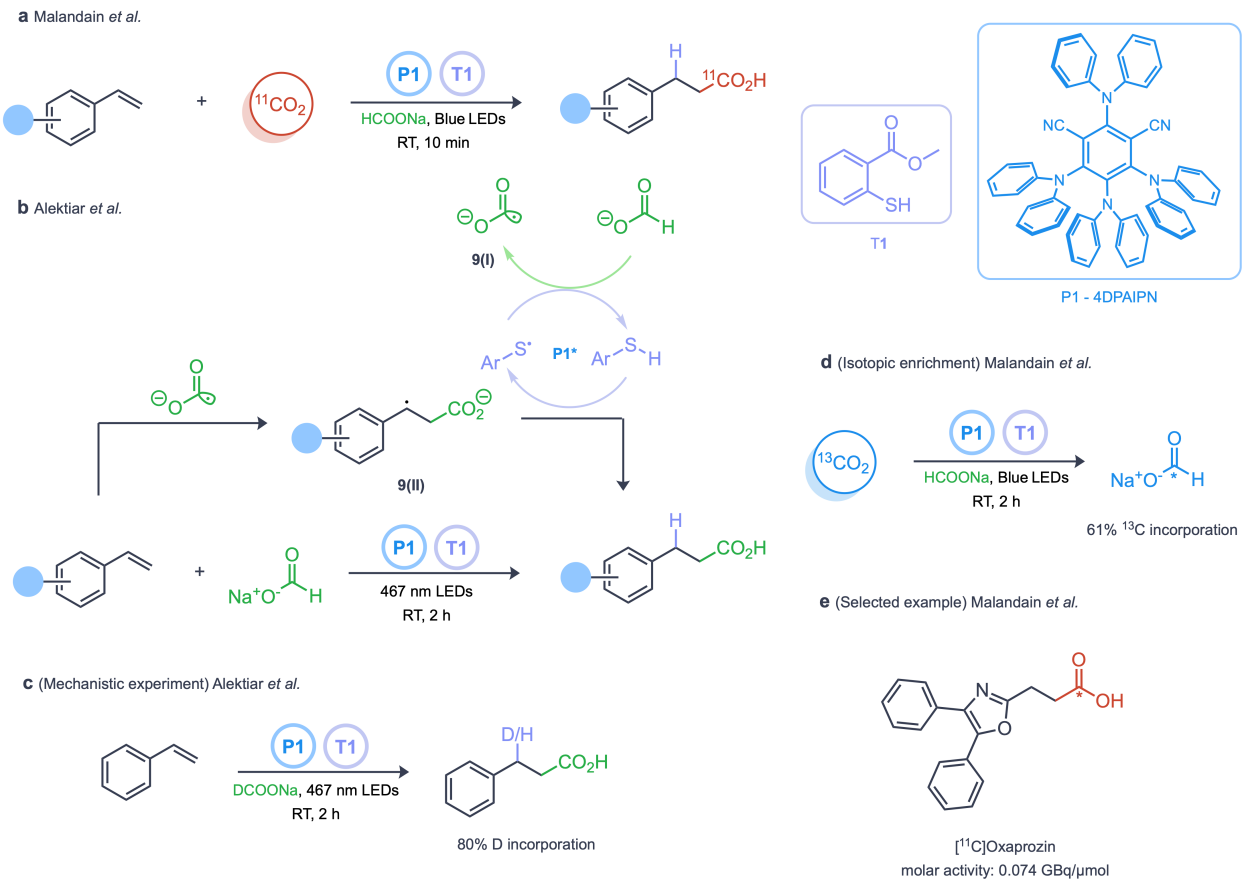

Figure 9 Photocatalysed hydrocarboxylation of benzylic styrenes

1.2.4 Overarching theme of photocatalysis with carbon-11

This section highlighted carbon-11 photocatalysis reports against corresponding non-radioactive methods from which they have been adopted for radiochemistry. Importantly, mechanistic insights from the non-radioactive method carry-over to the radiochemical method. For instance, one approach with $[^{11}C]CO_2$ is to activate the substrate for carboxylation, where the formation of an anion at the α-position of the substrate through reduction is the key step. Another approach is to activate $[^{11}C]CO_2$ through the initiation of an equilibrium with a formate radical anion, where the reaction proceeds through a radical mechanism. Furthermore, the purpose of this section was to specifically highlight key strategies employed to adopt non-radioactive methods for radiochemistry –

- Reduction of total reaction volumes from ~2 mL for most non-radioactive methods to <500 μL for the radiochemical methods to account for trace concentrations of carbon-11 produced.

- Increased concentration loading of catalyst for radiochemical methods (up to 9-fold increase in concentration from the non-radioactive method) for short reaction times (<10 mins) required due to carbon-11's physical half-life of 20.4 minutes.

1.3 The current state of photocatalysed carboxylation

As observed with photochemical methods for carbon-11, olefins have received the most attention for functionalization. The interest extends to non-radioactive methods where extensive research has been conducted for the functionalization of CO_2 onto olefins. Carbonyl compounds and imines have been far less explored for CO_2 carboxylation. These substrates give rise to α-substituted carboxylic acids, which are important functionalities in various bioactive molecules.

Carboxylation of imines yields α-amino carboxylic acids, commonly referred to as amino acids. Amino acids are a commonly found moiety in various pharmacophores and are present endogenously in all living systems. Consequently, carboxylation of carbonyl compounds gives rise to α-hydroxy carboxylic acids, a functionality found in various metabolites and bioactive ligands. Thus far, only a handful of methods have been reported to prepare these compounds. The subsequent sections will highlight the mechanistic similarities between non-radioactive carboxylation methods for olefins described in earlier sections and notable carboxylation methods for imines and carbonyl compounds.

Fan *et al.*[30] reported their photocatalysed CO_2 fixation to prepare diaryl α-amino acids. This method formed the basis for umpolung reactivity across C=X (X = N,O) bonds as the earliest published report within this section. The method employs imines derived from ketone substrates for carboxylation. Upon irradiation, the neutral photocatalyst reduces the imine **10(S)** to **10(ii)** through a single electron transfer, which is in resonance with the carbanion **10(iii)** (Figure 10). **10(iii)** has been proposed to be the reactive intermediate, supported by a computational spin density study. Unlike olefins, which would require a SSET for the formation of the reactive carbanion, the charge on **10(iii)** is localised at the carbon to react with CO_2. The carboxylation forms the free acid which undergoes and methylation workup to yield the product **10(P)**. The scope includes diaryl α-amino acid methyl esters with various stereoelectronic

substituents and an aryl-methyl amino acid. The lack of any reported free α-amino acids could be due to the reversible nature of such carboxylation reactions. Reversibility of the carboxylation makes the free amino acid less stable for isolation. Experiments on alkyl-phenyl ketoimines did not yield any carboxylated product, potentially due to poor stabilization of the carbanion **10**(iii) formed and clearly highlighting a limitation of the method. Regardless, the method hinges on the activation and subsequent reduction of the substrate for to form an anion for carboxylation of the imine.

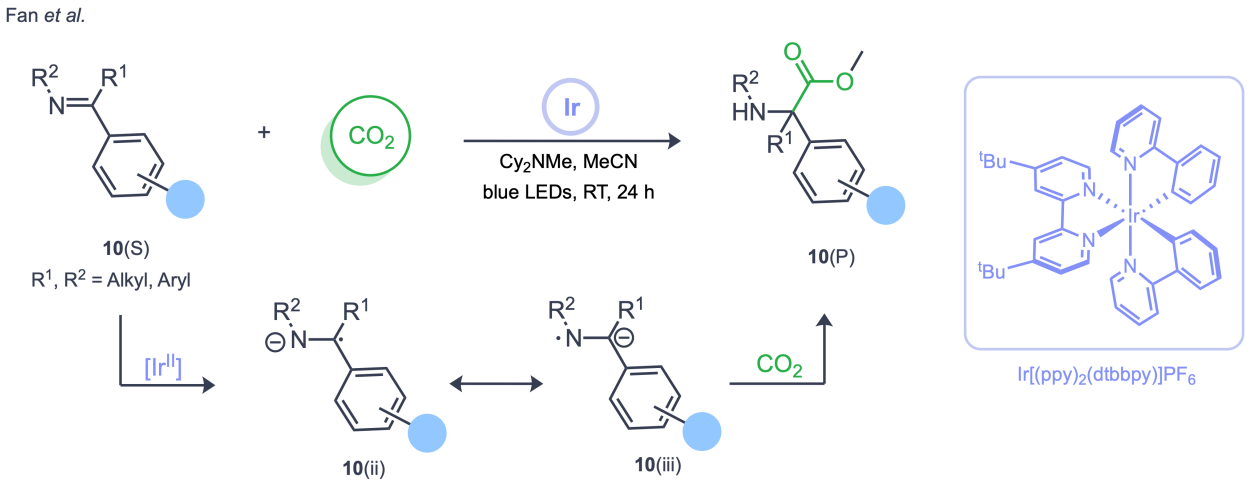

Figure 10 Umpolung photocarboxylation of imines with CO_2

Development of a photocarboxylation with imines set up works by Cao *et al.*[31] and Okumura *et al.*[32,33] on photocarboxylation of ketone substrates to prepare α-hydroxy acids. On theme with olefins, both methods propose different intermediates, but the mechanisms rely on SSET to form a reactive carbanion intermediate that undergoes carboxylation. Cao *et al.* proposes the formation of a silyl ether-like carbanion **11(iii)** while Okumura *et al.* propose a carbonate-stabilized carbanion **12(iii)**.

Cao *et al.* (Figure 11.a) employs a silane chloride to improve selectivity of carboxylation **11(P)**, compared to the primary unwanted ketone dimer product **11(U)**. The selectivity improves due to the bulkiness of the trimethylsilane (TMS) group (Figure 11.b). The mechanism utilizes TMS through covalently bonding to the ketone oxygen upon the first reduction to **11(ii)**. The covalency helps to stabilize the carbanion intermediate **11(iii)** upon SSET.

Similar to previous methods, the first reduction of the SSET occurs on the oxygen due to the transient formation of a carbanion on the oxygen followed by the α-carbon. CO_2 undergoes an electrophilic addition onto **11(iii)** to furnish the α-hydroxy acid **11(P)** (Figure 11.a). The proposed mechanism is supported by a radical trapping experiment using TEMPO, highlighting the formation of **11(ii)** and reduction experiments using D_2O confirming the formation of **11(iii)** (Figure 11.b). The substrate scope is highly diverse, from diaryl α-hydroxy carboxylic acids to carboxylation of alkyl-aryl ketones, alkyl-ketoester ketones and aldehydes, clearly demonstrating the versatility of this method. A majority of this scope has been reported as the free hydroxy acid. However, substrates with carbanion destabilizing motifs were isolated as hydroxy acid methyl ester perhaps due to the reversibility of the carboxylation step.

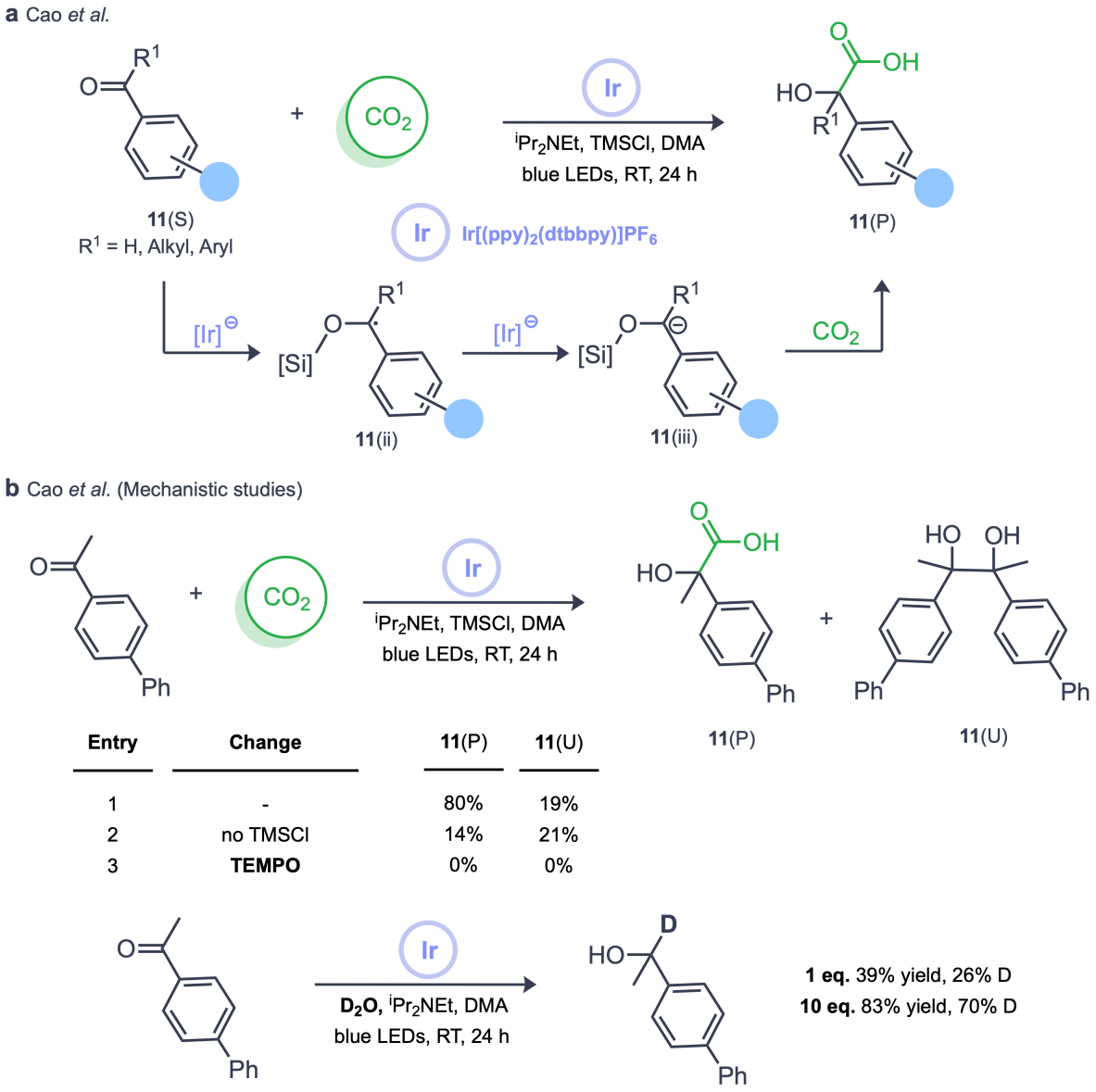

Figure 11 Photocarboxylation of ketones with silane-directed selectivity

Concurrently, yet independently, Okumura *et al.*[32] reported a photocarboxylation method for ketone and aldehyde substrates using an iridium photocatalyst coupled with 1,3-dimethyl-2-phenyl-2,3-dihydro-1H-benzimidazole (DMBI) as an electron and proton donor (Figure 12.a). The reported mechanism follows a SSET route where the first reduction occurs on the oxygen due to its electronegativity and forms the carbonate radical **12(ii)**. The subsequent reduction forms a familiar carbanion intermediate **12(iii)**. Formation of these intermediates are supported by the low formation of the reduced ketone **12(iv)** in the absence of CO_2. Finally, the reported mechanism suggests that intermediate **12(iii)** reacts with CO_2 to yield the α-hydroxy acid **12(P)** (Figure 12.a).

Notably missing among mechanistic experiments is the reaction performed in the presences of a radical scavenger such as TEMPO. Such an experiment would better suggest formation of proposed intermediates. The dual electron-proton (SET-HAT) donating nature of DMBI would suggest a possible mechanistic route similar to the mechanism reported by Fan *et al.*[30] for this reaction is through the formation of a ketyl-carbanion. Rather than considering a SET for the first step, consider the first step to form a ketyl radical through hydrogen atom transfer from DMBI followed by a SET to form a ketyl-carbanion. This ketyl-carbanion would be similar to **12(iii)** with the notable absence of carbonate. A standard carboxylation after would furnish the desired hydroxy acid.

Regardless, the substrate scope ranges from diaryl ketones, alkyl-aryl ketones and aldehydes. Recently, this method was adapted to use an organic *N*-BAP (diazabenzoacenaphthenium cation, **P1**) photoredox catalyst.[33] Importantly, the fundamental mechanism for both reports remain ambiguous.

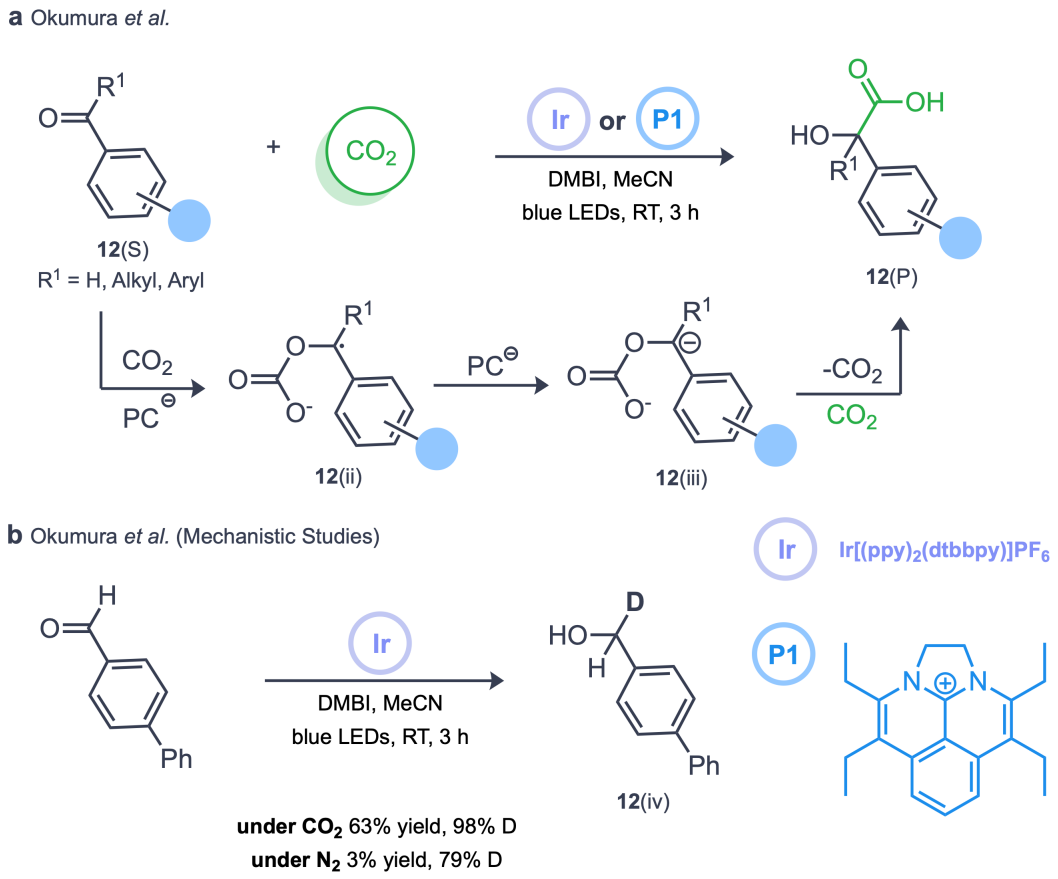

Figure 12 Photocarboxylation of ketones using an [Ir]/DMBI couple

1.3.1 Potential for adapting non-radioactive methods with carbon-11

Mechanistic similarity between radioactive and non-radioactive methods implies that majority of mechanistic basis for a potential method to be adopted for radiochemistry comes from non-radioactive studies. The low concentration and short physical half-life of carbon-11 imposes limitations on mechanistic experimentation to quantitatively measure reactivity as analytical measurements are not sufficiently sensitive.

A requirement to adopt non-radioactive methods must be a thorough mechanistic understanding of the reaction supported by experimental evidence. Such understanding should be extended beyond reactivity to understand kinetics and stability. The smaller scale and shorter reaction times demand fast kinetics and, the analysis of non-radioactive products (ex. NMR, LC-MS) differs vastly from radioactive products (ex. radioHPLC) requiring an understanding of the stability of products under varied conditions.

1.4 Bayesian Optimisation

Every method described in earlier sections had a screening and optimisation phase during method development. Traditionally, the optimisation campaign is undertaken by varying one variable at a time (OVAT). For example, consider a reaction is being optimized for the highest yield. To begin, a component of the reaction is switched based on the chemist's intuition and tested. There are three possible outcomes – an improvement in yield, near identical yields or a decrease. Generally, an improvement leads to another component being changed and tested, while the latter two cases call for a change of the same component. The cycle is repeated until the yield improves to a satisfactory range and the optimisation is declared to be completed.

An OVAT optimisation doesn't necessarily lead to the highest yielding conditions. When it does, the conditions generally are not obtained within the least number of experiments. OVAT campaigns treat each component independently. Using a Bayesian optimizer (BO), each experiment performed towards the optimisation campaign is quantified, accounting for inter-component dependencies. The two key pillars of a BO framework are:[34]

- A prior distribution function that enables defining prediction functions (or surrogate models)
- An acquisition function to determine the optimal series of queries (here, experiments to perform) that fit the surrogate model

Experimental Design via Bayesian Optimisation (EDBO+)[35] is a software to enable reaction optimisation using BO. The platform is fine-tuned to encode chemical reactions, defining an appropriate surrogate model to determine the experiments to perform. The general workflow for EDBO+ involves:

- Determination of a reaction space (ex. concentrations, catalysts, etc.) and the objectives (ex. yield, selectivity, etc.) to be optimized by the user, which is mathematically represented by the optimizer.
- The optimizer determines a batch of experiments to be performed using the acquisition function.
    - The initial set of experiments determined by the optimizer engage the maximum number of variables to represent the reaction space

- The experimental data is input into the optimizer, where the surrogate model provides predictions and concurrently, refines the acquisition function to suggest new experiments.

The primary benefit of such an approach is the use of statistically driven predictions, where data backs up every subsequent experiment. To maximize output parameters (such as yields), a maximum is found within the prediction function. Such a maximum, that fits well to the prediction function, represents the true optimal conditions in each reaction space.

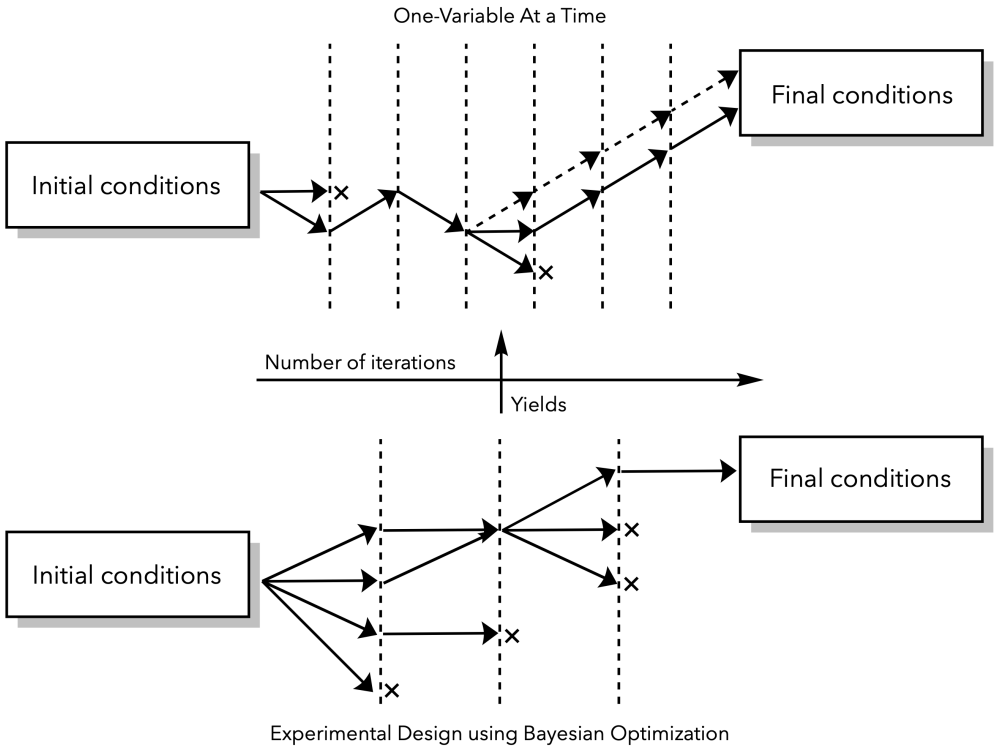

Figure 13 Comparison of an OVAT workflow with Bayesian optimisation
*Dashed line represents a potentially higher yielding condition that was not realized during optimisation

1.5 α-Hydroxy carboxylic acids in PET imaging

α-Hydroxy carboxylic acids are prevalent as a functional moiety in various disconnected niches. Notably, they are found in active ingredients for skincare products[36,37], as important metabolites in plants and animals[38,39] and in various muscarinic acetylcholine receptor (mAChR) antagonists.[40]

The latter two have been explored in the context of PET imaging in humans. Lactic acid, or lactate (due to its deprotonated state under physiological conditions) is a metabolite found in humans and a by-product of the glycolytic cycle. Furthermore, high lactate concentrations in the blood have been associated with diseased states including cancer[41] and cardiovascular disease.[42] L-3-^{11}C-lactate has been synthesized for PET imaging and evaluated for feasibility. Unfortunately, due to back diffusion of unmetabolized labelled lactate, the estimations from the study were poor. To introduce a metabolic endpoint for lactate, a potential strategy is to synthesize L-1-^{11}C-lactate. The proposed tracer has a clear metabolic endpoint through decarboxylation (verified by L-1-^{14}C-lactate) and consists of functionalization to a α-hydroxy acids moiety (Figure 14.a).

mAChRs are a part of the muscarinic cholinergic system, which controls the parasympathetic nervous system (PNS), or the vagal nervous system. The role of PNS has not been elucidated in diseased states.[43,44] A large focus of muscarinic PET imaging is on brain imaging, however some studies have been undertaken for cardiovascular PET imaging.[45] Various mAChR ligands have been radiolabelled with carbon-11 and evaluated *in vivo* for humans, including [^{11}C]*N*-Methyl Quinuclidinyl benzilate ([^{11}C]MQNB)[46], [^{11}C]Tropanyl benzilate ([^{11}C]TRB)[47] and [^{11}C]*N*-methyl-4-piperidyl benzilate ([^{11}C]NMPB)[48] (Figure 14.b).

While the tracers consist of α-hydroxy acid moieties, these tracers have been prepared through ^{11}C-methylation of native mAChR antagonist ligands. [^{11}C]Quinuclidinyl benzilate ([^{11}C]QNB) has been prepared through di-lithiation of benzophenone using Li metal, followed by carboxylation with [^{11}C]CO_2 to yield benzilic acid, which was coupled to quinuclidinol to yield [^{11}C]QNB.[49] However, to the best of our knowledge, [^{11}C]QNB has not been evaluated *in vivo*. As alluded to earlier, methylation of a ligand can

impact its pharmacokinetics. For example, the cationic nature of [^{11}C]MQNB by virtue of being a quaternary ammonium salt, leads to the tracer's impermeability through the blood-brain barrier.[46]

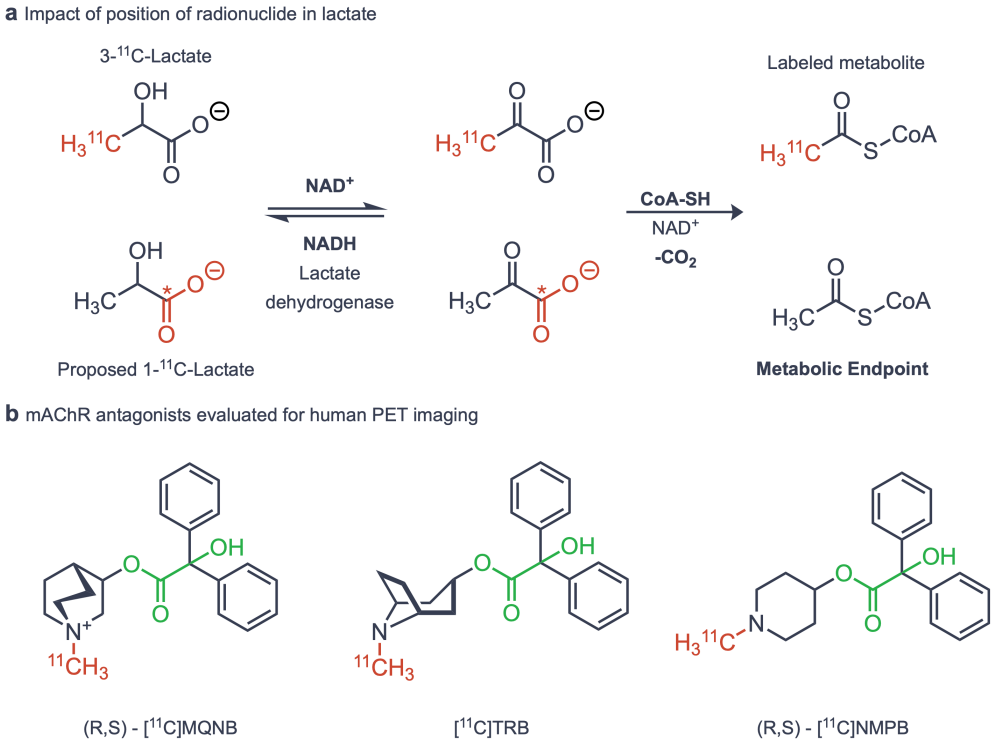

Figure 14 α-Hydroxy acids in metabolism and mAChR antagonists

1.6 Research Objectives

The general maturation of chemical methods has made direct fixation of [^{11}C]CO_2 an efficient and appealing route for carbon-11 radiolabelling. Furthermore, photocatalysis with carbon-11 precursors for radiolabelling is an emerging methodology to prepare PET tracers. For widespread adoption, photocatalysed methods must be extended to prepare a variety of functionalities found in existing and unrealized PET ligands. We were interested in radiolabelling α-hydroxy carboxylic acids, since PET tracers for muscarinic receptor ligands, that consist of this α-hydroxy acids moieties, have not been labelled natively for *in vivo* evaluation. We believed that a method to prepare α-hydroxy ^{11}C-carboxylic acids would enable the preparation of multiple mAChR targeting PET ligands within two steps.

We sought to develop a method for carboxylation for readily available ketone substrates with [^{11}C]CO_2 to prepare α-hydroxy ^{11}C-carboxylic acids. Given the breadth of non-radioactive methods for carboxylation of carbonyls derivatives (ketones, aldehydes and imines), the process of adapting a non-radioactive method for radiochemistry presented a broad scope of conditions. To this end, we intended to use a Bayesian optimizer to determine optimal radiochemical conditions in the least number of experiments. To demonstrate the versatility of the method, we wanted to radiolabel various carbonyl substrates and evaluate the impact of stereoelectronic groups. We hope that by establishing mild photocatalysed conditions to prepare α-hydroxy ^{11}C-acids, we provide straightforward access to a novel functionality in every radiochemist's toolbox.

Chapter 2

Results and Discussion

2.1 Preliminary experiments for ^{11}C-carboxylation of benzophenone

We commenced our investigation with a non-radioactive reaction for carboxylation of benzophenone to prepare 2,2-diphenyl-2-hydroxyacetic acid (benzilic acid). Based on radioactive photocatalytic conditions developed by our group and reported non-radioactive conditions, we determined preliminary conditions. The photocatalyst was picked for its high $E°_{RP}[Ir^{III}/Ir^{II}]$ = -1.61 eV and concurrently, the amine (**^{i}Pr$_2$NEt**) was picked for its low oxidation potential and widespread use as an electron donor, the base (**Cs_2CO_3**) was picked for its mild strength to buffer acidity from the oxidised amine and the solvent was directly adopted from a previous method for its tolerance of blue light.[20,31] Our preliminary experiment was set up using non-radioactive CO_2 and synthesised benzilic acid with a 62% yield (Figure 15.a).

Based on this result, we adopted this reaction with radioactive CO_2 by reducing the reaction scale from 0.2 mmol (in 2 mL solvent) down to 0.05 mmol (in 0.5 mL solvent) substrate, proportionally reducing other components. This scale was the minimum volume required for efficient delivery of radioactive CO_2. Although the scale was reduced to the minimum usable scale, the substrate remained in excess as [^{11}C]CO_2 is produced in nanomole quantities (Section 1.1.2). Nevertheless, this reaction yielded [^{11}C]benzilic acid with a 39% RCY (Figure 15.b) and we deemed the yield to be satisfactory.

However, qualitative observations of the radioHPLC UV chromatogram suggested a higher than anticipated presence of benzilic acid. We suspected that cesium carbonate introduced non-radioactive CO_2 into the reaction through equilibration with CO_3^{2-}. To this end, we replaced gaseous CO_2 in our non-radioactive conditions with an inert argon atmosphere. The conditions still yielded benzilic acid with a lower but comparable yield of 39% (Figure 15.c). Introduction of non-radioactive CO_2 from carbonate necessitated exploring conditions free of carbonate bases or bases that hold "masked" forms of CO_2. Non-radioactive CO_2 in the reaction can reduce the molar activity (A_m) of the radioactive product.

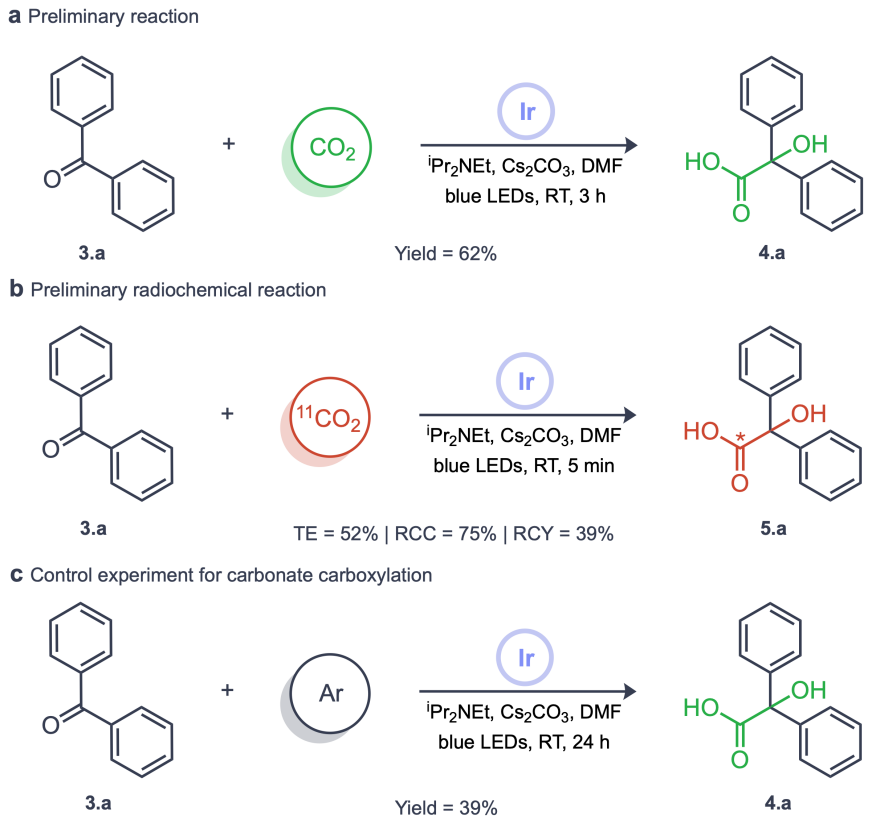

Figure 15 Preliminary experiments for ^{11}C-carboxylation of benzophenone

To employ conditions free of carbonate bases, we had a choice between two non-radioactive methods - Okumura's DMBI-mediated carboxylation and Cao's silyl-directed carboxylation. We adopted the silyl-directed method for its well understood mechanism supported by multiple experiments. As alluded to earlier, a concrete mechanism enables troubleshooting and improving a non-radioactive method for radiochemistry. We made two key changes to the method for radiochemistry –

- Reduced reaction scale to 1/4th the original scale from 0.2 mmol (in 2 mL solvent) down to 0.05 mmol (in 0.5 mL solvent)
- Increased photocatalyst concentration 4-fold from 0.5 mol% to 2 mol%

The reaction was productive, yielding [^{11}C]benzilic acid with a 17% RCY. The reactivity under this condition went down drastically, with radiochemical conversion nearly being 1/3rd of the carbonate conditions. The primary reduction of yield in the new conditions comes from the new base in KOPiv. Non-radioactive CO_2 from carbonate contributes to the overall concentration of CO_2 in the reaction which could

drive faster kinetics for a rate-law directly proportional to CO_2. Nevertheless, we ran control experiments to verify the reaction was photocatalytic in nature (Figure 16). First, we removed the iridium photocatalyst **Ir** which yielded no conversion. Next, we removed the sacrificial electron donor **iPr_2NEt**, which is responsible for the reducing nature of **Ir** upon irradiation, and as earlier, this yielded no conversion. The control experiments established the conditions were photocatalytic in nature (Figure 17.a).

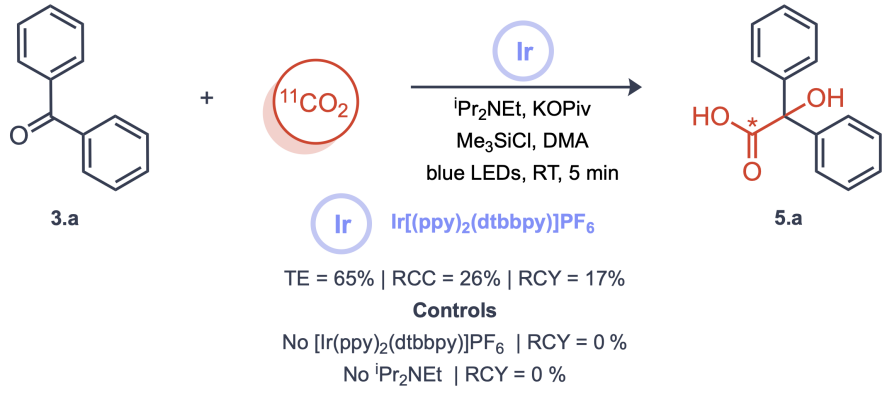

Figure 16 Carbonate-free preliminary conditions

2.2 Optimisation campaign

2.2.1 Bayesian Optimisation

The goal of the optimisation campaign was to identify the highest yielding chemical conditions. Given consistent physical conditions, we believed that radiochemical conversion (RCC) would have greater variation from the chemical nature of the reagents compared to trapping efficiency (TE). We identified the role of each component in the reaction based on the reported non-radioactive mechanism (Figure 17.a). The four components in the carbonate-free conditions are –

- Photocatalyst (PC): (ex. **$[Ir(ppy)_2(dtbbpy)]PF_6$**) undergoes excitation through irradiation, responsible for reduction of the substrate
- Sacrificial Electron Donor (SED): (ex. **$^iPr_2NEt$**) generally a nitrogenous base, undergoes oxidation from the PC to enable the reduction of the substrate

- Base: (ex. **KOPiv**) generally a weak and non-nitrogenous base, maintains basic pH and provides counter-ions during substrate reduction
- Additive (A): (ex. **Me_3SiCl**) Lewis acid-like behaviour, to improve the stability of the ketyl carbanion **int. B** (Figure 17.a). Furthermore, acts as a bulky group to improve selectivity towards carboxylation compared to the pinacol product.

Through a literature review for reported photocarboxylation methods, we compiled a variety of reagents to screen, categorized based on the four components mentioned above (Figure 17.b). The photocatalysts were picked based on reduction potentials and lifetime of excited states. For instance, the iridium complex **Ir** and **4-DPAIPN** have similar reduction potentials ($E°_{RP}[PC/PC^-]$ = -1.5 to -1.6 eV). However, the metal complex **Ir** has a much longer lifetime. A similar argument applies for the ruthenium complex **Ru** and **4-CzIPN** ($E°_{RP}[PC/PC^-]$ = -1.3 to -1.4 eV). The sacrificial electron donors were picked based on their oxidation potentials, ranging from ($E°_{RP}[SED^+/SED]$ = -0.8 to -1.1 eV) with **iPr_2NEt** being the weakest and **DABCO** being the strongest to oxidize.

Bases were picked to compare against the starting conditions with **KOPiv** – a stronger base in **KO^tBu** to improve quenching of the oxidized amine **SED^+** and a softer counter ion in **CsOPiv** to improve stability of **Int. B** upon formation. Strong differences in yields from the base used could highlight the role of the base in the reaction. However, the reported non-radioactive mechanism does not suggest a significant role of the base. Finally, the additive was not varied significantly as the non-radioactive method by Cao *et al.* explored various silane and non-metallic halides as additives. Although a bulkier **Ph_3SiCl** was screened alongside **Me_3SiCl** to explore whether added bulk can improve reactivity.

Using Bayesian optimisation, we sought to screen through the fewest possible combinations of the four categories, while quantifying the interactions of all the components in the reaction to converge towards the highest yielding conditions.

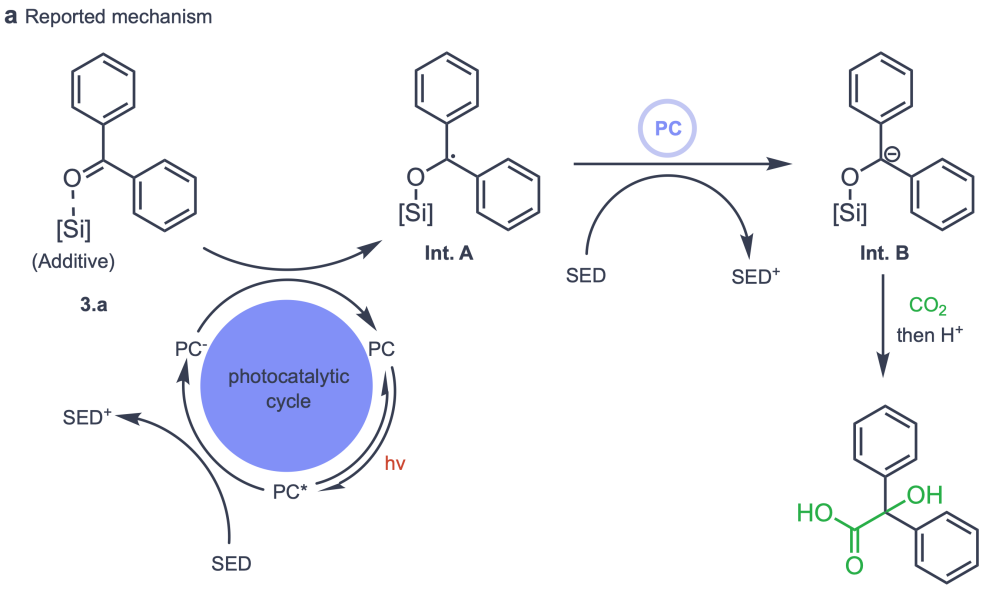

b Table of reagents to screen

Photocatalysts	Sacrificial e- Donors	Bases	Additives
$[Ir(dtbpy)(ppy)_2](PF_6)$	iPr_2NEt	KOtBu	Ph_3SiCl
$[Ru(bpy)_3](PF_6)_2$	Cy_2NMe	KOPiv	Me_3SiCl
4-DPAIPN	DABCO	CsOPiv	—
4-CzIPN	—	—	—

Figure 17 Mechanism driven screening using Bayesian optimisation

We decided to run the screening campaign in sets of four experiments using EDBO+. Our workflow used the command-line interface (CLI) in tandem with Microsoft Excel to input and access data from the optimizer. We set up the optimizer with each of the reagents as a variable in the requisite category. For example, 'Additive' was set up as a category of two variables – **Me_3SiCl** and **Ph_3SiCl**. Then we added the independent result parameters to maximize – radiochemical conversion (RCC) and trapping efficiency (TE). After the set up, the optimizer generated a spreadsheet with four suggested experiments.

For round 1, this is chosen through an initial random exploration by the optimizer. Subsequent rounds used previously input experimental data to determine new predictions. The conditions suggested for each round by the optimizer and their experimental results are presented in **Table 1.** Furthermore, the optimizer reported predictions after we input experimental data from round 1. The average variance of the

predictions (for the next round, at the end of each round) has been reported under the tables to represent the optimizer's confidence in predictions.

Table 1 Experiments during the Bayesian optimisation campaign

3.a 5.a

a Round 1

Entry	Photocatalyst	Sacrificial e⁻ Donor	Base	Additive	TE	RCC
1	$[Ru(bpy)_3](PF_6)_2$	Cy_2NMe	CsOPiv	Me_3SiCl	45%	1%
2	$[Ir(dtbbpy)(ppy)_2]PF_6$	iPr_2NEt	KOtBu	Me_3SiCl	65%	26%
3	4DPAIPN	iPr_2NEt	KOPiv	Me_3SiCl	77%	23%
4	4CzIPN	iPr_2NEt	KOtBu	Ph_3SiCl	72%	0%

Next round prediction's variance TE = 13% | RCC = 14%

b Round 2

Entry	Photocatalyst	Sacrificial e⁻ Donor	Base	Additive	TE	RCC
5	$[Ru(bpy)_3](PF_6)_2$	iPr_2NEt	KOPiv	Ph_3SiCl	60%	0%
6	4DPAIPN	iPr_2NEt	CsOPiv	Ph_3SiCl	68%	15%
7	4DPAIPN	DABCO	KOtBu	Me_3SiCl	37%	0%
8	$[Ir(dtbbpy)(ppy)_2]PF_6$	Cy_2NMe	KOPiv	Ph_3SiCl	31%	73%

Next round prediction's variance TE = 4% | RCC = 8%

c Round 3

Entry	Photocatalyst	Sacrificial e⁻ Donor	Base	Additive	TE	RCC
9	$[Ir(dtbbpy)(ppy)_2]PF_6$	DABCO	KOtBu	Me_3SiCl	70%	0%
10	4DPAIPN	Cy_2NMe	KOPiv	Ph_3SiCl	23%	47%
11	4DPAIPN	iPr_2NEt	KOtBu	Me_3SiCl	21%	1%
12	$[Ir(dtbbpy)(ppy)_2]PF_6$	iPr_2NEt	CsOPiv	Ph_3SiCl	25%	63%

Next round prediction's variance TE = 8% | RCC = 3%

The optimizer included every variable from each category during round 1, barring **DABCO** as an SED. Potentially, this initialized every variable for the optimizer but the predictions for this round were not strong given the average variance of the predictions given by the optimizer were >10% (Table 1.a). An important result here were the conditions with **4-CzIPN** (Table 1.4) which yielded no product. As highlighted in earlier works[25,26], **4-CzIPN** might undergo an initiation phase through the alkylation of the photocatalyst which improves the catalyst's reduction potential. The reduced photocatalyst is either a poor reductant for the substrate or the excited photocatalyst is poor at oxidising **iPr_2NEt** to reduce itself, hence displaying no conversion. Since the rest of the components are present in other conditions, **4-CzIPN** is ruled out by the optimizer for subsequent rounds of optimisation.

The second round yielded polarized results. Notably the conditions in Table 1.8 performed significantly better than the initial conditions (Figure 16) with an RCC of 73%. Two conditions produced no product (Table 1.5/1.7). The conditions involving the ruthenium complex (Table 1.5) are unsurprising as very poor conversion was observed in the previous round. The reduction potential of the complex is within the range of **4-CzIPN** and does not display any conversion for the same reasons. Another interesting observation in round 2 was obtaining 0% RCC with **DABCO** (Table 1.7). Given the non-zero trapping efficiency recorded, and further observing similar results with the base in the next round (Table 1.9), we theorized the formation of a strong **CO_2-DABCO** adduct (Figure 18.a) which prevented carboxylation. **DABCO** is a sterically unhindered and strained nitrogenous base, it exhibits properties like nitrogenous superbases used trap [^{11}C]CO_2[50] (Figure 18.b). Superbases such as **DBU** and **BEMP** trap CO_2 to form intermediate carbamates that can be decoupled for further reactivity.

The metal photocatalyst **$[Ir(ppy)_2(dtbbpy)]PF_6$]** and phthalonitrile based organic photocatalyst **4-DPAIPN** were preferred for the next round as the only yield producing catalysts. (Table 1.c) Intuitively, we expected such preference given both photocatalysts have a higher $E°_{RP}$ (PC^*/PC^-) compared to the ruthenium complex and **4-CzIPN**. The predictions this round improved with variances of the predictions decreasing to <10% (Table 1.b). Since the predictions aligned with our intuition for conditions of future

experiments, we decided to screen another round of conditions with the optimizer. We expected the optimizer to narrow conditions down to the best performing photocatalyst between **[Ir(ppy)$_2$(dtbbpy)]PF$_6$]** and **4-DPAIPN** coupled with the optimal SED and base for the photocatalyst.

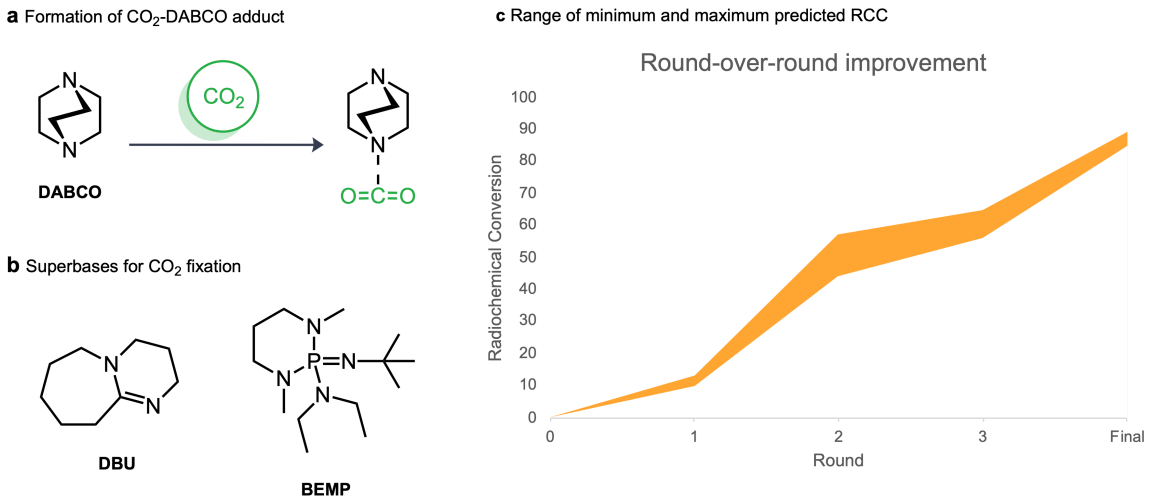

Figure 18 Observations from the Bayesian optimisation campaign

After running experiments for the third round, while conditions involving **4-DPAIPN** showed promise, the optimizer had converged its top predicted RCCs for conditions employing the iridium complex (**[Ir(ppy)$_2$(dtbbpy)]PF$_6$]**) as a photocatalyst (Table 2.a). We anticipated identical conditions with 4-DPAIPN and the iridium complex to yield fairly equally, given their similar reduction potentials. However, the lower lifetime of the organic photocatalyst could lead to poorer performance. The conditions with the highest predicted RCC (Table 2.1) after 12 experiments had not been run in previous rounds. The top 5 predictions after round 3 were different combinations of the iridium complex with one of the pivalate bases **(CsOPiv/KOPiv)** along with **Cy$_2$NMe** or **^{i}Pr$_2$NEt** as the sacrificial electron donor. The predictions highlighted key intuitive observations –

- Reduction potential and lifetime of the excited state of the photocatalyst are essential to reactivity
- Weak bases are sufficient to quench the oxidized amine formed and increased strength of the base does not improve reactivity
- The additive plays an electronic effect, not a steric effect

- Amines with a low oxidation potential perform the best coupled with a photocatalyst with the highest reduction potential

Note: The effect of the counter-ion on **Int. B** could not be explained as **CsOPiv** showed very poor solubility in the reaction mixture compared to **KOPiv**, significantly impacting light penetration into the reaction vial and hampering reactivity.

To our surprise, the top predicted condition (Table 2.1) ended up being the condition with the highest RCC in the campaign. Notably, the only difference in the final condition compared to the initial was switching out the amine from **$^{i}Pr_2NEt$** to **Cy_2NMe** highlighting the importance of the photocatalyst-SED combination. While **$^{i}Pr_2NEt$** has the lower oxidation potential, factors such as constrained sterics might make the **iridium-Cy_2NMe** couple more favoured. The experimental result outperformed the prediction, and we believed this to be the highest performing condition given the low average predicted variance of other predictions (Table 2.a). Furthermore, the predicted RCCs improved round-over-round and the range of yields from predictions for suggested experiments continued to narrow (Figure 18.c). This suggested the optimizer had narrowed to the most optimal conditions and no further screening was required.

Table 2 Final conditions after Bayesian optimisation campaign

a Top 3 predictions after 12 experiments

Entry	Photocatalyst	Sacrificial e⁻ Donor	Base	Additive	RCC	Predicted RCC
1	$[Ir(dtbbpy)(ppy)_2]PF_6$	Cy_2NMe	KOPiv	Me_3SiCl	89%	79±3%
2	$[Ir(dtbbpy)(ppy)_2]PF_6$	iPr_2NEt	CsOPiv	Ph_3SiCl	61%*	58±2%
3	$[Ir(dtbbpy)(ppy)_2]PF_6$	Cy_2NMe	KOPiv	Ph_3SiCl	72%*	71±2%

Next round prediction's variance TE = 6% | RCC = 2%
*From earlier rounds

b Final conditions after optimization

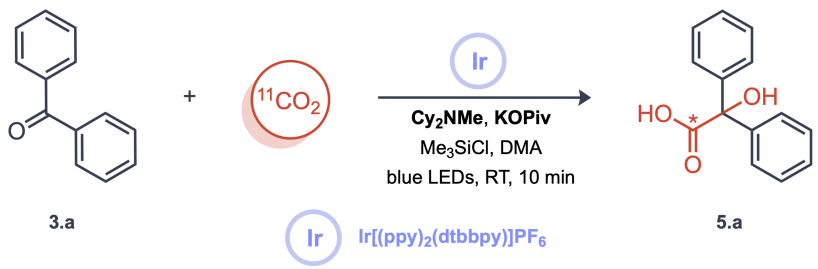

An important facet of this campaign has not been discussed intentionally – trapping efficiency. After the first round, we believed TE was driven by the base and SED. Like Figure 18.a, we believed the amines present in the reaction mixture formed CO_2-adducts or interacted non-covalently at the least. However, we couldn't find any evidence to support this theory. We continued with the Bayesian optimisation solely focusing on RCC. We believed that conversion only depended on the chemical nature of the conditions, given the physical conditions remained the same. Supported by round-over-round average variance of predictions, the predictions for RCC became stronger while the predictions for TE remained uncertain. We believed that TE was not only driven by the chemical nature of the conditions. To improve TE, stoichiometric changes were required. To this end, we decided to screen various concentrations for identical chemical conditions (Table 3).

Table 3 Impact of concentration of reagents to optimized conditions

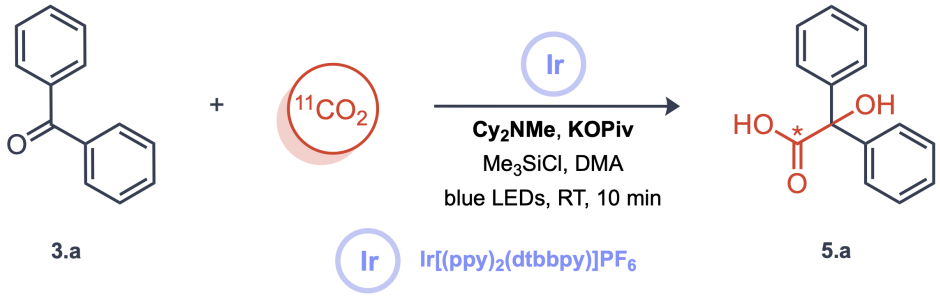

Entry	Benzophenone (M)	Cy_2NMe (M)	KOPiv (M)	TE	RCC
1	0.1	0.2	0.2	40	71
2	0.2	0.2	0.1	39	79
3	0.1	0.2	0.1	36	72
4	0.1	0.4	0.01	25	53
5	0.2	0.02	0.2	49	6

First, we established a baseline using standard concentrations (Table 3.1). Varying concentration ratios of the components at the same order of magnitude has negligible impact on TE and RCC (Table 3.2/3.3). While there might be a notable impact on the rate constant, short reaction times lead to negligible change in conversion. Further, these concentrations were at the limit of dissolution, a higher concentration of base (>0.2 M) would remain suspended in the solvent, hindering the irradiated light to penetrate.

When the concentration of the components is decreased by an order of magnitude with respect to the substrate, we observe significant impact on TE and RCC (Table 3.4/3.5). The data strongly suggests a direct proportionality to concentration of the components in the rate constant, leading to a significant decrease in conversion. A decrease in concentration of the base slightly reduced both TE and RCC suggesting a dual role. The basic conditions improve CO_2 solubility in the reaction improving TE and quenching oxidized SED improves turnover of the photocatalytic cycle improving RCC. Decrease in concentration of the SED majorly attenuated reactivity (RCC) highlighting its role in the photocatalytic cycle being turnover. Hence, we continued with the standard stoichiometry for the substrate scope. We theorized that other than the base in the reaction improving TE, the physical set up has a role to play with TE performance.

2.2.1.1 An outlook on Bayesian optimisation for reaction optimisation

Through this campaign we found EDBO+ to be an unbiased guide for optimisation experiments. Reports[35,51] have found Bayesian optimisation to outperform human decision-making by requiring fewer number of experiments and displaying lower variance in outcomes from the initial set of experimental data. We found Bayesian optimisation to display its true potential when multiple dependent variables are screened. For instance, we know based on the reported mechanism (Figure 17) that the photocatalyst and SED are dependent variables. Intuitively, it is difficult to envision the performance of each combination. Bayesian optimisation accounts for such dependencies *de novo*, taking the human out of the loop. We believe Bayesian optimisation in everyday laboratory practices could facilitate more efficient optimisation campaigns by enabling data-driven decisions for future experiments.

2.2.2 Physical set up changes to improve trapping efficiency

Over the course of the optimisation campaign and the substrate scope we identified multiple parts of our reaction set up hindering reaction performance. Common to all iterations of our set ups is a tapered microwave vial attached with an attached stainless-steel needle for [^{11}C]CO_2 delivery and an exhaust needle. Our initial radiochemistry set up used a sodium hydroxide (Ascarite) cartridge directly attached to the

exhaust needle. This was sufficient to ensure isotopic CO_2 did not escape into the atmosphere after delivery and cause unnecessary radiation exposure. However, we found it difficult to identify at what timepoint does the delivery of activity end, to determine the time point to slow down bubbling of the He push gas through the reaction mixture as excess bubbling releases trapped isotopic CO_2. It was not possible to obtain a measure of escaped $[^{11}C]CO_2$ during delivery after reaction completion to determine the endpoint, as addition of 1 M HCl released unreacted $[^{11}C]CO_2$ adding to total escaped $[^{11}C]CO_2$.

Note: Since TE and RCC are dependent on each other, unreacted $[^{11}C]CO_2$ escaping out of the reaction mixture is accounted for by a lower TE but higher RCC. Conversely, if none of the unreacted $[^{11}C]CO_2$ escaped, it would be accounted for by a higher TE but lower RCC.

Since both processes were continuous, we thought the measurement of activity escaping from the reaction vessel in real-time would enable monitoring both parameters. Hence, we extended the tubing between the exhaust and Ascarite cartridge that led into a Capintec dose calibrator, enabling real-time activity monitoring (Figure 19.a).

Next, we found gas flow to reduce over subsequent experiments until the Ascarite cartridge was replaced. The cartridge was manually packed with Ascarite and held together with cotton. The cartridge was reused for multiple experiments and stored under sealed conditions. However, the cartridge was exposed to the atmosphere during the reaction which introduced moisture into the cartridge. Ascarite is a granular material, which clumps under moisture. Formation of such clumps blocked gas flow within the cartridge and downstream, in the entire reaction vessel. The issue required a straightforward solution, loose packing of the cartridge, which significantly reduced Ascarite clumping. Concurrently, we switched out cotton for glass wool to reduce any moisture in the packed Ascarite's vicinity. Together, the solution improved gas flow without any impact to trapping activity.

Importantly, the blockage highlighted the importance of air flow, or the lack thereof. We found that activity was largely delivered as a bolus from the $[^{11}C]CO_2$ trap. Hence, bubbling push gas beyond the

delivery of most activity only reduced trapped activity. We found 45 seconds of bubbling at 20 mL/min to be sufficient to deliver activity from the trap, improving our TE significantly (Figure 19.b.2).

Our final inconsistency was identified while performing a scope on various ketone substrates. After experimenting with our initial scope of substrates, we sought to duplicate results for successful substrates. After performing duplicate experiments, we found >5% deviations in RCYs. Initially a pattern could not be identified, although upon inspecting sets of experiments (often multiple radiochemistry experiments were performed sequentially), we found experiments performed later in the set consistently yielded poorly. We theorized the source of reduction of performance was from the degradation of the synthesized product. An acid quench using 1 M HCl led to decarboxylation of synthesized α-hydroxy acids. The delay in radioHPLC injections of the later experiments led to greater degradation before injection, leading to the inconsistency. While radioHPLC analysis could be undertaken without quenching the reaction, an acid quench provides sharper chromatograms, improving accuracy of peak integrations.

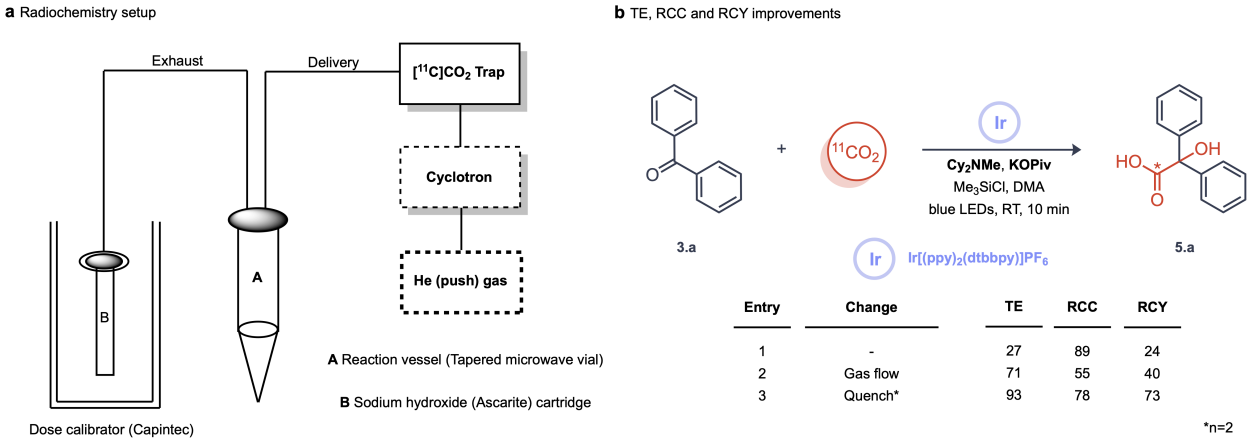

Figure 19 Diagram of radiochemistry set up and impact of physical set up changes made

Since [^{11}C]benzilic acid **5.a** was required in the highest yields for further experiments, we developed a gradient to isolate the compound **5.a** without an acid quench (Figure 19.b.3). The rest of the scope used an acid quench performed right before radioHPLC injections, since optimisation of chromatographic conditions for each substrate was impractical. Delaying the quench to the last moment ensured minimal

impact to TE and RCC from degradation. More importantly, the set up led to consistent TE between all radiochemical experiments.

2.3 Synthesis of non-radioactive standards

After completion of the optimisation campaign, the next step was to scope a variety of substrates. Unlike non-radioactive chemistry, the carbon-11 compounds prepared cannot be characterized using traditional methods such as NMR and MS (due to radioactive decay and trace concentrations of the isotope). Hence, characterization relies on co-injection of the non-radioactive compound (standard) with the radioactive compound into a radioHPLC set up. Since both compounds have identical physical and chemical properties, they co-elute during an HPLC injection. The carbon-11 compound is detected through a **γ**-detector while the non-radioactive compound is visible on the UV chromatogram.

To this end, we employed the method reported by Cao *et al.*[31] to prepare the non-radioactive standards. We picked 4-acetylbiphenyl **3.b** to replicate the reported conditions, primarily to make NMR analysis more straightforward. The reaction was performed as reported, unfortunately the reaction yielded the dimer (pinacol-like product) **4.b(i)** as the major product (Figure 20.1). Since this result was in-line with the absence of a silane (TMSCl), we attempted the reaction with fresh bottle of TMSCl. The reaction continued to yield **4.b(i)** as the major product, however we isolated our desired product **4.b** at a low 8% yield (Figure 20.2). We had observed the formation of benzilic acid **4.a** with Cs_2CO_3 in the absence of CO_2 during our control experiments (Figure 15). Hence, we decided to switch bases (Figure 20.3) to push the carboxylation through introducing CO_2 in solution from the carbonate base. However, these conditions yielded **4.b** poorly with a yield of 6%.

The goal of non-radioactive synthesis for radiochemistry is solely for the purpose of characterization of the radioactive compound. Yields are not relevant if sufficient material is obtained for such. However, we were unable to replicate the reported selectivity for **4.b** after multiple attempts. The only variation we had compared to the reported method was the absence of a glovebox to prepare the reaction flask. We used Schlenk techniques instead to procure a CO_2 atmosphere in the flask.

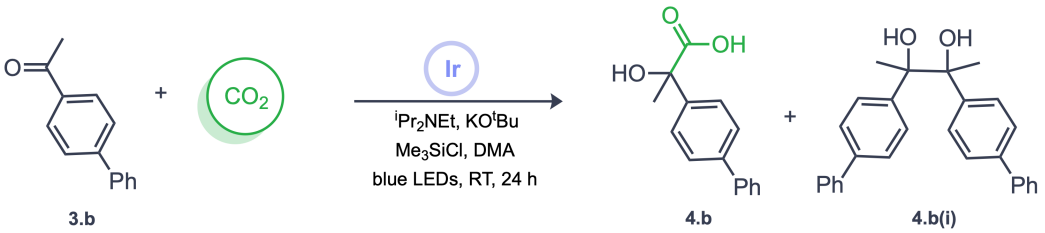

Entry	Change	4.b	4.b(i)
1	-	n.d.	45%
2	TMSCl	8%	-*
3	-KO^{t}Bu, +Cs_2CO_3	6%	-*

*not isolated

Ir $Ir[(ppy)_2(dtbbpy)]PF_6$

Figure 20 Initial experiments to synthesize non-radioactive standards

2.3.1 Serendipitous discovery of photocarboxylation conditions

We decided to search for conditions that were less sensitive to air. Our suspicions for the conditions (Figure 20) performing poorly to yield **4.b** was the lack of a sufficiently inert atmosphere. We found photocarboxylation or electrocarboxylation to be the only routes to prepare α-hydroxy carboxylic acids within a single step from ketone substrates. The established thermal route was multistep, requiring the cyanation of the ketone substrate to prepare a cyanohydrin, then hydrolysis to obtain the α-hydroxy acid.

Given the mechanistic similarities of photocarboxylation of alkenes, imines and ketones highlighted in Chapter 1, we looked at photocarboxylation methods reported for all functionalities, specifically for conditions that can be performed without a strict CO_2 atmosphere created in glovebox. We found the method reported by Xu *et al.*[52] for dicarboxylation of alkenes using formate, carbonate and CO_2 (Figure 21.a). Interestingly, the reaction in the absence of CO_2 gas yielded the monocarboxylation product with very good yields.

Based on this observation, we set up an experiment using 4-Acetylbiphenyl (**3.b**) as our substrate with the reported conditions, albeit switching out CO_2 for Ar. The reaction was performed at room temperature due to set up limitations. However, no conversion (favourable or unfavourable) was observed in the reaction. Then, we performed the reaction as reported with 4-Acetylbiphenyl and we were pleased to find the reaction yielded **4.a** as the major product with a 51% yield (Figure 21.b). A formate mediated

photocarboxylation has not been reported for carbonyl substrates.[53] Determination of whether formate is a carboxylate source, a reductant or both in the reaction would require mechanistic studies. Observing no conversion in the absence of CO_2 strongly suggests the gas being the primary carboxylate source and the reaction likely follows a SSET-type mechanism. Further efforts would involve replacing reaction components with isotopic reagents to identify roles and could be an avenue for future investigations.

This method provided sufficient material for co-injection in radioHPLC and characterization. Hence, no further optimisation was undertaken. We decided to use these conditions to synthesize non-radioactive standards for substrates with non-zero RCC during radiochemistry experiments. We synthesised a library of 13 compounds with yields up to 94%.

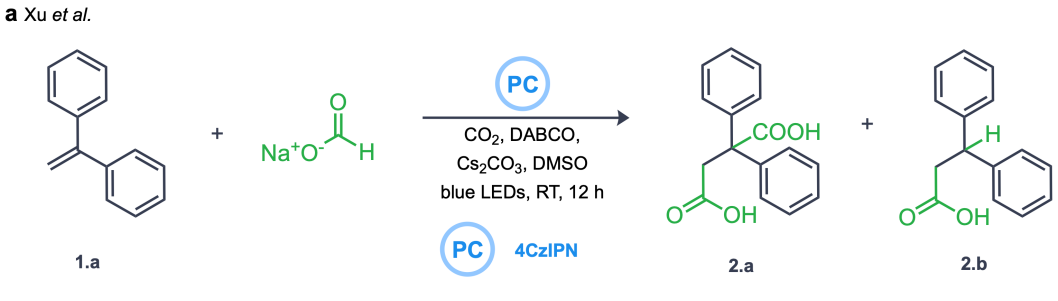

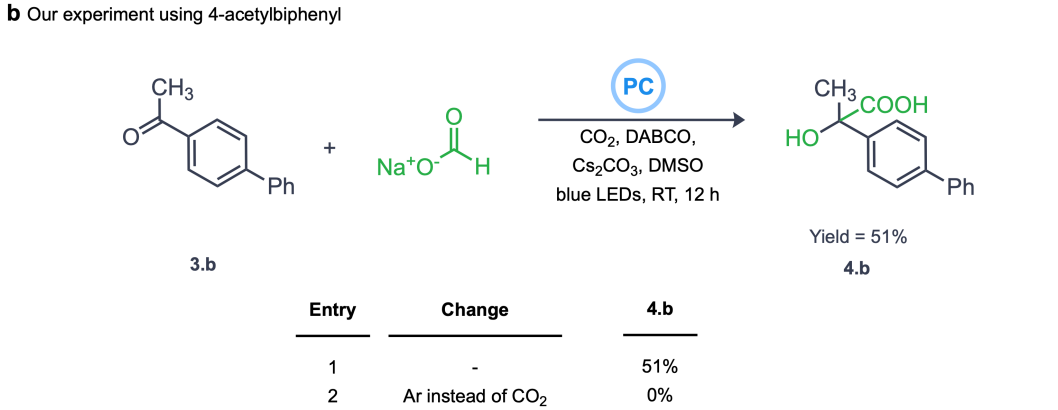

Figure 21 Formate mediated synthesis of non-radioactive standards

Table 4 Scope of non-radioactive standards synthesized using formate mediated photocarboxylation
*Isolation using Workup 2 (without Chromatography) #Isolated, degraded during characterization

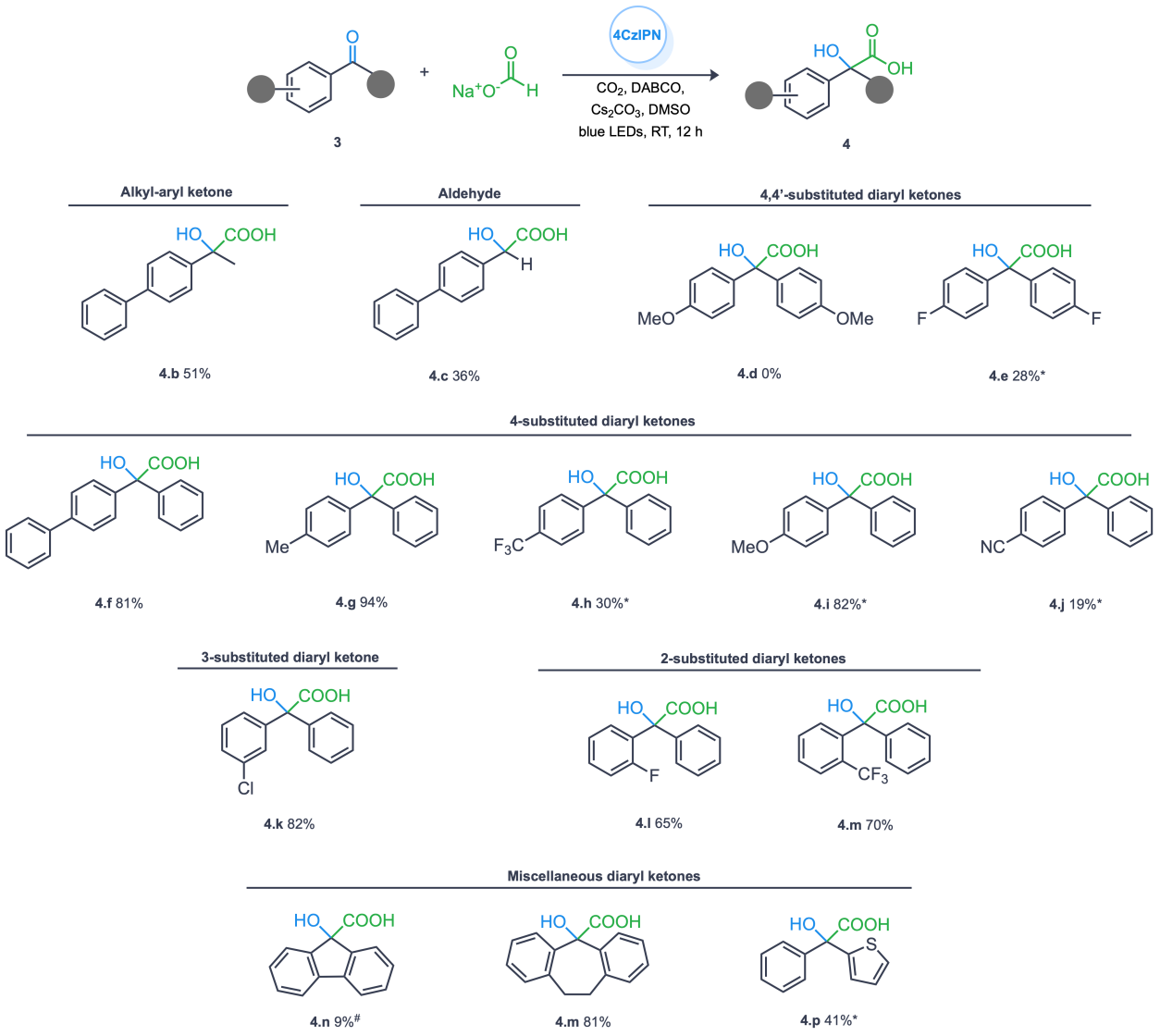

A chromatography-free workup was adopted from the report by Okumura *et al.*[32] (Workup 2) for certain substrates, potentially at the cost of lower yields as sufficient material was obtained regardless. The method was employed to carboxylate an aldehyde to synthesize **4.c**, with a yield of 36%. Although much of the starting material went through unfavourable conversions. Based on our radiochemistry experiments we moved on to primarily diaryl ketone substrates. The dimethoxy substituted **4.d** showed no conversion, while other substrates with electron donating group (EDG) substitutions (**4.g, 4.f** and **4.m**) had the highest yields and were the most stable to decarboxylation. We found some electron withdrawing group (EWG)

substitutions (**4.k** and **4.f**) to show high yields, however often these compounds readily decarboxylated in solution, especially under acidic conditions. Compounds **4.m** and **4.n** significantly degraded in NMR solvents, and sampling a compound in DMSO led to signals that corresponded to the starting material. Nonetheless, our threshold for yields were >20%, as this provided sufficient material for characterization and co-injection in radioHPLC. All yields obtained were over our determined threshold.

2.4 Substrate scope of α-hydroxy-^{11}C-carboxylic acids

We were interested in the isotopic labelling of ketone substrates activated by at least one phenyl group. Radiochemistry conditions and reaction set up (Figure 19) were employed for all substrates successfully labelled with carbon-11. Since TE was primarily driven through physical changes to our reaction set up (2.2.2), it remained consistent at 92±7% (n=24) for all substrates.

Our initial interest was to establish the breadth of ketone substrates (Table 5). First, we looked at the impact of strong stereoelectronic groups on RCC. We picked 4,4'-disubstituted ketones to prepare **5.d** and **5.e** to represent a strong EDG and a strong EWG respectively. We found no formation of **5.d** suggesting that EDGs are not favourable due to destabilization of the carbanion on **int. B** (Figure 17)**,** which prevents carboxylation. On the other hand, a lower yield from the difluoro substituted **5.e** suggests a greater stabilization of **int. B** leading to either slower kinetics, or a greater rate of decarboxylation of the product **5.e** leading to a lower observed yield. Either way, **5.e** yielding lower than benzilic acid (**5.a**).

Next, we moved to carboxylation of 4-substituted ketones to test functional group tolerance of the method. **5.f** and **5.g** are simple aryl and alkyl substituted benzilic acid forms presenting similar yields, albeit performing slightly worse than benzilic acid (**5.a**). The decline in the yield for **5.f** stems from a negative mesomeric effect, which stabilizes the carbanion **int. B**, preventing carboxylation. During the formation of **5.g**, the carbanion intermediate **int. B** is minorly destabilized, which reduced carboxylation. The impact of a stronger electron-withdrawing trifluoromethyl substitution (**5.h)** followed a similar trend to **5.a** from its negative inductive effect. Surprisingly, a nitrile substitution led to poor conversion to form **5.j** due to the strong mesomeric nature of nitrile that stabilizes **int. B** to a greater degree than **5.e.**

Through the methoxy substituted **5.i** we found the limit of tolerating an electron donating substitution. While the dimethoxy substituted **5.d** shows no conversion, monomethoxy is tolerated with a significantly lower yield compared to **5.a**. Lastly, we looked at the impact of EWGs at the *ortho*-aryl and *meta*-aryl positions. *Meta*-chloro substituted **5.k** provided an unexpectedly high yield, due to a lowered inductive effect from a *meta*-substitution, which minorly destabilized **int. B** similar to **5.g**. Substrates **5.l** and **5.m** furnished similar yields to **5.h**, highlighting the mechanism being driven primarily by electronic effects and not being impacted by any steric effects.

Afterwards, we looked at conformationally restricted **5.n** and **5.o**. No conversion was observed for the fluorenone derived **5.n**, the corresponding **int. B** formed is aromatized by the formation of the carbanion, making the carboxylation highly unfavoured. Meanwhile, **5.o** performed similar to other electron-withdrawing substrates. However, the lower yield compared to **5.a** is due to the restricted conformation destabilizing **int. B**, and not from slower kinetics due to stabilization. Lastly, we prepared an α-hydroxy acid **5.p** with a heterocyclic ketone substrate benzothiophene which performed worse than **5.a** due the heterocycle replacing a formal benzene ring.

Table 5 RCYs for substrate scope of α-hydroxy-^{11}C-carboxylic acids

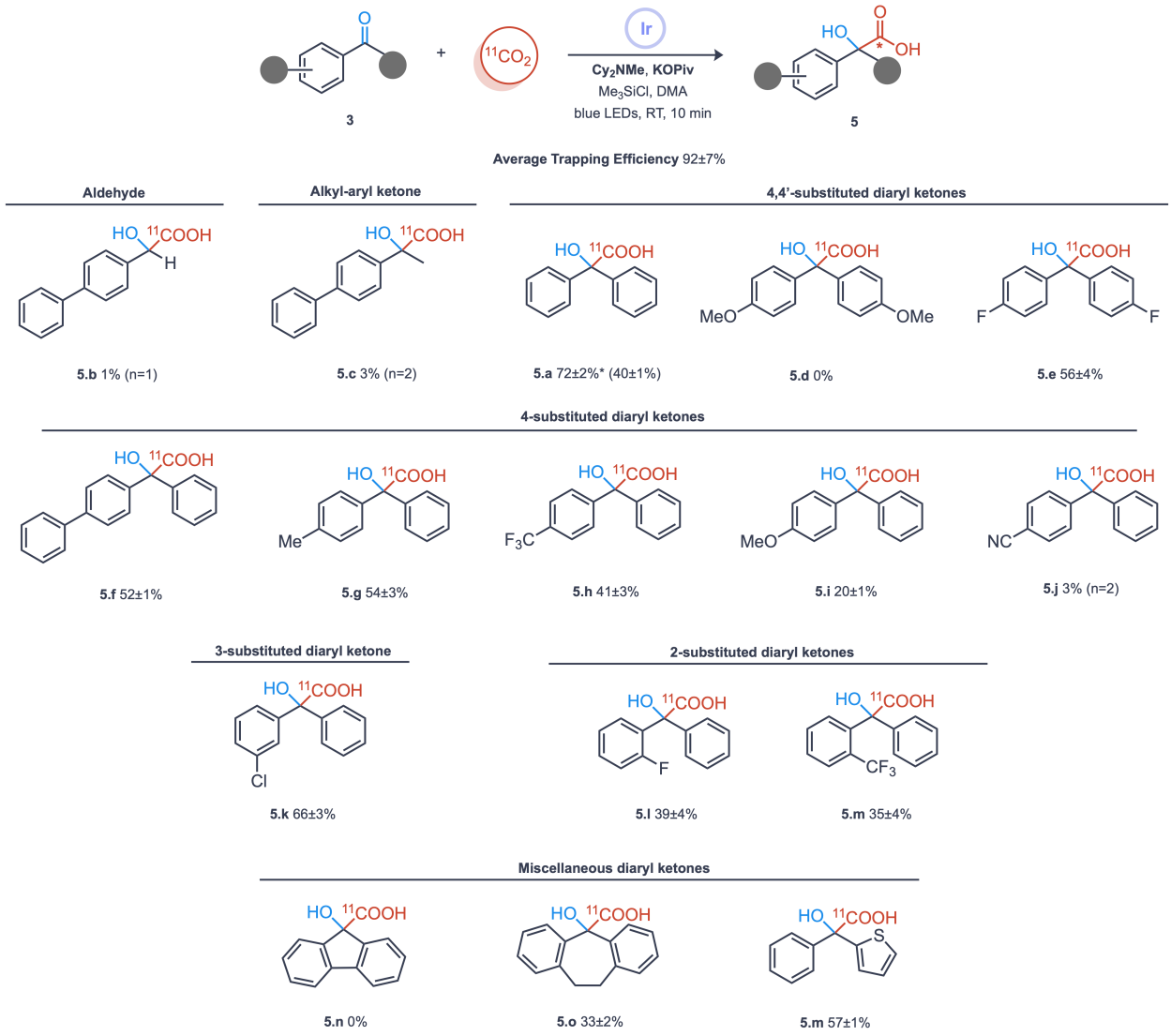

2.4.1 Attempts to improve reactivity with low yielding substrates

We attempted to carboxylate 4-acetylbiphenyl **3.b** and 4-biphenylcarboxaldehyde **3.c** which were an aldehyde and alkyl-aryl ketone activated by a biphenyl group. While both led to formation of their respective products, they had RCC values <5% which is not a usable range for further chemistry. We theorized the activation of the substrate to generate **int. B** (Figure 17) had slow kinetics leading to low RCCs. Due to the low yields obtained for **5.b** and **5.c** we looked at modifications for existing conditions to improve RCC.

Our first solution was to introduce sodium formate into the current conditions (Table 6.2), with the expectation a radical mechanism proceeding from **int. A**. Malandain *et al.* used a formate mediated mechanism to drive reactivity without SSET by generating a radical anion of CO_2 and proceeding through a radical addition. However, the conversion remained the same suggesting no change in the mechanism being followed. While the photocatalyst-SED couple can reduce the substrate, it is unable to reduce CO_2 to form the radical anion species.

To attempt the formation of the radical anion, we attempted an entirely formate mediated condition, switching our SED to DABCO and adding sodium formate to the conditions (Table 6.3). DABCO-formate mediated methods have been employed for non-radioactive carboxylation of olefins and imines. These methods rely on DABCO to reduce formate to the radical anion, followed by subsequent reduction or carboxylation by the radical anion. Since the optimisation campaign revealed that no conversion is observed with DABCO as the SED (Table 1.7/1.9), an alternative mechanism driven by formate carboxylation would have been required for these conditions to be successful. Unfortunately, no conversion was observed.

Finally, finding little success in employing a formate mediated mechanism, we decided to adopt the method reported by Okumura *et al.*[32], which uses 1,3-Dimethyl-2-phenyl-2,3-dihydro-1*H*-benzoimidazole (DMBI) as a reductant (Table 6.4). DMBI is a strong reductant and hydrogen atom transfer agent being commonly used in semiconductors.[54] Given the success with alkyl-aryl ketones and aldehydes in their non-radioactive work, a DMBI mediated route could improve reactivity with less activated substrates. As alluded to earlier, given the dual nature of DMBI, the reaction could proceed through a radical

polar crossover mechanism to furnish the product with lower activation energies. However, no conversion was observed here either.

Given these results, we believe the stabilization of **int. B** plays a crucial role in dictating the kinetics of synthesis of **5**. Attempts to access alternate mechanisms require significantly revised conditions. Hence, poor stabilization of the intermediate in alkyl-aryl ketones and aldehydes is characteristic of the substrates and will remain a limitation for this method.

Table 6 Attempts to carboxylate 4-acetylbiphenyl with [^{11}C]CO_2

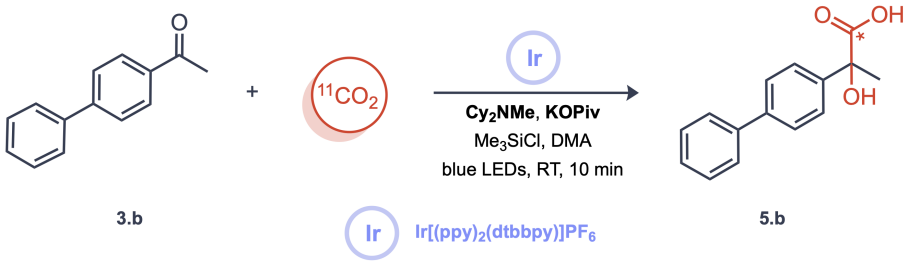

3.b 5.b

Ir Ir[(ppy)$_2$(dtbbpy)]PF$_6$

Entry	Change	RCY
1	-	3%
2	+HCOONa	3%
3	-Cy$_2$NMe, +HCOONa,+DABCO	0%

3.b 5.b

Ir Ir[(ppy)$_2$(dtbbpy)]PF$_6$

Entry	Change	RCY
4	-	0%

2.5 Synthesis of [^{11}C]Quinuclidinyl Benzilate (QNB)

Our successful synthesis of benzilic acid (**5.a**) enables the radiolabelling of a host mAChR targeting PET tracers in their native form. To demonstrate one such application, we decided to prepare [^{11}C]QNB. The preparation of [^{11}C]QNB has been reported previously[49], although the synthesis involves the use of metallic lithium to prepare a lithiated **int. B** which reacts with [^{11}C]CO_2 to yield [^{11}C]benzilic acid. The conditions are likely not easily reproducible under clinical settings, as the tracer has not been evaluated in humans to our knowledge.

We employed a straightforward nucleophilic substitution to prepare [^{11}C]QNB. We prepared the mesylate of quinuclidinol **6** to enable direct substitution of benzilic acid **4.a**. Preliminary evidence from LC-MS using nonradioactive benzilic acid **4.a** with the mesylate **6** in the presence of DIPEA as a weak base suggested formation of QNB (Figure 22.a). Given the preliminary data suggested that the substitution worked, we attempted to telescope the substitution directly after preparing radioactive benzilic acid **5.a**. Unfortunately, both at room temperature and heating the reaction up to 150°C yielded no conversion to **7**. However, precipitation in experiment (Figure 22.b.2) suggested that due to the stoichiometric presence of pivalate in the reaction, a competing adduct is forming with the mesylate **6** instead of QNB **7**. Future efforts will focus on isolating radioactive benzilic acid **5.a** to prevent the competing substitution reaction.

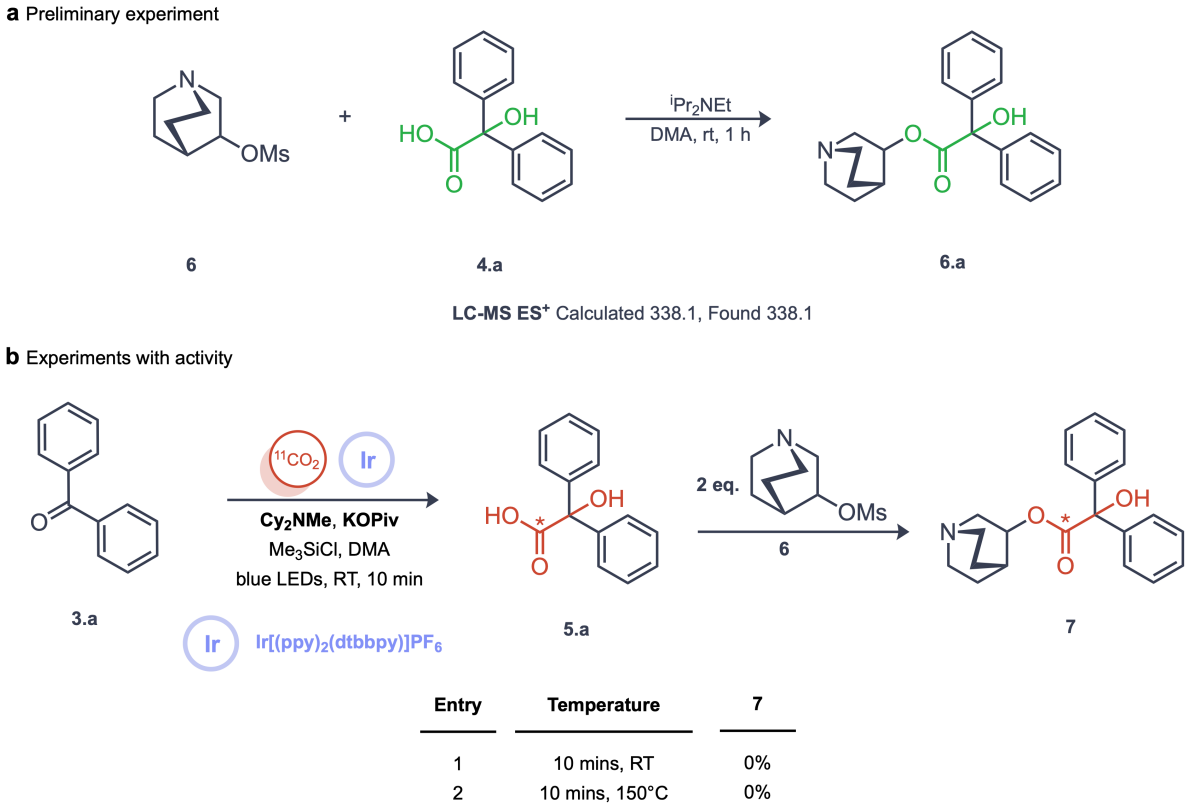

Entry	Temperature	7
1	10 mins, RT	0%
2	10 mins, 150°C	0%

Figure 22 Attempts at synthesis of [^{11}C]QNB

Chapter 3

Conclusions and Future Directions

3.1 Conclusion

Direct fixation of [^{11}C]CO_2 is a highly efficient route to prepare carbon-11 labelled PET tracers. Photocatalysis is an emerging methodology to incorporate [^{11}C]CO_2 for carbon-11 radiolabelling. To this end, we have developed a photocatalysed synthesis of α-hydroxy ^{11}C-carboxylic acids. This method leverages readily available ketones as precursors for radiolabelling with [^{11}C]CO_2, assisted by an iridium-based photocatalyst. We employed a Bayesian optimisation software (EDBO+) during an optimisation campaign. Bayesian optimizers are data-driven tools providing greater efficiency and consistency in reaction optimisation compared to human decision-making. Using EDBO+, we improved synthetic yields of [^{11}C]2-hydroxy-2,2-diphenylacetic acid from an RCC of 17% to 72%, bringing it to a useful range for production of PET tracers. α-hydroxy acids are found in bioactive ligands and metabolites, enabling native radiolabelling of existing PET tracers and opening a route to unrealized PET tracers.

We demonstrated the versatility of this method by synthesizing a scope of 14 carbon-11 labelled α-hydroxy acids with radiochemical yields ranging from 20-73%. The scope includes 2/3/4-substituted benzilic acids with heteroatomic functional groups, a heterocyclic ketone and a mono-hydroannulene core commonly found in drug molecules. Furthermore, we developed a metal-free photocatalytic method to prepare α-hydroxy acids with non-radioactive CO_2 to characterize the radioactive compounds. We synthesized a scope of 14 compounds including 3 unreported molecules with yields up to 82%.

3.2 Future Directions

An immediate goal for the project is the preparation of [^{11}C]Quinuclidinyl Benzilate ([^{11}C]QNB). The ligand is a very potent inhibitor of mAChRs (K_d = 0.27 nM) and its methiodide salt [^{11}C]*N*-methyl QNB has been evaluated *in vivo* with human subjects. The charged nature of [^{11}C]MQNB makes the tracer impermeable through the blood-brain barrier. The native ligand [^{11}C]QNB would not suffer from such impermeability, and a mild and efficient synthesis of the tracer would enable a more straightforward clinical production of the tracer.

In the near future, a goal for the project would be the exploration of strongly electron withdrawing substrates to understand the impact of electronics on the proposed intermediate **int. B** that forms prior to carboxylation. Mechanistic experiments described for non-radioactive methods in earlier sections highlight the formation of such an intermediate for carboxylation. Potential substrates to inquire the electronic effects of **int. B** include trifluoromethoxy substituted ketones, aldehydes and α-keto ester substrates. Such substrates consist of strong electron withdrawing groups at the α-position to the reactive carbon and could enable access to substrates which are not substituted by aromatic groups. An application to probe at the electronic limit of the method is through the preparation of [1-^{11}C]lactate. While [1-^{11}C]lactate is potentially very difficult to be synthesized using this method on account of its highly inactivated precursor, the synthesis of a 3-trifluoromethyl derivative of lactic acid could still be possible as a bioisostere. The purpose of attempting to carboxylate such substrates is to identify the performance limits of the method beyond diaryl species. Key performance parameters include reduction potentials of the photocatalyst, the nitrogenous base and the substrate, and the lifetime of the photocatalyst.

Finally, a logical next step to carboxylation of carbonyls is the carboxylation of imine substrates to yield α-amino acids. Especially, imine substrates derived from previously successful ketone substrates serve as a useful starting point. α-Amino acids are prevalent in various bioactive molecules and are found in many endogenous molecules in our body. Such prevalence of α-amino acids makes them a highly appealing target to radiolabel with carbon-11, especially with high activity yields and molar activities.

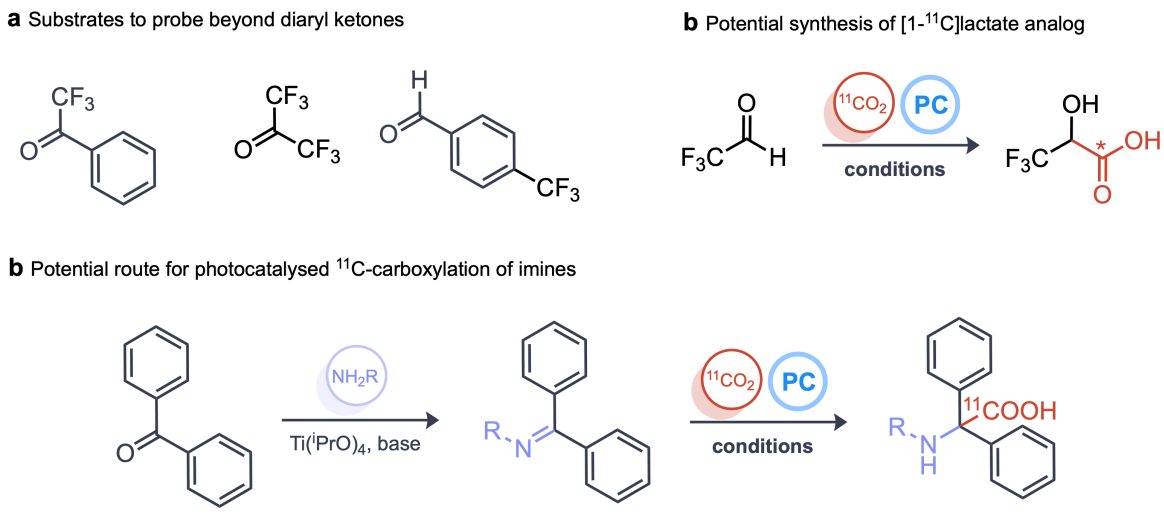

Figure 23 Future directions

Expanding mild and efficient photocatalytic methods to a broad scope of functionalities would make them more adaptable in clinical settings, making the methods practical resource in every radiochemist's toolbox.

Chapter 4

Experimental

4.1 Materials

4.1.1 General

All reactions were set up under inert atmosphere with anhydrous reagents unless otherwise specified. Commercially available chemicals were obtained from Sigma-Aldrich, TCI Chemicals, Oakwood Chemicals and Thermo Scientific, and were used as received.

4.1.2 Radioactive reactions

Before commencing all radiochemical reactions, isotopic [^{11}C]CO_2 was generated through a Siemens Eclipse HP/RP Hybrid Cyclotron located at the National Cardiac PET Centre at the University of Ottawa Heart Institute. Unless otherwise mentioned, cyclotron parameters were default and the N_2 target (with additive O_2) was beamed at 40 μA for 2 mins. The irradiated target enriched with [^{11}C]CO_2 was delivered to a Synthra MeI plus module, where a CO_2 trap cooled to -180 °C using liquid nitrogen freezes [^{11}C]CO_2 over a coil, generally yielding ~4 GBq of activity.

All photochemical reactions were performed in a sealed tapered microwave vial (2 dram) placed between two Kessil A160WE Tuna Blue lamps (maximum intensity, white to blue light), 2.5 cm from the reactor vessel. A delivery line from the Synthra MeI plus module was attached to the reactor vessel using a stainless-steel needle. Helium is used as a push gas to deliver isotopic CO_2 from the heated coil into the reaction vessel. A sodium hydroxide (Ascarite) cartridge was attached over the exhaust needle to measure escaped [^{11}C]CO_2 after delivery.

Activity measurements for the reactor vessel and Ascarite cartridge were made using Capintec CRC-15 Dual PET dose calibrator. Yield calculations were performed using radioHPLC (Agilent 1100 Series HPLC + Raytest Gabi radio detector OR Waters 2695 HPLC + Custom radio detector) set up.

Measured activity and radioHPLC integrations were decay-corrected for yield calculations using $t_{1/2}[^{11}C]$ = 20.364 min.

4.1.3 Non-radioactive reactions

All photochemical reactions were performed using standard Schlenk techniques and carried out under a carbon dioxide atmosphere unless otherwise noted. Reactions were set up in a 10 mL Schlenk flask and placed in a water bath to maintain room temperature. Kessil A160WE Tuna Blue lamp (maximum intensity, blue light) was placed 1 cm from the water bath (2 cm from Schlenk flask).

Reactions were monitored using liquid chromatography-mass spectrometry (LC-MS), recorded on Waters Xevo-TQD and thin-layer chromatography (TLC) using UV light as visualizing agents and $KMnO_4$ as developing agents. ^1H and ^{13}C NMR were recorded on Bruker Avance II 400 (^1H: 400 MHz and ^{13}C: 101 MHz). Chemical shifts (δ) for ^1H and ^{13}C NMR spectra are given in ppm relative to tetramethyl silane (TMS). The residual solvent signals were used as references for ^1H and ^{13}C NMR spectra and the chemical shifts converted to the TMS scale ($CDCl_3$: δH = 7.26 ppm, δC = 77.16 ppm; $(CD_3)_2SO$: δH = 2.50 ppm, δC = 39.52 ppm).

4.2 Radioactive Methods

4.2.1 General synthesis of ^{11}C-α-hydroxy carboxylic acids (Optimisation Campaign)

An oven-dried microwave vial with a stir bar was charged with all solid reagents, doubly sealed and then evacuated backfilled with Ar (3x). Reagents used: 50 μmol (1 equiv.) ketone, 100 μmol (2 equiv.) base, 100 μmol (2 equiv.) amine, 65 μmol (1.3 equiv.) silane and 2 μmol (2 mol%) photocatalyst. The leftover liquid reagents along with 500 μL of solvent were dissolved together in a vial. Before attaching the delivery line and Ascarite cartridge to the reactor vessel, the mixture of liquid reagents was dissolved with other solid reagents. The reactor vessel was placed between the lamps and the delivery line and exhaust were attached. Immediately after, the production of [^{11}C]CO_2 was started. When isotope production was completed, the microwave vial was irradiated with the lamps and isotope delivery is commenced. Helium is bubbled at 20 mL/min until all activity has been delivered, then slowed down to 10 mL/min until the reaction is complete. The reaction was stirred for 5 minutes under irradiation. After 5 minutes, the delivery line was raised out of solution, and the reaction is quenched with 1 mL of 1 M HCl. The reaction was stirred for 1 minute until no further activity is collected in the exhaust cartridge. Finally, activity measurements were made and 100 μL of the reaction mixture was used for radioHPLC.

4.2.2 Synthesis of ^{11}C-α-hydroxy carboxylic acids (Substrate Scope)

An oven-dried microwave vial with a stir bar was charged with 50 μmol (1 equiv.) ketone and 14 mg (2 equiv.) potassium pivalate. In a sealed vial was prepared the mixture (A) of 21.4 μL (2 equiv.) Cy_2NMe and 8.2 μL (1.3 equiv.) TMSCl in 400 μL of dimethylacetamide (DMA). 1 mg (2 mol%) $[Ir(dtbbpy)(ppy)_2]PF_6$ was obtained from a 10 mM stock solution (B) of the complex in DMA. Mixture A was added to the vial and vortexed until homogenous, then the vessel was placed between the lamps and the delivery line and exhaust were attached. Immediately after, the production of [^{11}C]CO_2 was started. Before completion of production, 100 μL of mixture B was added to the reactor vessel. When isotope production was completed, the microwave vial was irradiated with the lamps and isotope delivery was commenced. Helium was bubbled at 20 mL/min for exactly 45 seconds, until all activity had been delivered.

The reaction was stirred for 10 minutes under irradiation. After 10 minutes, activity measurements were made on the reaction vessel and exhaust. Finally, 100 μL of the reaction mixture was dissolved in 300 μL of freshly prepared 2:1 solution of 1 M HCl/ACN for radioHPLC analysis.

4.3 Non-radioactive methods

4.3.1 Synthesis of phthalonitrile-based photocatalysts

4-DPAIPN

An oven-dried 25 mL Schlenk flask with a stir bar was charged with 3.6 mmol (6 equiv.) diphenylamine (DPA) and 4.8 mmol (8 equiv.) sodium hydride. The vial was sealed, evacuated and backfilled with argon, then 4 mL of dimethylformamide (DMF) was added. The mixture was stirred for 1 h at 50 °C. Then 0.6 mmol of tetrafluoroisophthalonitrile (4-F-IPN) was dissolved in 2 mL DMF and added dropwise to the Schlenk flask. The mixture was further stirred for 4 h at 50°C. After stirring the reaction was cooled down to room temperature and quenched with 0.5 mL water. The reaction mixture was further diluted with water and extracted with EtOAc. The organic layer was then washed with 10% LiCl in water (w/v) to remove extracted DMF and the organic layer was concentrated *in vacuo.* Flash chromatography was performed using DCM in hexanes 0% → 70%. The product fractions were concentrated, then redissolved in DCM and precipitated using pentanes. 4-DPAIPN was isolated with a 26% yield (187 mg), spectral data were consistent with literature reports.[55]

4-CzIPN

To an oven-dried 50 mL Schlenk flask with a stir bar was charged with 5.0 mmol (5 equiv.) 9H-carbazole (Cz) and 7.5 mmol (7.5 equiv.) sodium hydride. The vial was sealed, evacuated and backfilled with argon, then 15 mL of tetrahydrofuran (THF) was added. The mixture was stirred for 30 mins at room temperature. Then 1.0 mmol of tetrafluoroisophthalonitrile (4-F-IPN) was dissolved in 5 mL THF and added dropwise to the Schlenk flask. The mixture was further stirred for 16 h at room temperature. After stirring the reaction was quenched with 1 mL water. The reaction mixture was further diluted with water and extracted with EtOAc and the organic layer was concentrated *in vacuo.* Flash chromatography was performed using DCM in hexanes 0% → 55%. The product fractions were concentrated, then redissolved in DCM and precipitated using pentanes. 4-CzIPN was isolated with a 38% yield (299 mg), spectral data were consistent with literature reports.[55]

4.3.2 Synthesis of non-radioactive standards (General procedure)

An oven-dried 10 mL Schlenk flask with a stir bar was charged with 0.2 mmol (1 equiv.) ketone, 0.004 mmol (2 mol%) photocatalyst, 0.6 mmol (3 equiv.) sodium formate, 0.06 mmol (30 mol%) 1,4-diazabicyclooctane (DABCO) and 0.5 mmol (2.5 equiv.) cesium carbonate. The vial was sealed, evacuated and backfilled with CO_2, then 2 mL of dimethyl sulfoxide (DMSO) was added. The flask was placed in a water bath to maintain the flask at room temperature, in front of a lamp to be irradiated for 3 hours to 6 hours. Reaction completion was monitored using thin-layer chromatography (TLC) in 80% EtOAc (with 0.5% AcOH)/Hexanes. The reaction was quenched using 4 mL 1 M HCl and stirred for 5 minutes. The reaction mixture was extracted using EtOAc and the organic layer was washed with brine to remove DMSO. One of the following workups was performed for each substrate –

Workup 1 - The organic layer was concentrated *in vacuo* and dissolved in 20% EtOAc/Hexanes to load on silica for flash chromatography. Flash chromatography was performed using EtOAc (with 0.5% AcOH) in Hexanes 20% → 50% to isolate the product.

Workup 2 – The organic layer was extracted with 10% $NaHCO_3$. The aqueous layer was acidified using dropwise addition of 12 M HCl until pH<2.5. The neutralized aqueous layer was extracted with EtOAc and this organic layer was concentrated *in vacuo* to isolate the product.

4.3.3 NMR Spectral data

2-([1,1'-biphenyl]-4-yl)-2-hydroxypropanoic acid (4.b)

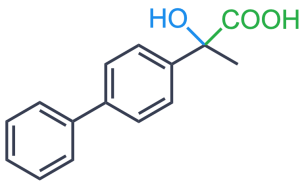

Synthesised using **General procedure (Workup 1)**, 51% yield, white solid

^{1}H NMR (600 MHz, DMSO) δ 7.70 – 7.55 (m, 6H), 7.46 (t, 2H) 7.36 (t, 1H) 1.64 (s, 3H) **^{13}C NMR** (151 MHz, DMSO) δ 176.0, 143.7, 139.9, 138.9, 128.9, 127.4, 126.7, 126.1, 104.4, 74.8, 68.3. Spectra were consistent with data reported in literature.[31]

2,2-bis(4-fluorophenyl)-2-hydroxyacetic acid (4.e)

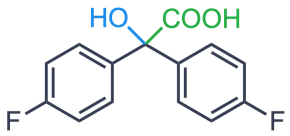

Synthesised using **General procedure (Workup 2)**, 28% yield, yellow solid

^{1}H NMR (600 MHz, DMSO) δ 7.41 – 7.35 (t, 4H), 7.19 – 7.10 (t, 4H) **^{13}C NMR** (151 MHz, DMSO) δ 174.4, 160.6, 139.9, 129.1, 114.5, 104.4. Spectra were consistent with data reported in literature.[31]

2-([1,1'-biphenyl]-4-yl)-2-hydroxy-2-phenylacetic acid (4.f)

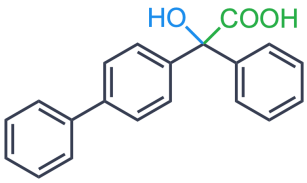

Synthesised using **General procedure (Workup 1)**, 81% yield, white solid

^{1}H NMR (600 MHz, DMSO) δ 7.68 – 7.60 (dd, 4H), 7.48 – 7.40 (m, 6H), 7.38 – 7.32 (m, 3H), 7.31 – 7.26 (t, 1H) **^{13}C NMR** (151 MHz, DMSO) δ 174.7, 143.7, 142.9, 139.8, 139.1, 129.0, 127.8, 127.8, 127.5, 127.4, 127.1, 126.7, 126.1, 80.2. Spectra were consistent with data reported in literature.[31]

2-hydroxy-2-phenyl-2-(p-tolyl)acetic acid (4.g)

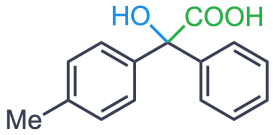

Synthesised using **General procedure (Workup 1)**, 81% yield, white solid

^{1}H NMR (600 MHz, DMSO) δ 7.40 – 7.33 (m, 2H), 7.33 – 7.28 (t, 2H), 7.27 – 7.22 (d, 3H), 7.14 – 7.09 (d, 2H), 2.27 (s, 3H) **^{13}C NMR** (151 MHz, DMSO) δ 174.8, 144.0, 140.9, 136.3, 128.2, 127.6, 127.1, 127.1, 120.4, 104.4, 80.1. Spectra were consistent with data reported in literature.[31]

2-hydroxy-2-phenyl-2-(4-(trifluoromethyl)phenyl)acetic acid (4.h)

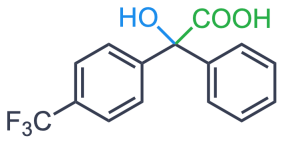

Synthesised using **General procedure (Workup 2)**, 30% yield, yellow oil

^{1}H NMR (600 MHz, DMSO) δ 7.72 – 7.67 (d, 2H), 7.62 – 7.58 (d, 2H), 7.39 – 7.33 (m, 5H). **^{13}C NMR** (151 MHz, DMSO) δ 174.2, 170.5, 143.2, 128.1, 128.0, 127.7, 127.0, 124.8, 124.7, 80.2. Spectra were consistent with data reported in literature.[31]

2-hydroxy-2-(4-methoxyphenyl)-2-phenylacetic acid (4.i)

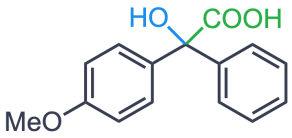

Synthesised using **General procedure (Workup 2)**, 82% yield, yellow oil

^{1}H NMR (600 MHz, DMSO) δ 7.35 (d, 2H), 7.31 (t, 2H), 7.27 (d, 3H), 6.88 (d, 2H), 3.73 (s, 3H). **^{13}C NMR** (151 MHz, DMSO) δ 174.9, 158.4, 144.0, 135.7, 128.4, 127.7, 127.2, 113.0, 104.4, 79.9, 55.1. Spectra were consistent with data reported in literature.[31]

2-hydroxy-2-(4-cyano)-2-phenylacetic acid (4.j)

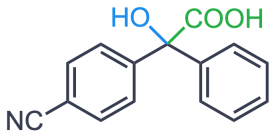

Synthesised using **General procedure (Workup 2)**, 19% yield, yellow oil

^{1}H NMR (600 MHz, DMSO) δ 7.79 (d, 2H), 7.56 (d, 2H), 7.38 – 7.26 (m, 5H). **^{13}C NMR** (151 MHz, DMSO) δ 173.8, 149.0, 142.9, 131.7, 128.1, 128.0, 127.7, 126.8, 118.7, 110.0, 80.1. Spectra were consistent with data reported in literature.[32]

2-(3-chlorophenyl)-2-hydroxy-2-phenylacetic acid (4.k)

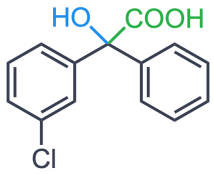

Synthesised using **General procedure (Workup 1)**, 82% yield, yellow oil

^{1}H NMR (600 MHz, DMSO) δ 7.40 – 7.25 (m, 9H). **^{13}C NMR** (151 MHz, DMSO) δ 174.2, 146.2, 143.2, 132.5, 129.7, 128.0, 127.4 (q), 126.9, 126.9, 126.0, 104.4, 80.1. Spectra were consistent with data reported in literature.[31]

2-(2-fluorophenyl)-2-hydroxy-2-phenylacetic acid (4.l)

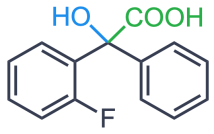

Synthesised using **General procedure (Workup 1)**, 65% yield, yellow solid

^{1}H NMR (600 MHz, DMSO) δ 7.53 (d, 2H), 7.40 – 7.25 (m, 4H), 7.16 (t, 1H), 7.08 (t, 1H), 6.94 (t, 1H). **^{13}C NMR** (151 MHz, DMSO) δ 174.1, 161.1, 159.5, 141.3, 129.8, 129.0, 127.3 (d), 123.6, 115.7, 104.4, 77.76, 68.3. Spectra were consistent with data reported in literature.[31]

2-(2-(trifluoromethyl)phenyl)-2-hydroxy-2-phenylacetic acid (4.m)

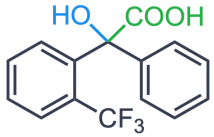

Synthesised using **General procedure (Workup 1)**, 70% yield, yellow oil

^{1}H NMR (600 MHz, DMSO) δ 7.77 (d, 1H), 7.53 – 7.40 (m, 7H), 6.77 (d, 1H). **^{13}C NMR** (151 MHz, DMSO) δ 174.7, 174.3, 142.9, 142.2, 131.3, 130.4, 128.2, 128.1, 128.0, 127.0, 126.9, 104.4, 81.0.

2-hydroxytricyclo[9.4.0.03,8]pentadeca-1(15),3,5,7,11,13-hexaene-2-carboxylic acid (4.o)

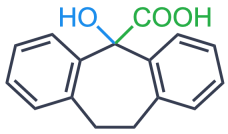

Synthesised using **General procedure (Workup 1)**, 81% yield, pale yellow solid

^{1}H NMR (600 MHz, DMSO) δ 7.76 – 7.70 (m, 2H), 7.18 – 7.12 (m, 4H), 7.11 – 7.06 (m, 2H), 3.29 – 3.20 (m, 2H), 2.92 – 2.81 (m, 2H). **^{13}C NMR** (151 MHz, DMSO) δ 174.2, 172.0, 142.0, 137.1, 129.7, 127.2, 125.4, 124.8, 78.1.

2-hydroxy-2-phenyl-2-(thiophen-2-yl)acetic acid (4.p)

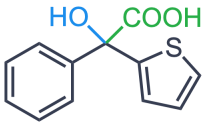

Synthesised using **General procedure (Workup 2)**, 41% yield, dark purple solid

^{1}H NMR (600 MHz, DMSO) δ 7.47 – 7.42 (m, 3H), 7.32 (t, 2H), 7.28 (t, 1H), 7.07 (s, 1H), 6.98 (s, 1H).

^{13}C NMR (151 MHz, DMSO) δ 173.7, 148.1, 143.5, 127.8, 127.6, 126.4, 126.2, 125.6, 125.5, 78.2.

Bibliography

[1] S. M. Ametamey, M. Honer, P. A. Schubiger, "Molecular Imaging with PET" *Chem. Rev.* **2008**, *108*, 1501–1516.

[2] J. Rong, A. Haider, T. E. Jeppesen, L. Josephson, S. H. Liang, "Radiochemistry for positron emission tomography" *Nat. Commun.* **2023**, *14*, 3257.

[3] S. Hoberück, K. Zöphel, M. G. Pomper, S. P. Rowe, A. Gafita, "One Hundred Years of the Tracer Principle" *J. Nucl. Med.* **2023**, DOI 10.2967/jnumed.123.266458.

[4] L. Deng, K. Pushpitha, C. Joseph, V. Gupta, R. Rajput, N. Chitranshi, Y. Dheer, A. Amirkhani, K. Kamath, D. Pascovici, J. X. Wu, G. H. Salekdeh, P. A. Haynes, S. L. Graham, V. K. Gupta, M. Mirzaei, "Amyloid β Induces Early Changes in the Ribosomal Machinery, Cytoskeletal Organization and Oxidative Phosphorylation in Retinal Photoreceptor Cells" *Front. Mol. Neurosci.* **2019**, *12*, DOI 10.3389/fnmol.2019.00024.

[5] P. W. Miller, N. J. Long, R. Vilar, A. D. Gee, "Synthesis of 11C, 18F, 15O, and 13N Radiolabels for Positron Emission Tomography" *Angew. Chem. Int. Ed.* **2008**, *47*, 8998–9033.

[6] D. Petroni, L. Menichetti, M. Poli, "Historical and radiopharmaceutical relevance of [18F]FDG" *J Radioanal. Nucl. Chem.* **2020**, *323*, 1017–1031.

[7] K. Suzuki, T. Yamazaki, M. Sasaki, A. Kubodera, "Specific activity of [11C]CO2 generated in a N2 gas target: effect of irradiation dose, irradiation history, oxygen content and beam energy" *Radiochim. Acta.* **2000**, *88*, 211–216.

[8] J. Andersson, P. Truong, C. Halldin, "In-target produced [11C]methane: Increased specific radioactivity" *Appl. Radiat. Isot.* **2009**, *67*, 106–110.

[9] H. H. Coenen, A. D. Gee, M. Adam, G. Antoni, C. S. Cutler, Y. Fujibayashi, J. M. Jeong, R. H. Mach, T. L. Mindt, V. W. Pike, A. D. Windhorst, "Consensus nomenclature rules for radiopharmaceutical chemistry — Setting the record straight" *Nucl. Med. Biol.* **2017**, *55*, v–xi.

[10] K. Dahl, T. Turner, N. Vasdev, "Radiosynthesis of a Bruton's tyrosine kinase inhibitor, [11C]Tolebrutinib, via palladium-NiXantphos-mediated carbonylation" *J. Label. Compd. Radiopharm.* **2020**, *63*, 482–487.

[11] A. Pees, M. Chassé, A. Lindberg, N. Vasdev, "Recent Developments in Carbon-11 Chemistry and Applications for First-In-Human PET Studies" *Molecules* **2023**, *28*, 931.

[12] P. Bellotti, H.-M. Huang, T. Faber, F. Glorius, "Photocatalytic Late-Stage C–H Functionalization" *Chem. Rev.* **2023**, *123*, 4237–4352.

[13] D. Lin, L. M. Lechermann, M. P. Huestis, J. Marik, J. B. I. Sap, "Light-Driven Radiochemistry with Fluorine-18, Carbon-11 and Zirconium-89" *Angew. Chem. Int. Ed.* **2024**, *n/a*, e202317136.

[14] R. W. Pipal, K. T. Stout, P. Z. Musacchio, S. Ren, T. J. A. Graham, S. Verhoog, L. Gantert, T. G. Lohith, A. Schmitz, H. S. Lee, D. Hesk, E. D. Hostetler, I. W. Davies, D. W. C. MacMillan, "Metallaphotoredox aryl and alkyl radiomethylation for PET ligand discovery" *Nature* **2021**, *589*, 542–547.

[15] P. Zhang, C. "Chip" Le, D. W. C. MacMillan, "Silyl Radical Activation of Alkyl Halides in Metallaphotoredox Catalysis: A Unique Pathway for Cross-Electrophile Coupling" *J. Am. Chem. Soc.* **2016**, *138*, 8084–8087.

[16] X. Wu, W. Chen, N. Holmberg-Douglas, G. T. Bida, X. Tu, X. Ma, Z. Wu, D. A. Nicewicz, Z. Li, "11C-, 12C-, and 13C-cyanation of electron-rich arenes via organic photoredox catalysis" *Chem* **2023**, *9*, 343–362.

[17] W. Chen, X. Wu, J. B. McManus, G. T. Bida, K.-P. Li, Z. Wu, D. A. Nicewicz, Z. Li, "Direct C–H Radiocyanation of Arenes via Organic Photoredox Catalysis" *Org. Lett.* **2022**, *24*, 9316–9321.

[18] J. B. McManus, D. A. Nicewicz, "Direct C–H Cyanation of Arenes via Organic Photoredox Catalysis" *J. Am. Chem. Soc.* **2017**, *139*, 2880–2883.

[19] Z. Zhu, X. Wu, G. T. Bida, H. Deng, X. Ma, S. Qian, Z. Wu, Z. Li, D. A. Nicewicz, "Carbon isotopic labelling of carboxylic acids enabled by organic photoredox-catalysed cyanation" *Nat. Synth.* **2024**, *4*, 97–105.
[20] D. Kong, M. Munch, Q. Qiqige, C. J. C. Cooze, B. H. Rotstein, R. J. Lundgren, "Fast Carbon Isotope Exchange of Carboxylic Acids Enabled by Organic Photoredox Catalysis" *J. Am. Chem. Soc.* **2021**, *143*, 2200–2206.
[21] G. Luurtsema, V. Pichler, S. Bongarzone, Y. Seimbille, P. Elsinga, A. Gee, J. Vercouillie, "EANM guideline for harmonisation on molar activity or specific activity of radiopharmaceuticals: impact on safety and imaging quality" *EJNMMI Radiopharm. Chem.* **2021**, *6*, 34.
[22] V. Pichler, T. Zenz, C. Philippe, C. Vraka, N. Berrotéran-Infante, S. Pfaff, L. Nics, M. Ozenil, O. Langer, M. Willeit, T. Traub-Weidinger, R. Lanzenberger, M. Mitterhauser, M. Hacker, W. Wadsak, "Molar activity – The keystone in 11C-radiochemistry: An explorative study using the gas phase method" *Nucl. Med. Biol.* **2018**, *67*, 21–26.
[23] D. Kong, P. J. Moon, E. K. J. Lui, O. Bsharat, R. J. Lundgren, "Direct reversible decarboxylation from stable organic acids in dimethylformamide solution" *Science* **2020**, *369*, 557–561.
[24] G. Destro, K. Horkka, O. Loreau, D.-A. Buisson, L. Kingston, A. Del Vecchio, M. Schou, C. S. Elmore, F. Taran, T. Cantat, D. Audisio, "Transition-Metal-Free Carbon Isotope Exchange of Phenyl Acetic Acids" *Angew. Chem. Int. Ed.* **2020**, *59*, 13490–13495.
[25] M. Munch, B. A. Mair, M. Adi, B. H. Rotstein, "Photocatalyzed radiosynthesis of 11C-phenylacetic acids" *J. Label. Compd. Radiopharm.* **2024**, *67*, 211–216.
[26] Q.-Y. Meng, T. E. Schirmer, A. L. Berger, K. Donabauer, B. König, "Photocarboxylation of Benzylic C–H Bonds" *J. Am. Chem. Soc.* **2019**, *141*, 11393–11397.
[27] Y. Kwon, J. Lee, Y. Noh, D. Kim, Y. Lee, C. Yu, J. C. Roldao, S. Feng, J. Gierschner, R. Wannemacher, M. S. Kwon, "Formation and degradation of strongly reducing cyanoarene-based radical anions towards efficient radical anion-mediated photoredox catalysis" *Nat. Commun.* **2023**, *14*, 92.
[28] A. Malandain, M. Molins, A. Hauwelle, A. Talbot, O. Loreau, T. D'Anfray, S. Goutal, N. Tournier, F. Taran, F. Caillé, D. Audisio, "Carbon Dioxide Radical Anion by Photoinduced Equilibration between Formate Salts and [11C, 13C, 14C]CO2: Application to Carbon Isotope Radiolabeling" *J. Am. Chem. Soc.* **2023**, *145*, 16760–16770.
[29] S. N. Alektiar, Z. K. Wickens, "Photoinduced Hydrocarboxylation via Thiol-Catalyzed Delivery of Formate Across Activated Alkenes" *J. Am. Chem. Soc.* **2021**, *143*, 13022–13028.
[30] X. Fan, X. Gong, M. Ma, R. Wang, P. J. Walsh, "Visible light-promoted CO2 fixation with imines to synthesize diaryl α-amino acids" *Nat. Commun.* **2018**, *9*, 4936.
[31] G.-M. Cao, X.-L. Hu, L.-L. Liao, S.-S. Yan, L. Song, J. J. Chruma, L. Gong, D.-G. Yu, "Visible-light photoredox-catalyzed umpolung carboxylation of carbonyl compounds with CO2" *Nat. Commun.* **2021**, *12*, 3306.
[32] S. Okumura, Y. Uozumi, "Photocatalytic Carbinol Cation/Anion Umpolung: Direct Addition of Aromatic Aldehydes and Ketones to Carbon Dioxide" *Org. Lett.* **2021**, *23*, 7194–7198.
[33] S. Okumura, T. Imuta, K. Kato, K. Shimosaka, H. Aoki, Y. Aoyagi, K. Hikichi, N. Ishida, "Metal-free carboxylation of aromatic ketones and aldehydes with CO2 by a diazabenzoacenaphthenium photoredox catalyst" *Chem. Lett.* **2025**, *54*, upaf135.
[34] B. Shahriari, K. Swersky, Z. Wang, R. P. Adams, N. de Freitas, "Taking the Human Out of the Loop: A Review of Bayesian Optimization" *Proc. IEEE* **2016**, *104*, 148–175.
[35] J. A. G. Torres, S. H. Lau, P. Anchuri, J. M. Stevens, J. E. Tabora, J. Li, A. Borovika, R. P. Adams, A. G. Doyle, "A Multi-Objective Active Learning Platform and Web App for Reaction Optimization" *J. Am. Chem. Soc.* **2022**, *144*, 19999–20007.
[36] R. C. Tung, W. F. Bergfeld, A. T. Vidimos, B. K. Remzi, "α-Hydroxy Acid-Based Cosmetic Procedures" *Am. J. Clin. Dermatol.* **2000**, *1*, 81–88.

[37] S.-C. Tang, J.-H. Yang, "Dual Effects of Alpha-Hydroxy Acids on the Skin" *Molecules* **2018**, *23*, 863.
[38] X. Li, Y. Yang, B. Zhang, X. Lin, X. Fu, Y. An, Y. Zou, J.-X. Wang, Z. Wang, T. Yu, "Lactate metabolism in human health and disease" *Sig Transduct Target Ther* **2022**, *7*, 1–22.
[39] V. G. Maurino, M. K. M. Engqvist, "2-Hydroxy Acids in Plant Metabolism" *Arabidopsis* **2015**, *2015*, DOI 10.1199/tab.0182.
[40] C. Bolden, B. Cusack, E. Richelson, "Antagonism by antimuscarinic and neuroleptic compounds at the five cloned human muscarinic cholinergic receptors expressed in Chinese hamster ovary cells." *J. Pharmacol. Exp. Ther.* **1992**, *260*, 576–580.
[41] M. V. Liberti, J. W. Locasale, "The Warburg Effect: How Does it Benefit Cancer Cells?" *Trends Biochem. Sci.* **2016**, *41*, 211–218.
[42] H. Zhang, J. Zhao, J. Yu, X. Zhang, S. Ran, S. Wang, W. Ye, Z. Luo, X. Li, Y. Hao, J. Zong, R. Li, L. Lai, K. Zheng, P. Huang, C. Zhou, J. Wu, Y. Li, J. Xia, "Lactate metabolism and lactylation in cardiovascular disease: novel mechanisms and therapeutic targets" *Front. Cardiovasc. Med.* **2024**, *11*, DOI 10.3389/fcvm.2024.1489438.
[43] P. S. Rajendran, J. Hadaya, S. S. Khalsa, C. Yu, R. Chang, K. Shivkumar, "The vagus nerve in cardiovascular physiology and pathophysiology: From evolutionary insights to clinical medicine" *Semin. Cell. Dev. Biol.* **2024**, *156*, 190–200.
[44] M. Tibensky, B. Mravec, "Role of the parasympathetic nervous system in cancer initiation and progression" *Clin. Transl. Oncol.* **2021**, *23*, 669–681.
[45] M. Ozenil, J. Aronow, M. Millard, T. Langer, W. Wadsak, M. Hacker, V. Pichler, "Update on PET Tracer Development for Muscarinic Acetylcholine Receptors" *Pharmaceuticals* **2021**, *14*, 530.
[46] J. Delforge, D. L. Guludec, A. Syrota, B. Bendriem, C. Crouzel, M. Slama, P. Merlet, "Quantification of Myocardial Muscarinic Receptors with PET in Humans" *J. Nucl. Med.* **1993**, *34*, 981–991.
[47] R. A. Koeppe, K. A. Frey, G. K. Mulholland, M. R. Kilbourn, A. Buck, K. S. Lee, D. E. Kuhl, "[11C]Tropanyl Benzilate—Binding to Muscarinic Cholinergic Receptors: Methodology and Kinetic Modeling Alternatives" *J. Cereb. Blood Flow Metab.* **1994**, *14*, 85–99.
[48] J.-K. Zubieta, R. A. Koeppe, G. K. Mulholland, D. E. Kuhl, K. A. Frey, "Quantification of Muscarinic Cholinergic Receptors with [11C]NMPB and Positron Emission Tomography: Method Development and Differentiation of Tracer Delivery from Receptor Binding" *J. Cereb. Blood Flow Metab.* **1998**, *18*, 619–631.
[49] C. Prenant, L. Barre, C. Crouzel, "Synthesis of [11C]-3-quinuclidinylbenzilate (QNB)" *J. Label. Compd. Radiopharm.* **1989**, *27*, 1257–1265.
[50] B. H. Rotstein, S. H. Liang, J. P. Holland, T. L. Collier, J. M. Hooker, A. A. Wilson, N. Vasdev, "11CO2 fixation: a renaissance in PET radiochemistry" *Chem. Commun.* **2013**, *49*, 5621.
[51] B. J. Shields, J. Stevens, J. Li, M. Parasram, F. Damani, J. I. M. Alvarado, J. M. Janey, R. P. Adams, A. G. Doyle, "Bayesian reaction optimization as a tool for chemical synthesis" *Nature* **2021**, *590*, 89–96.
[52] P. Xu, S. Wang, H. Xu, Y.-Q. Liu, R.-B. Li, W.-W. Liu, X.-Y. Wang, M.-L. Zou, Y. Zhou, D. Guo, X. Zhu, "Dicarboxylation of Alkenes with CO2 and Formate via Photoredox Catalysis" *ACS Catal.* **2023**, *13*, 2149–2155.
[53] J. Majhi, G. A. Molander, "Recent Discovery, Development, and Synthetic Applications of Formic Acid Salts in Photochemistry" *Angew. Chem. Int. Ed.* **2024**, *136*, e202311853.
[54] P. Wei, J. H. Oh, G. Dong, Z. Bao, "Use of a 1H-Benzoimidazole Derivative as an n-Type Dopant and To Enable Air-Stable Solution-Processed n-Channel Organic Thin-Film Transistors" *J. Am. Chem. Soc.* **2010**, *132*, 8852–8853.
[55] M. Garreau, F. Le Vaillant, J. Waser, "C-Terminal Bioconjugation of Peptides through Photoredox Catalyzed Decarboxylative Alkynylation" *Angew. Chem. Int. Ed.* **2019**, *58*, 8182–8186.

Appendix A

radioHPLC Chromatograms

[^{11}C]2-hydroxy-2,2-diphenylacetic acid (5.a)

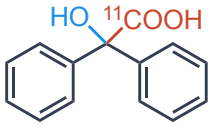

Without acid quench (n=2) –

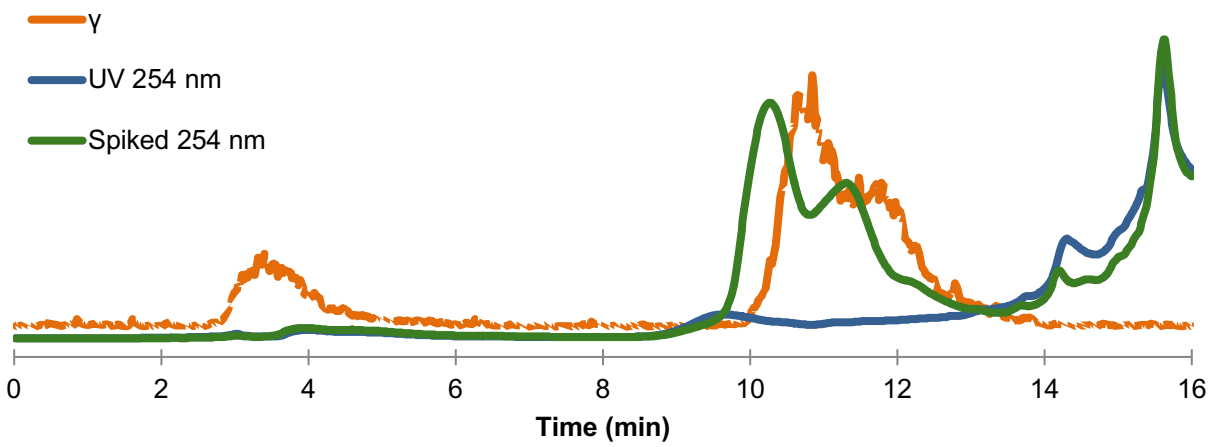

Standard (n=2) –

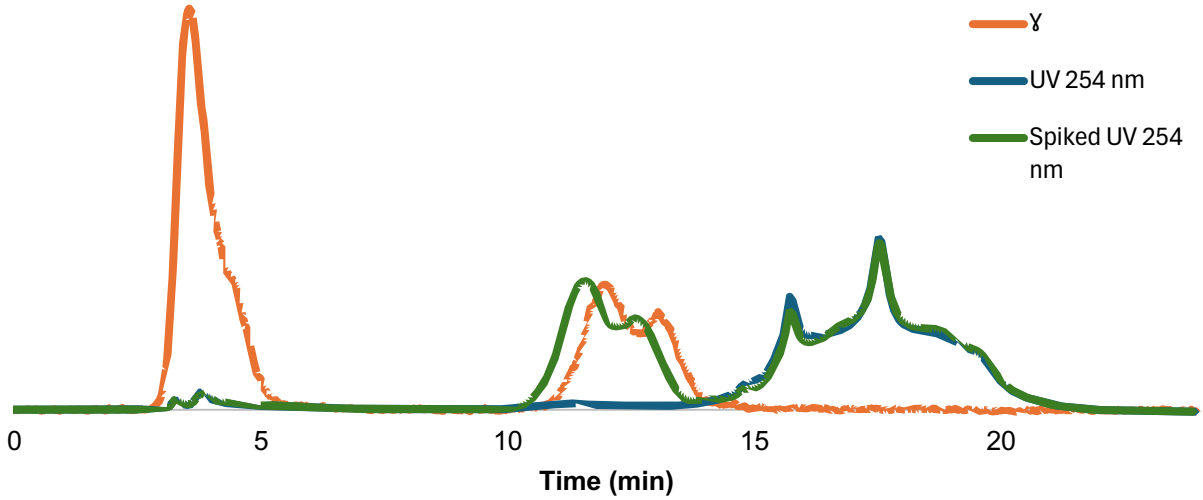

[^{11}C]2,2-bis(4-fluorophenyl)-2-hydroxyacetic acid (5.e)

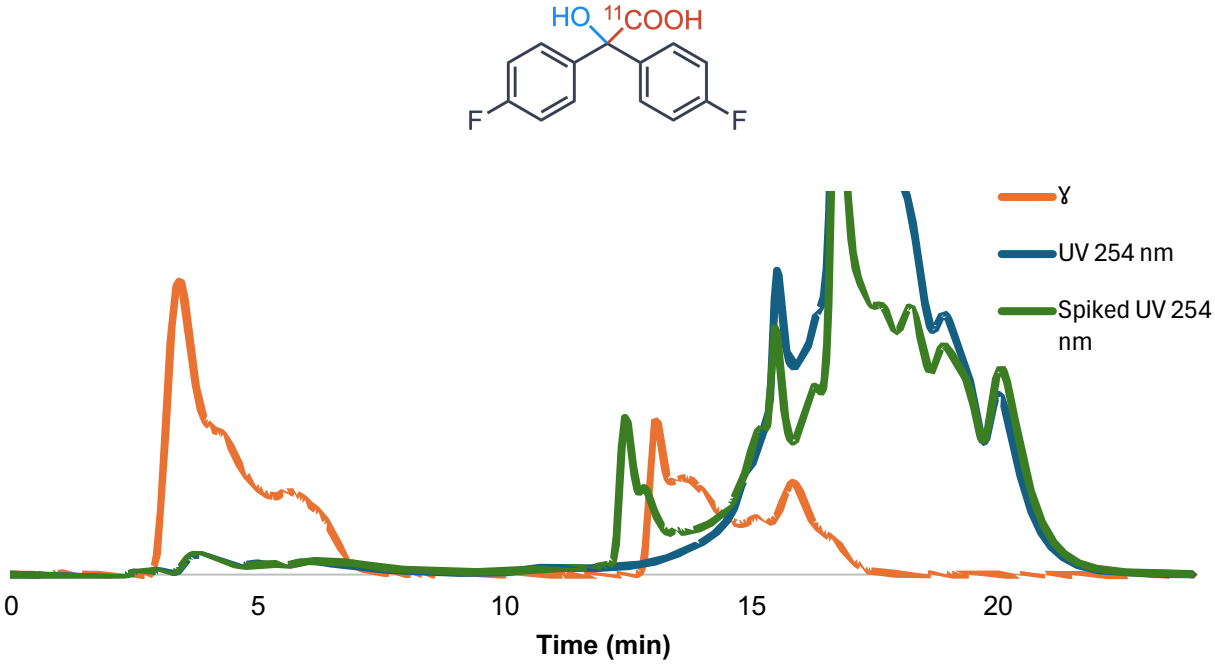

[^{11}C]2-([1,1'-biphenyl]-4-yl)-2-hydroxy-2-phenylacetic acid (5.f)

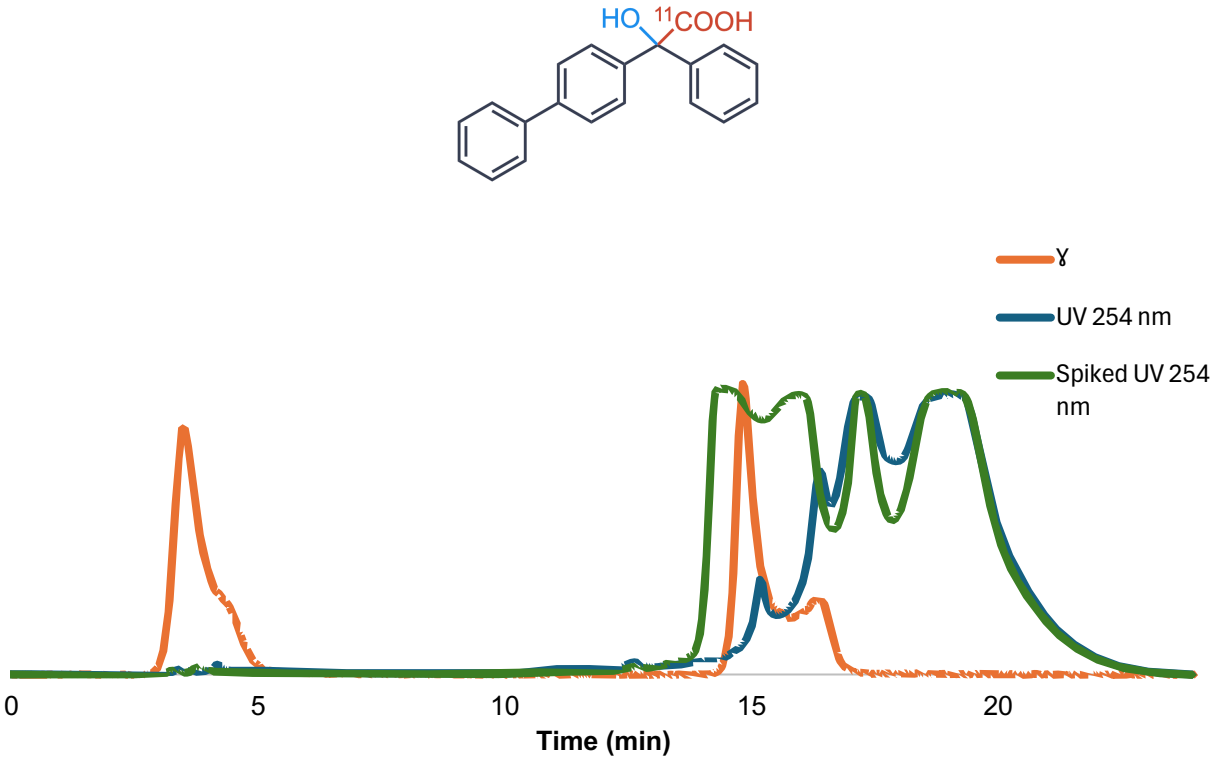

[^{11}C]2-hydroxy-2-phenyl-2-(p-tolyl)acetic acid (5.g)

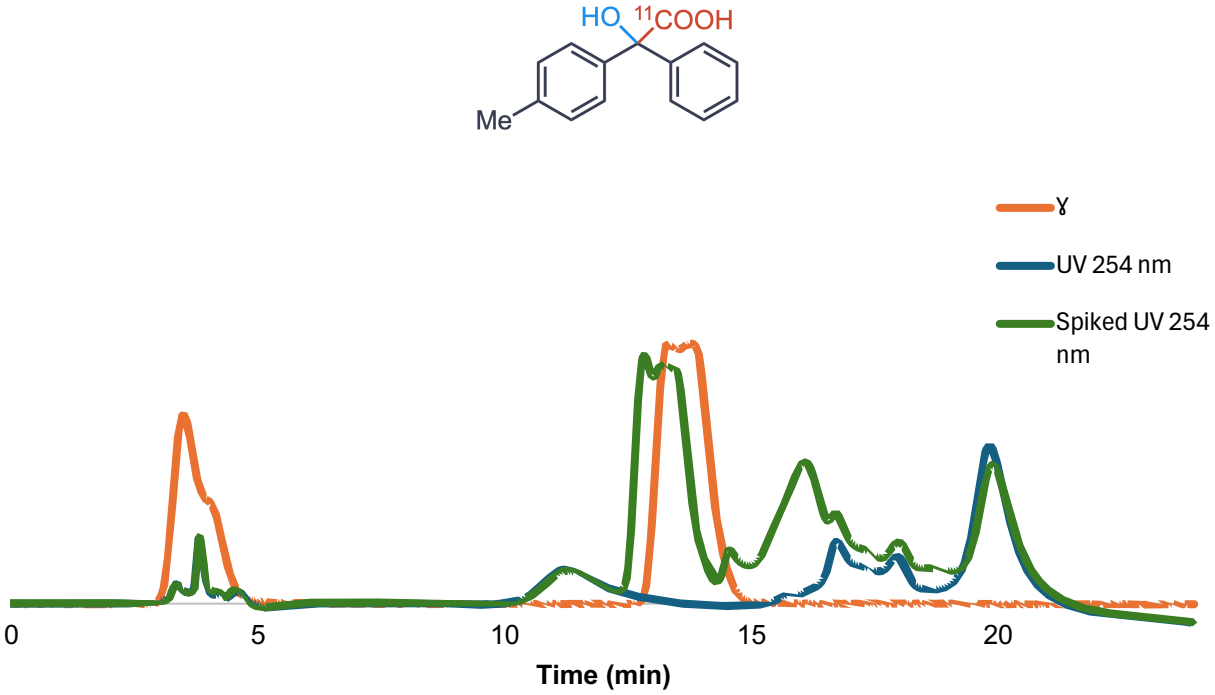

[^{11}C]2-hydroxy-2-phenyl-2-(4-(trifluoromethyl)phenyl)acetic acid (5.h)

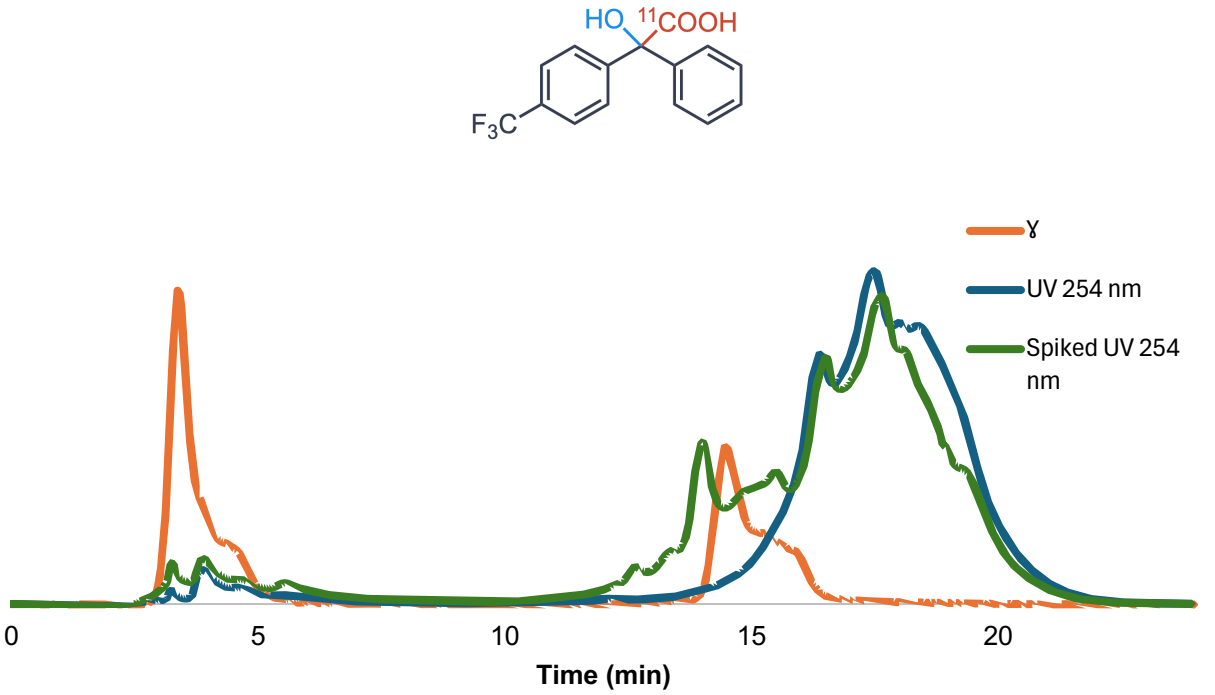

[^{11}C]2-hydroxy-2-(4-methoxyphenyl)-2-phenylacetic acid (5.i)

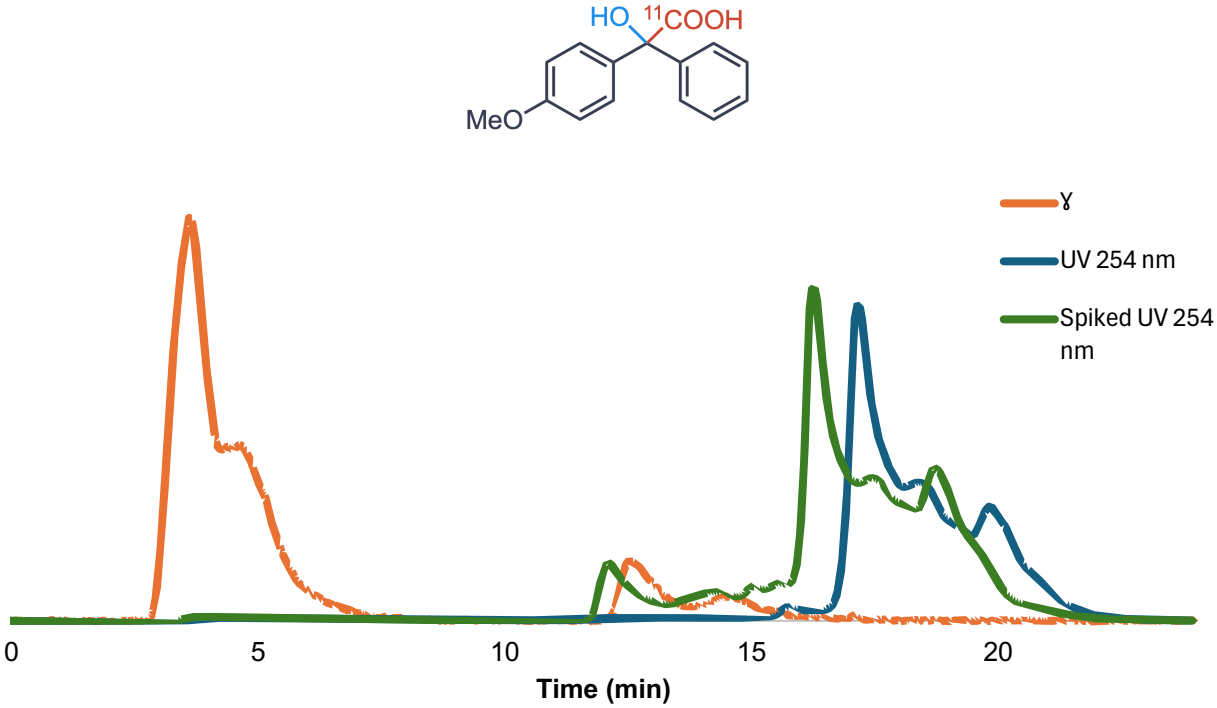

[^{11}C]2-hydroxy-2-(4-cyano)-2-phenylacetic acid (5.j)

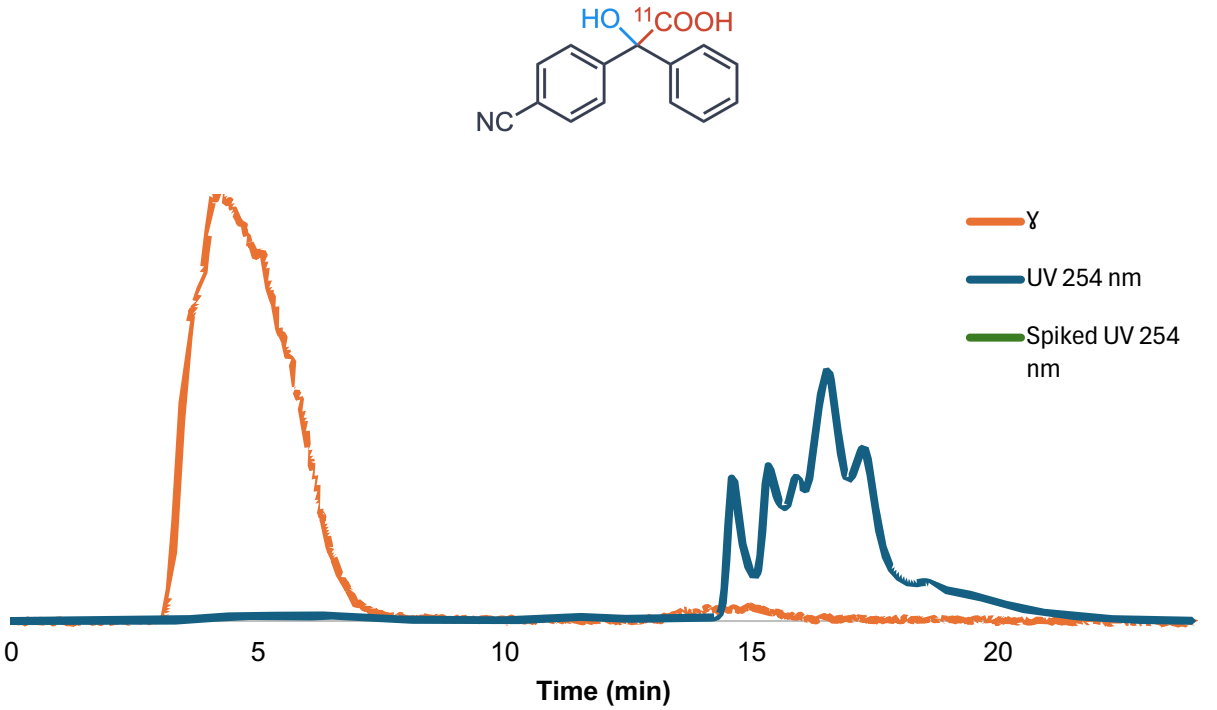

[^{11}C]2-(3-chlorophenyl)-2-hydroxy-2-phenylacetic acid (5.k)

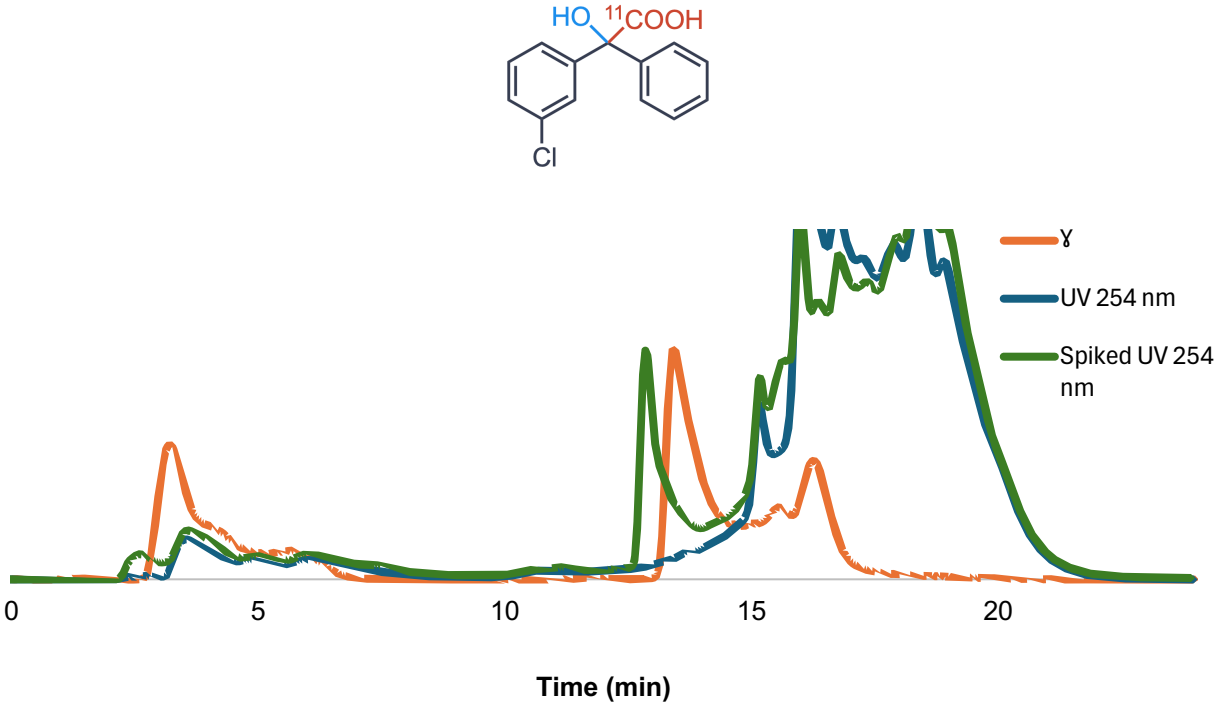

[^{11}C]2-(2-fluorophenyl)-2-hydroxy-2-phenylacetic acid (5.l)

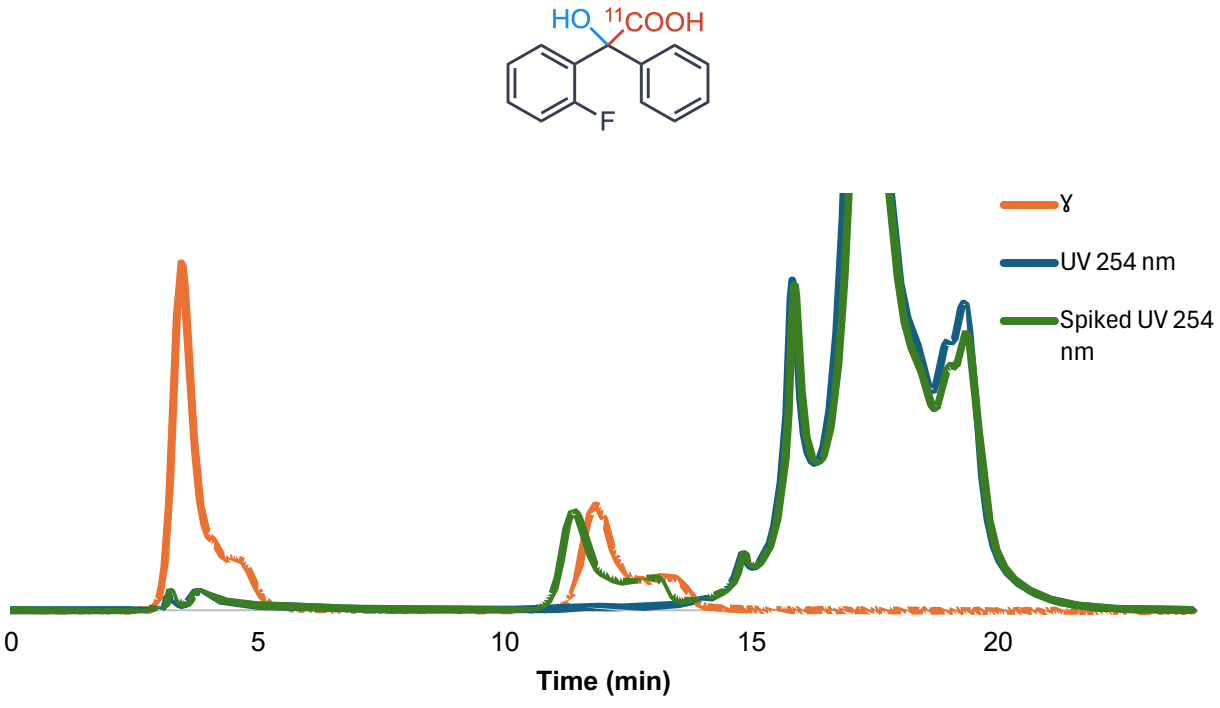

[^{11}C]2-(2-(trifluoromethyl)phenyl)-2-hydroxy-2-phenylacetic acid (5.m)

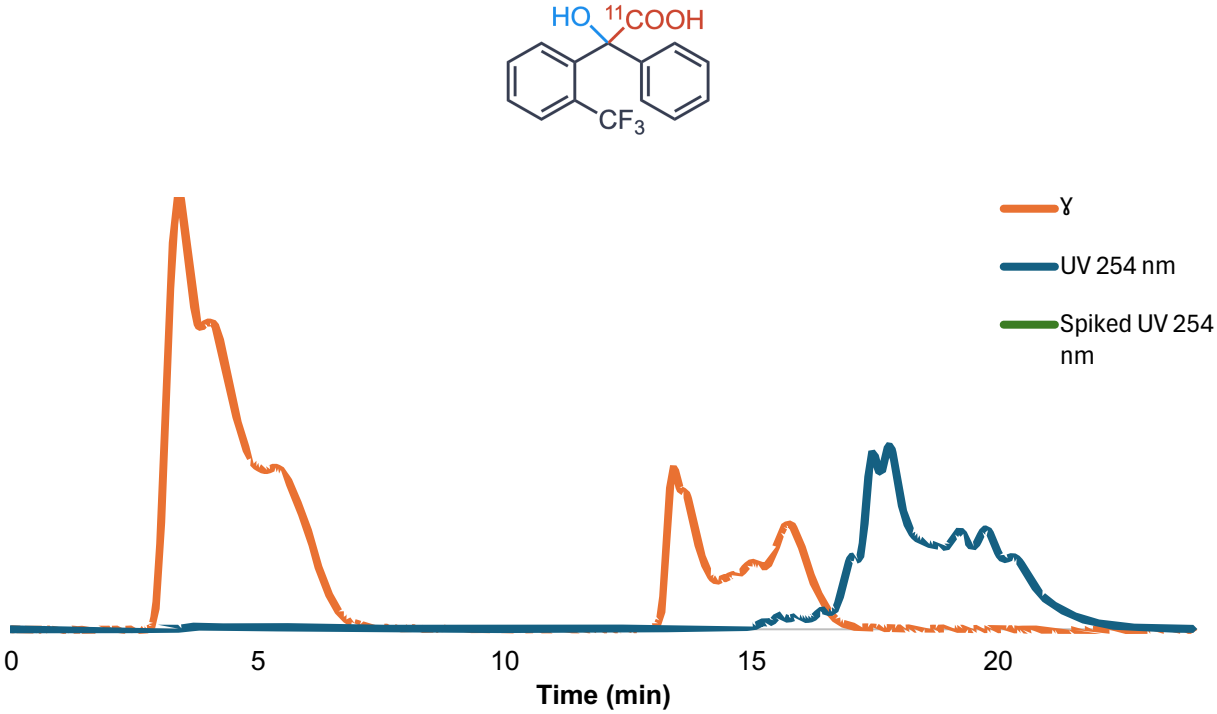

[^{11}C]2-hydroxytricyclo[9.4.0.03,8]pentadeca-1(15),3,5,7,11,13-hexaene-2-carboxylic acid (5.o)

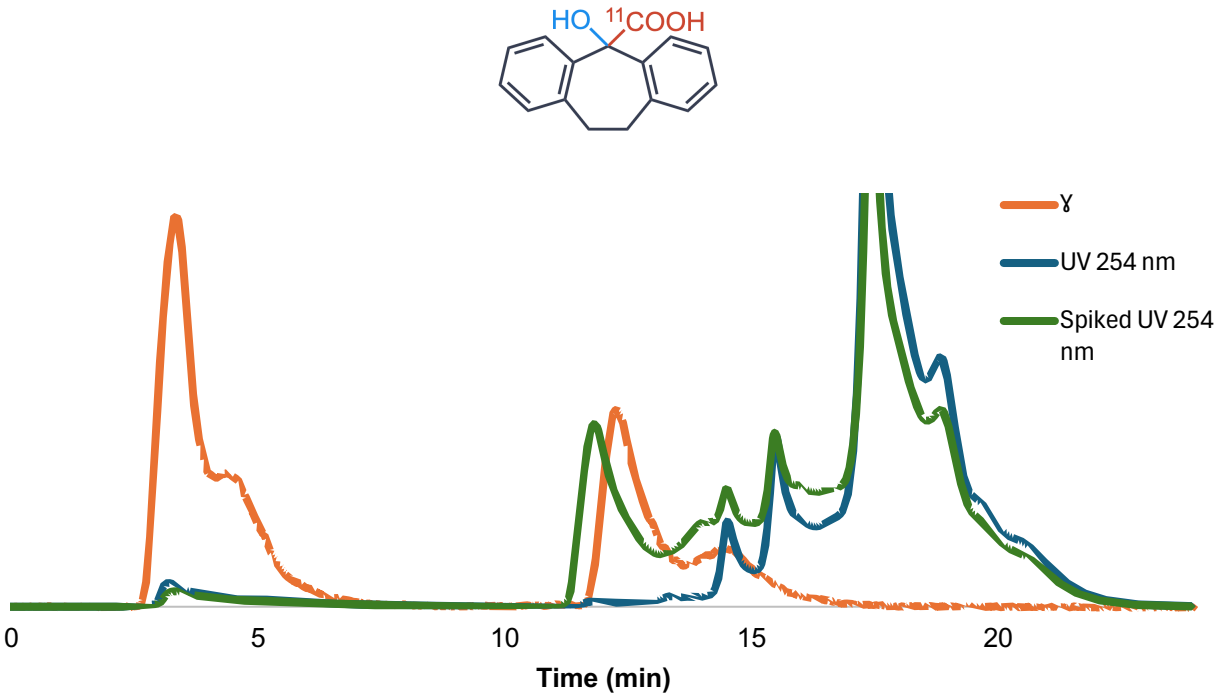

[^{11}C]2-hydroxy-2-phenyl-2-(thiophen-2-yl)acetic acid (5.p)

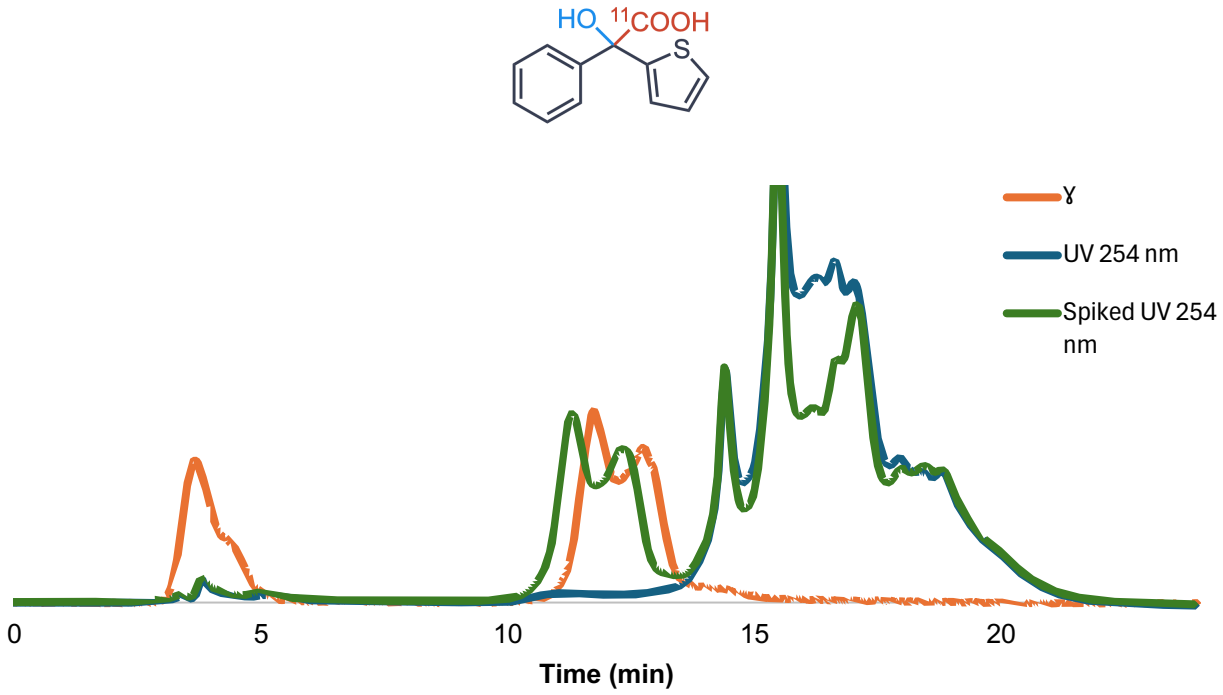

Appendix B

NMR Spectra

Note: Unassigned signals are from solvent impurities during the chromatography (workup 1) **or** direct isolation (workup 2) steps of **General procedure.** The impurities are limited to water, ethyl acetate, acetic acid (workup 1) and pivalic acid (from KOPiv, workup 2).

2-([1,1'-biphenyl]-4-yl)-2-hydroxypropanoic acid (4.b)

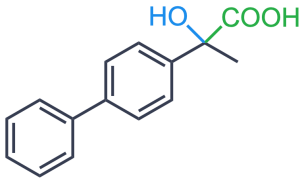

^{1}H NMR (600 MHz, DMSO)

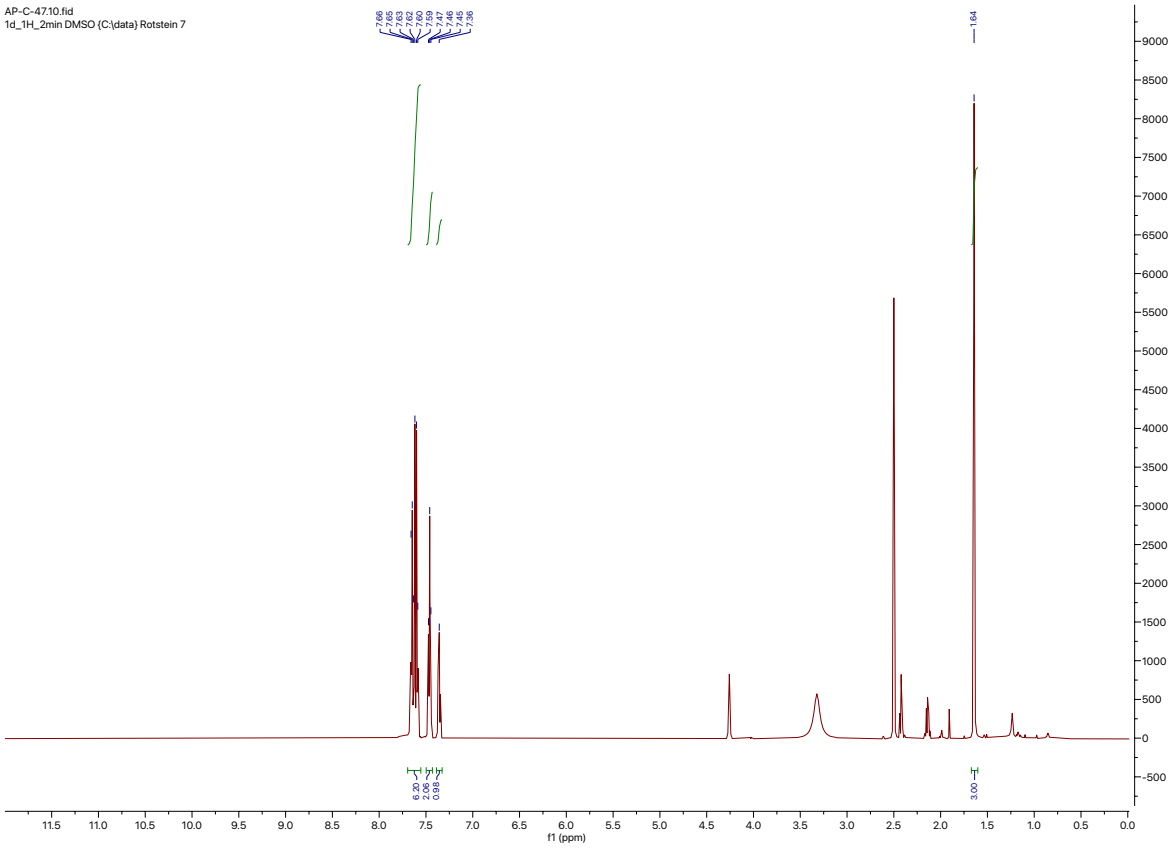

^{13}C NMR (151 MHz, DMSO)

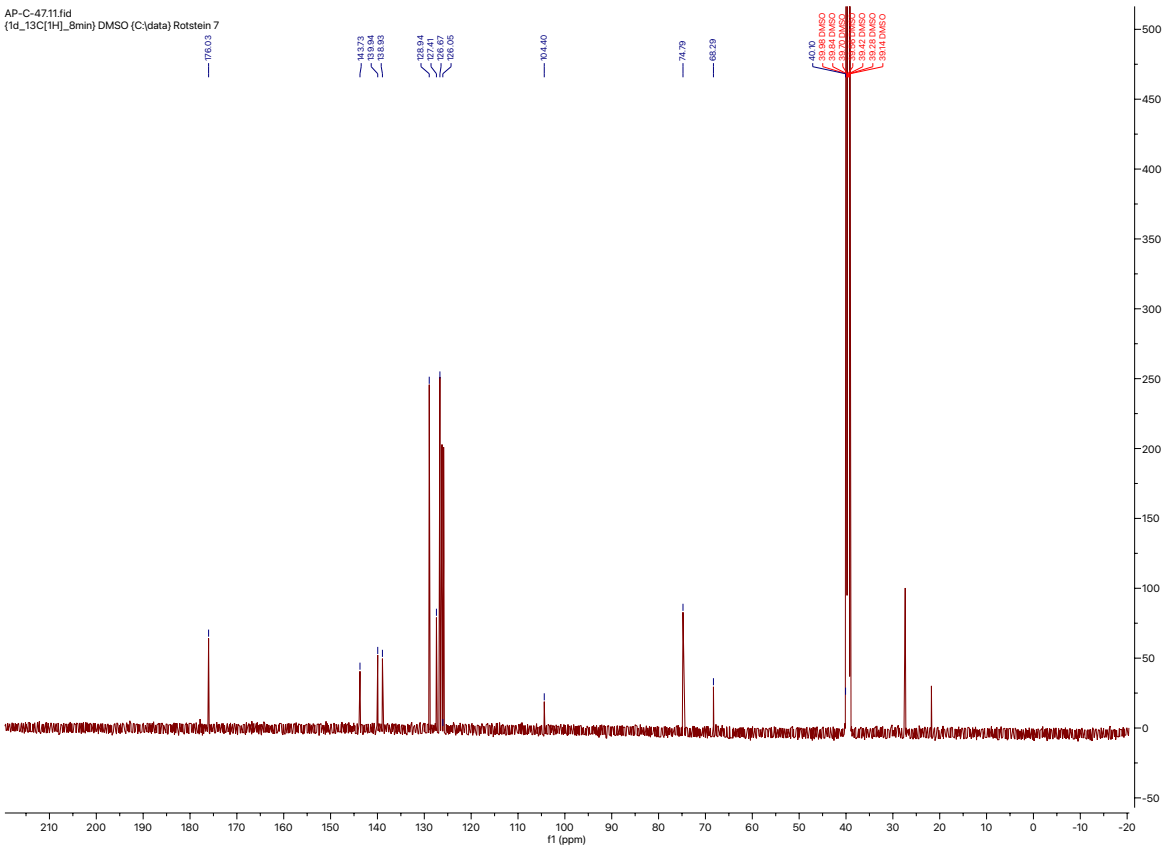

2,2-bis(4-fluorophenyl)-2-hydroxyacetic acid (4.e)

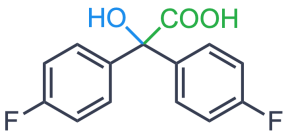

^{1}H NMR (600 MHz, DMSO)

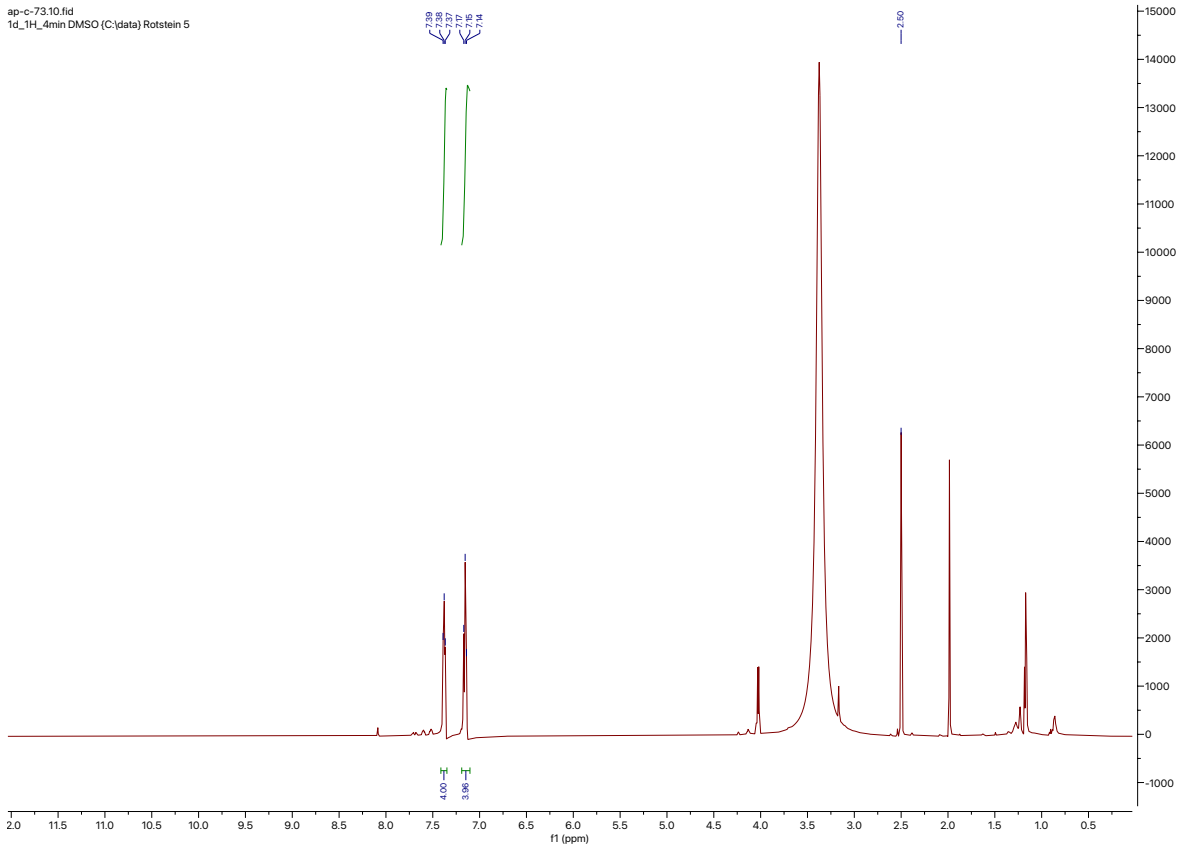

^{13}C NMR (151 MHz, DMSO)

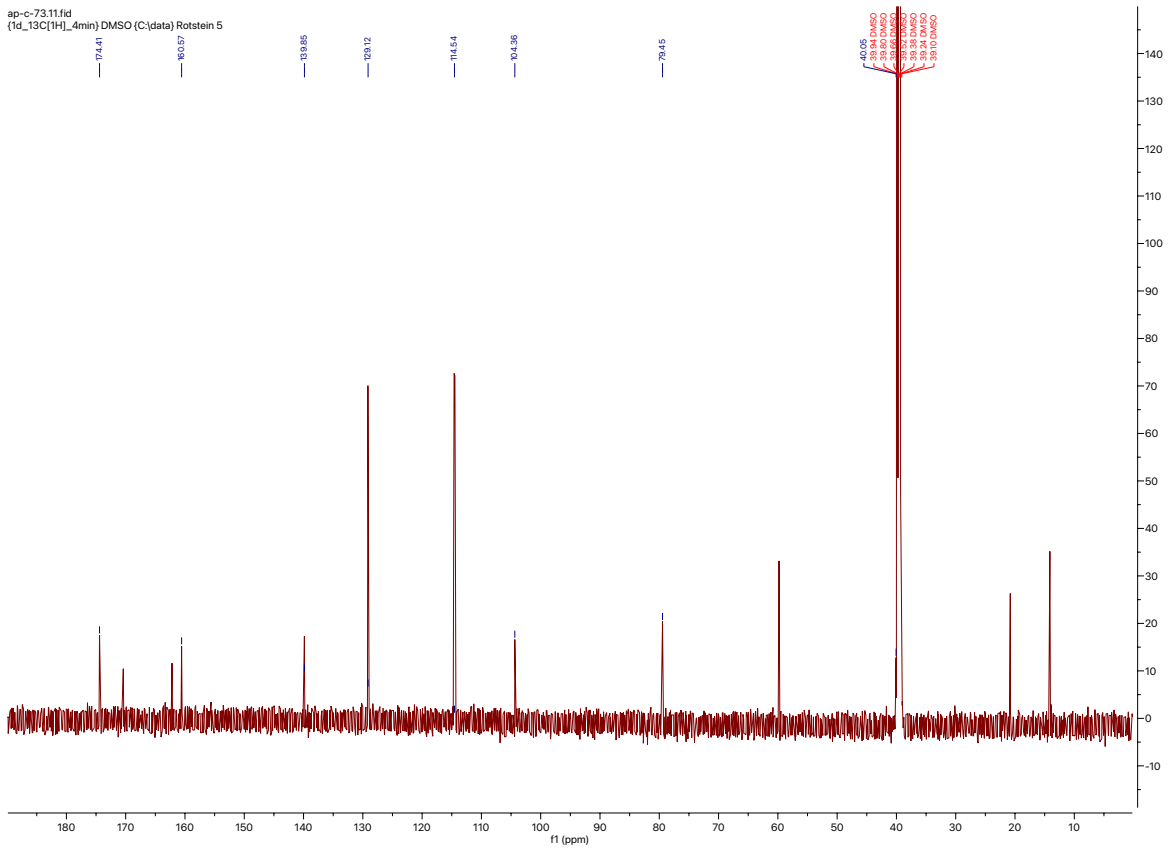

2-([1,1'-biphenyl]-4-yl)-2-hydroxy-2-phenylacetic acid (4.f)

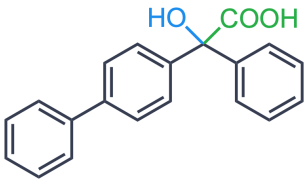

^{1}H NMR (600 MHz, DMSO)

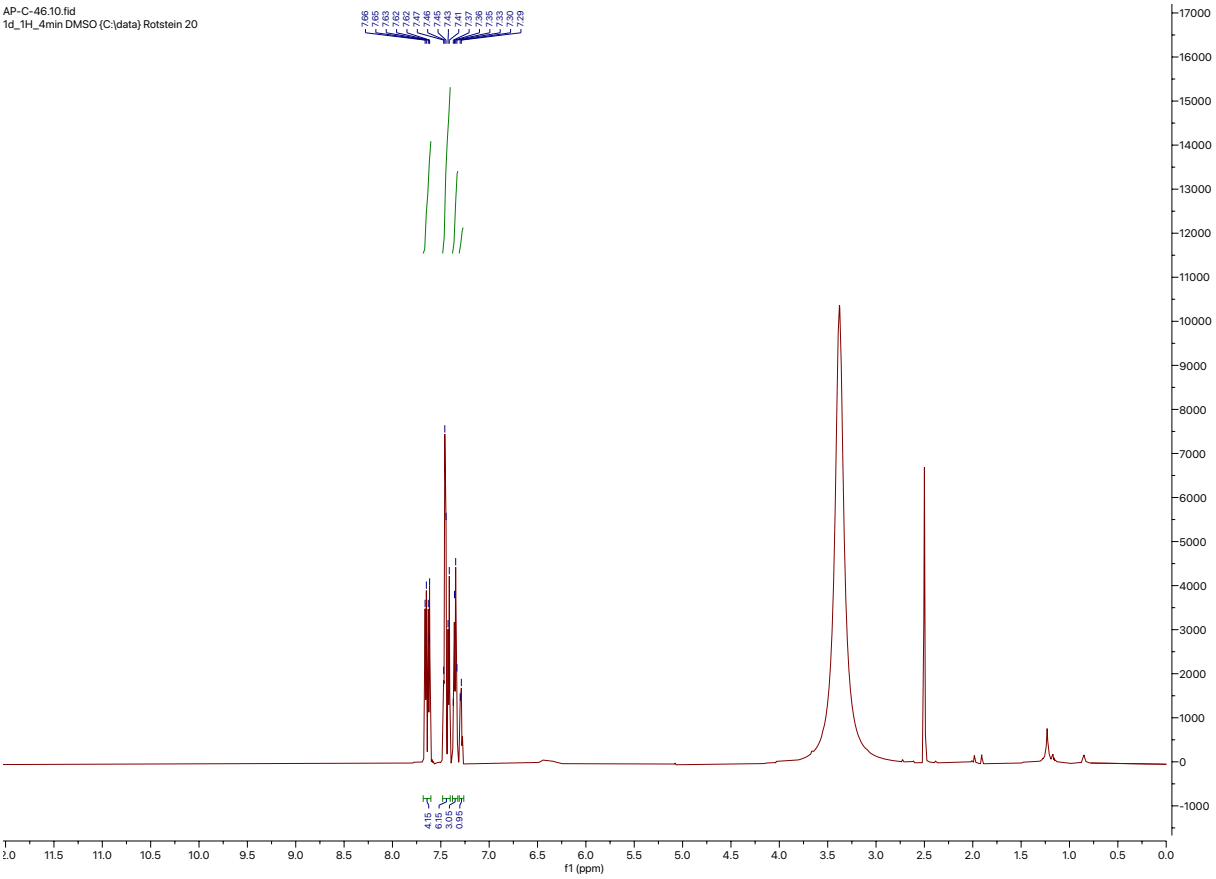

^{13}C NMR (151 MHz, DMSO)

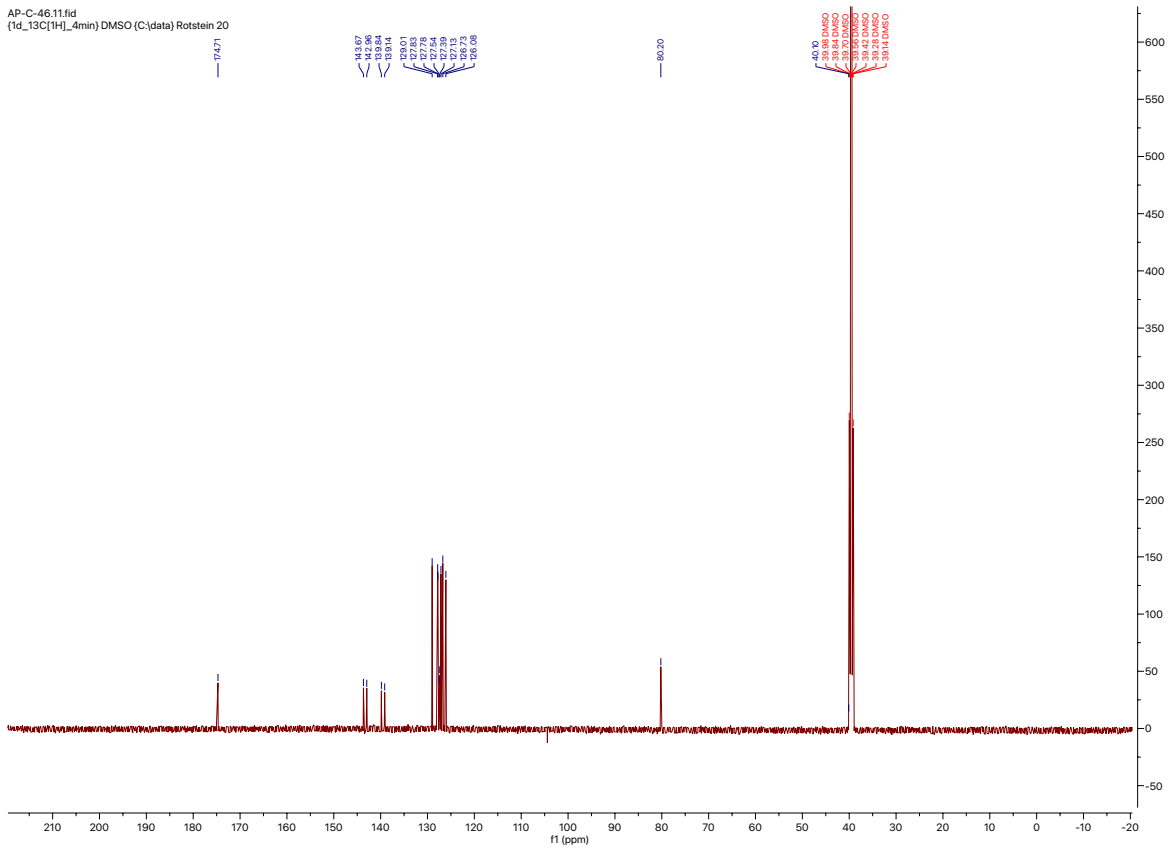

2-hydroxy-2-phenyl-2-(p-tolyl)acetic acid (4.g)

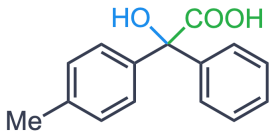

^{1}H NMR (600 MHz, DMSO)

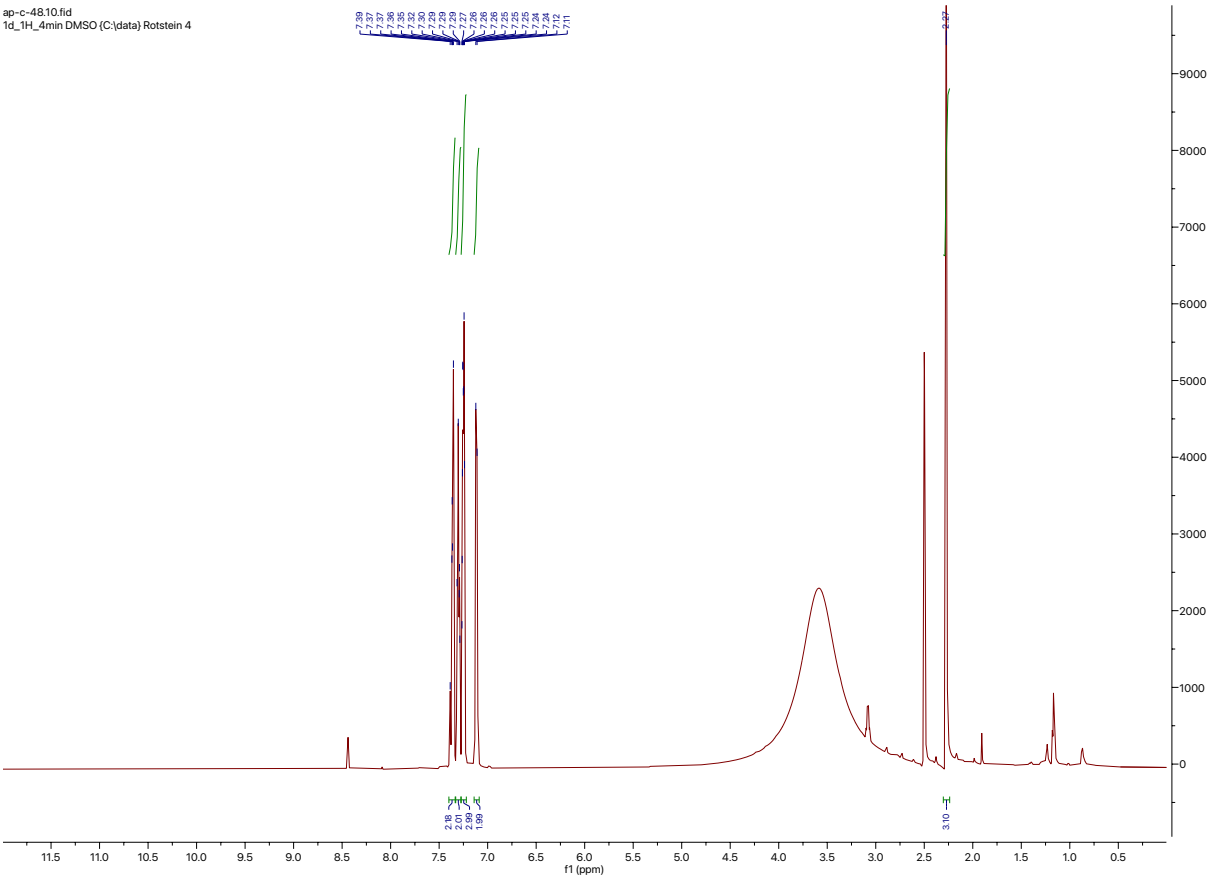

^{13}C NMR (151 MHz, DMSO)

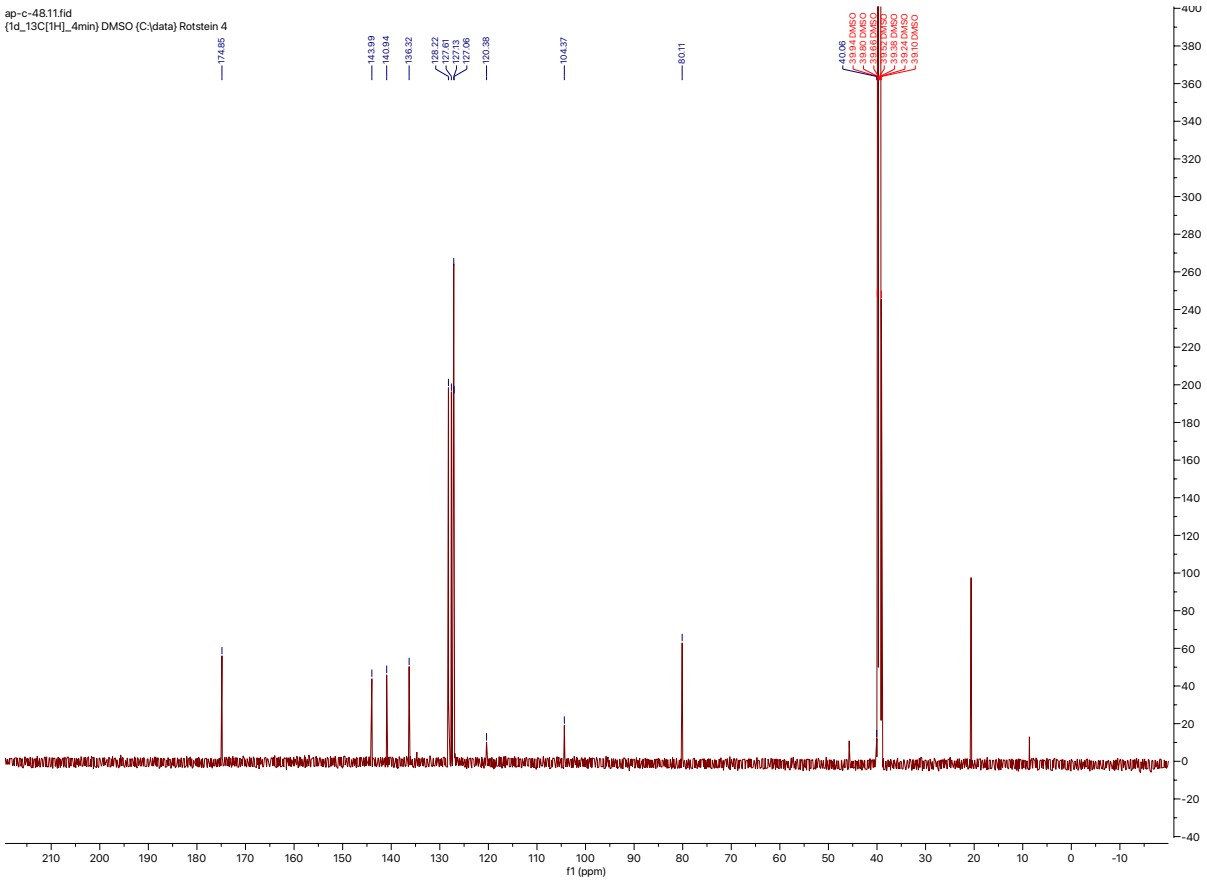

2-hydroxy-2-phenyl-2-(4-(trifluoromethyl)phenyl)acetic acid (4.h)

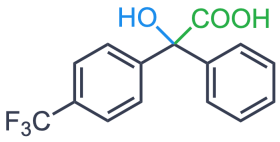

^{1}H NMR (600 MHz, DMSO)

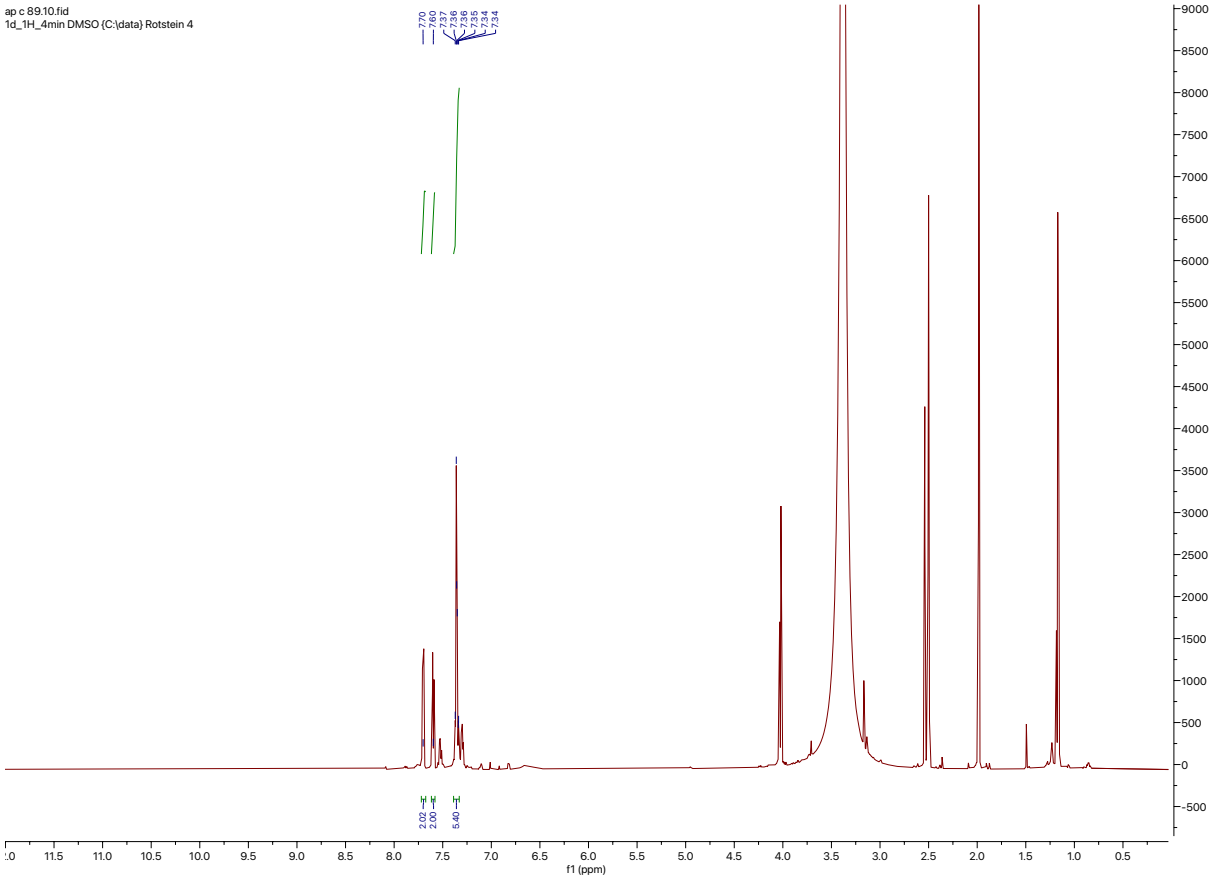

^{13}C NMR (151 MHz, DMSO)

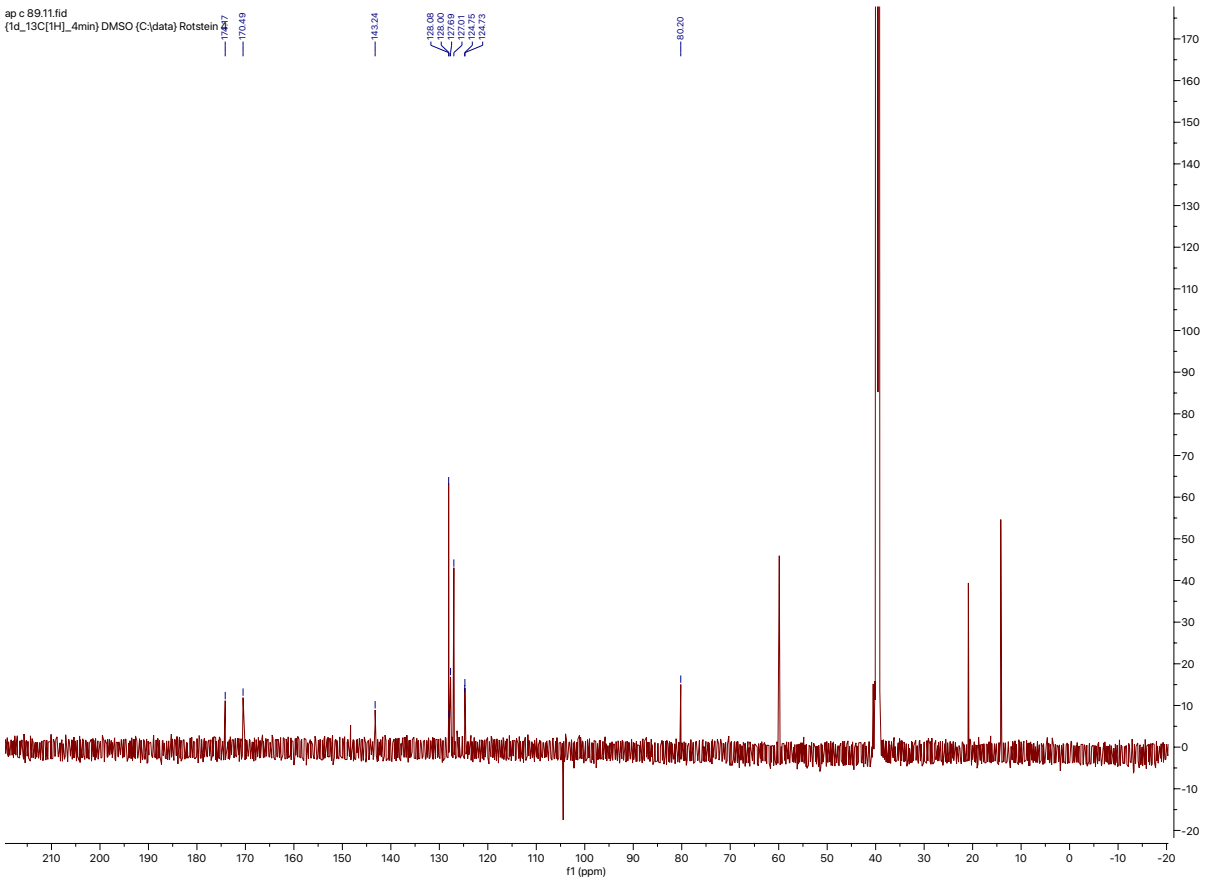

2-hydroxy-2-(4-methoxyphenyl)-2-phenylacetic acid (4.i)

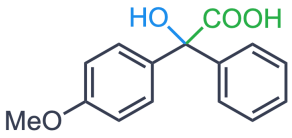

^{1}H NMR (600 MHz, DMSO)

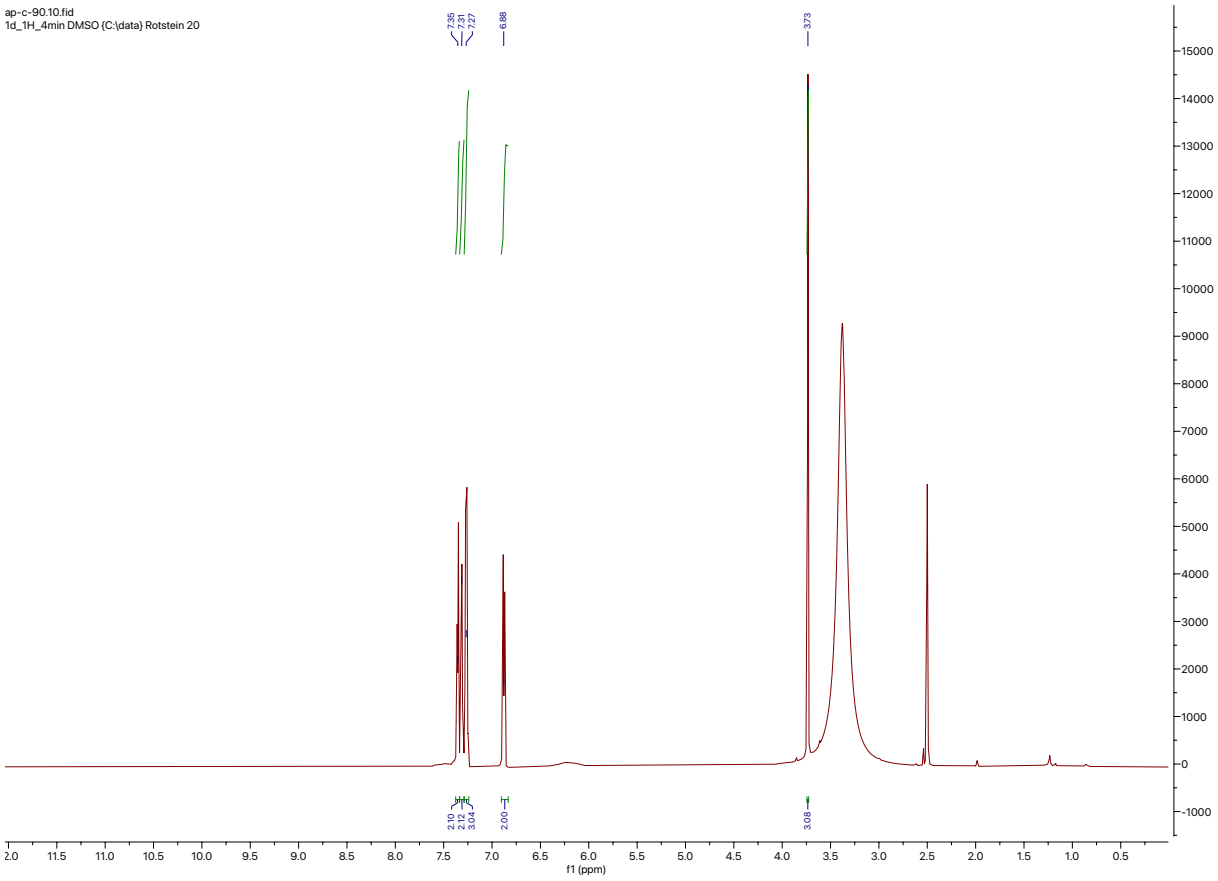

^{13}C NMR (151 MHz, DMSO)

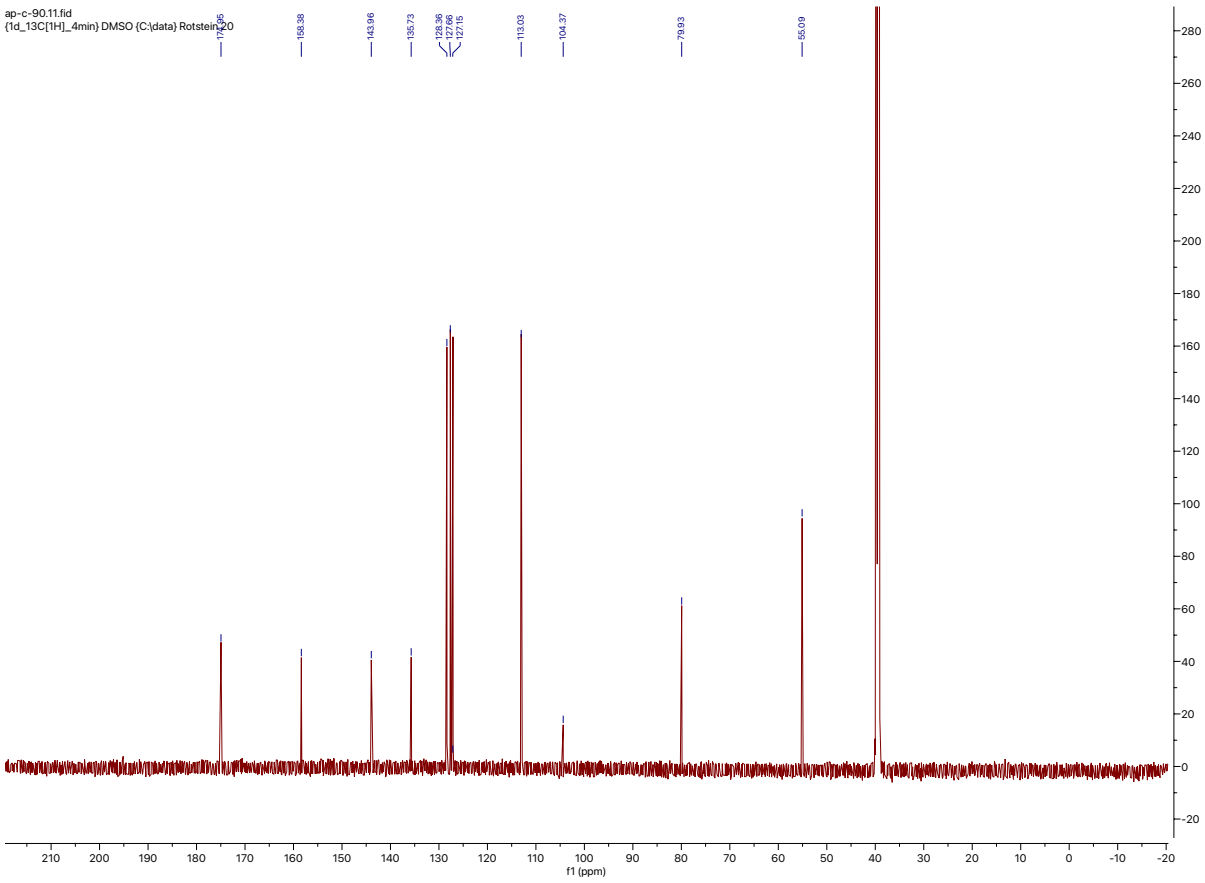

2-hydroxy-2-(4-cyano)-2-phenylacetic acid (4.j)

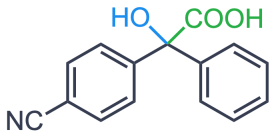

^{1}H NMR (600 MHz, DMSO)

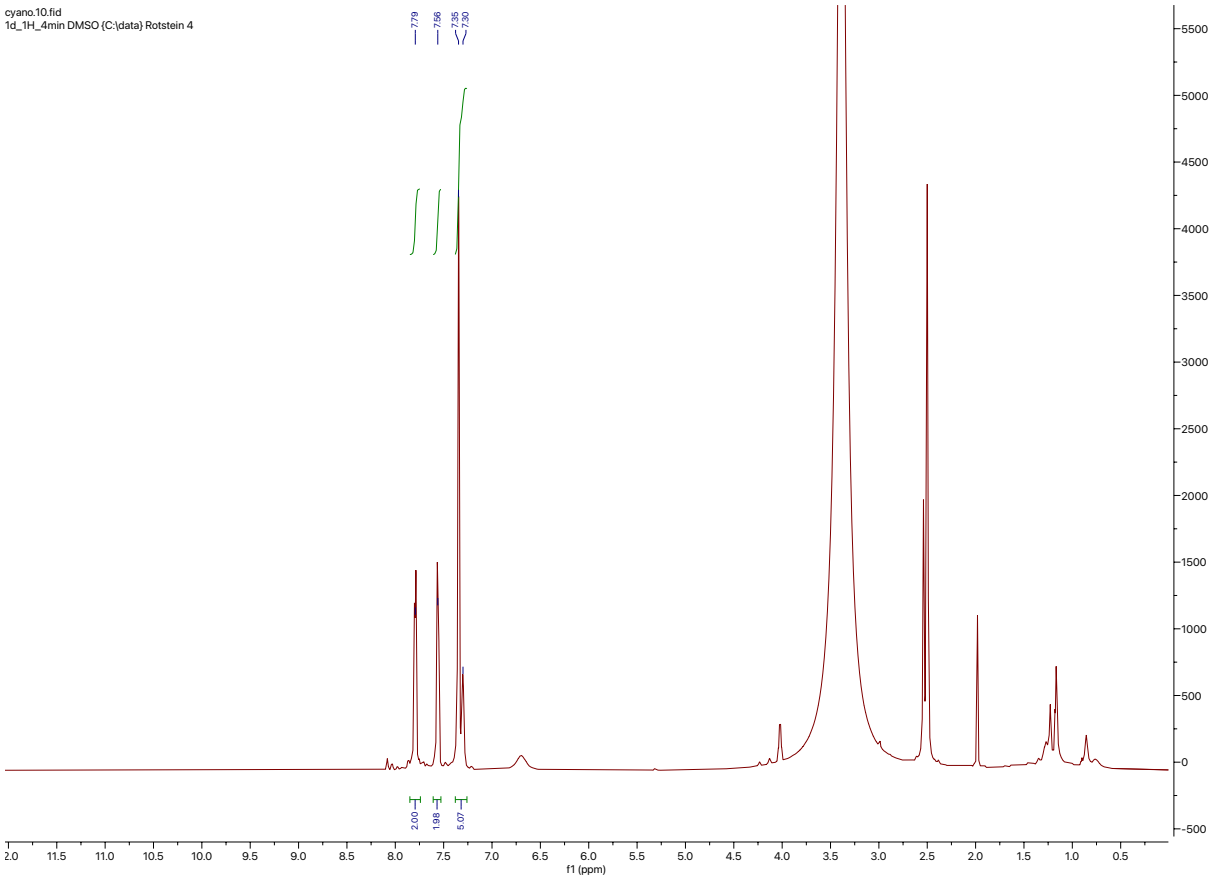

^{13}C NMR (151 MHz, DMSO)

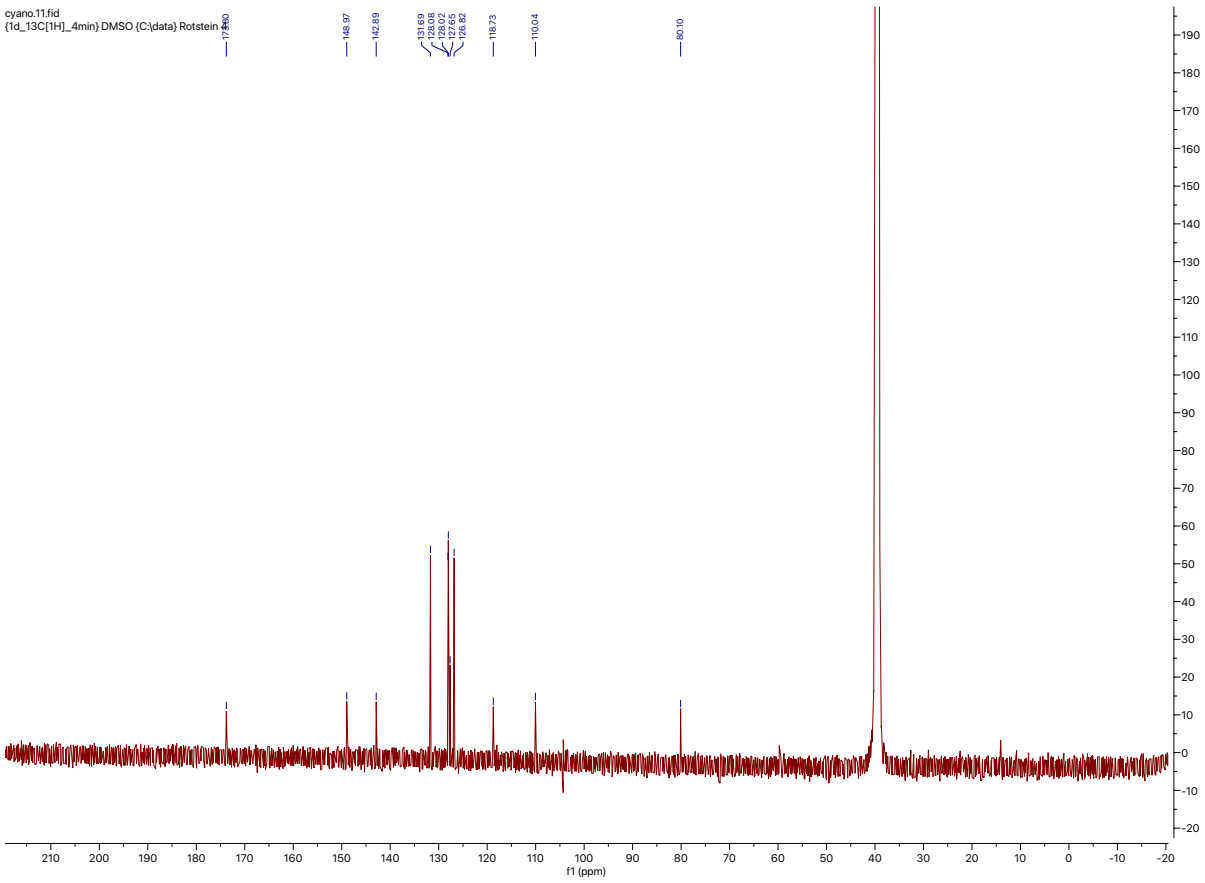

2-(3-chlorophenyl)-2-hydroxy-2-phenylacetic acid (4.k)

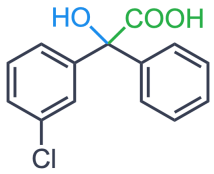

^{1}H NMR (600 MHz, DMSO)

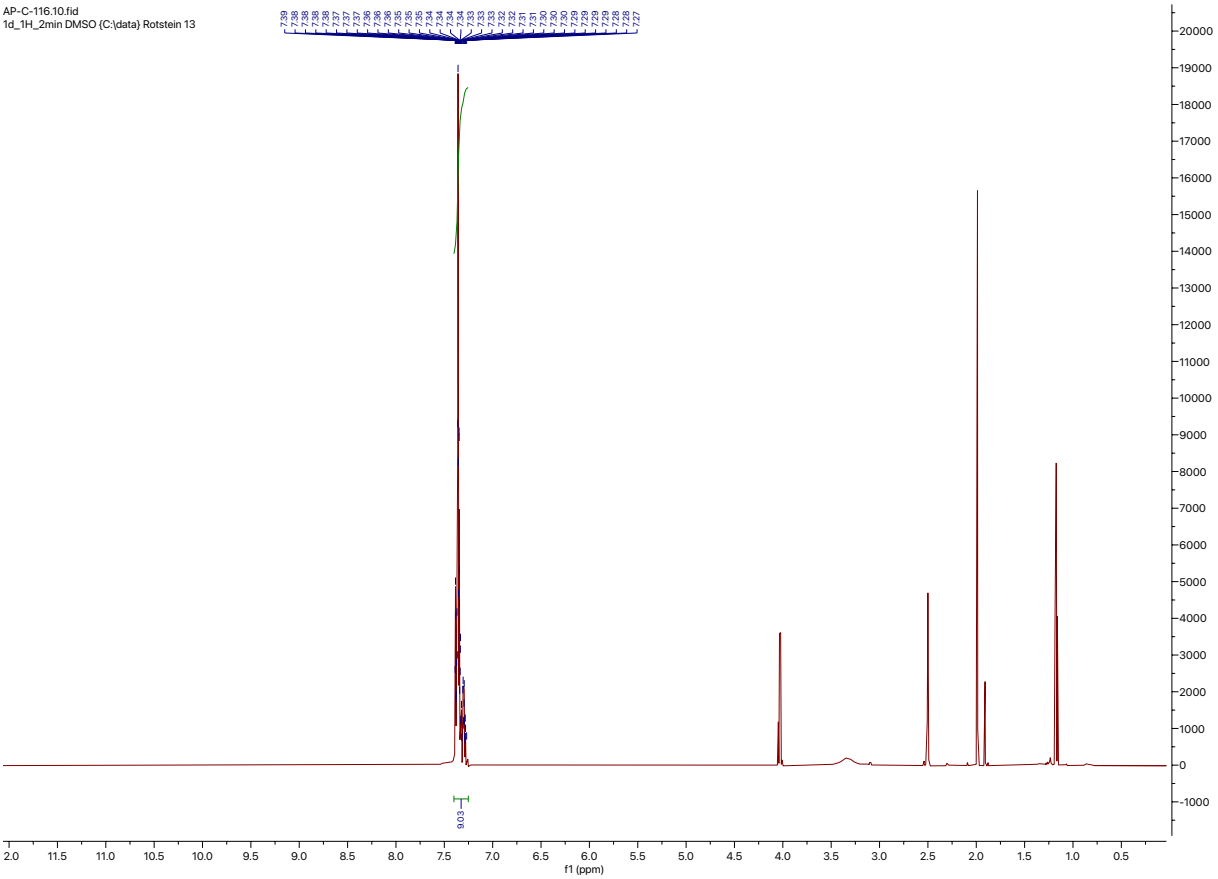

^{13}C NMR (151 MHz, DMSO)

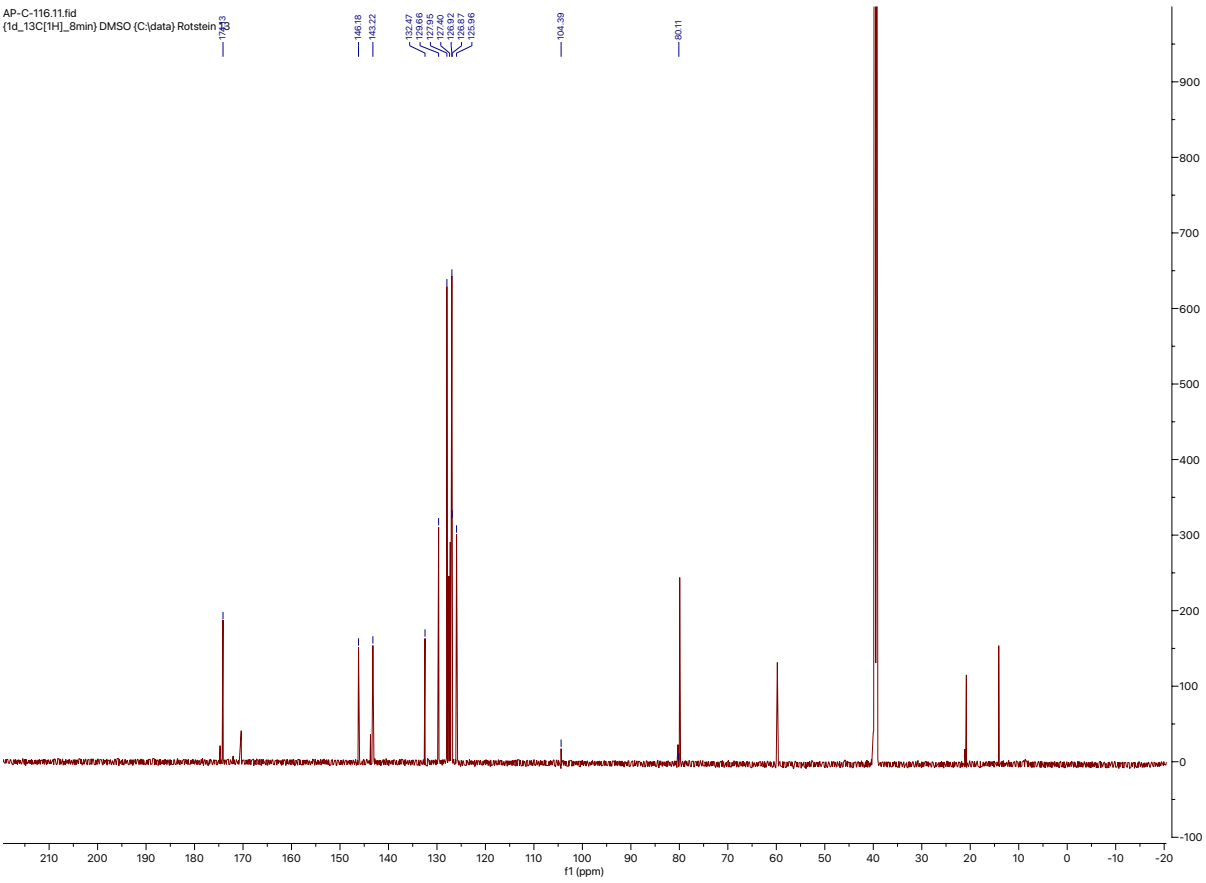

2-(2-fluorophenyl)-2-hydroxy-2-phenylacetic acid (4.l)

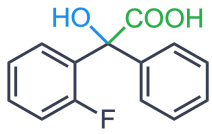

^{1}H NMR (600 MHz, DMSO)

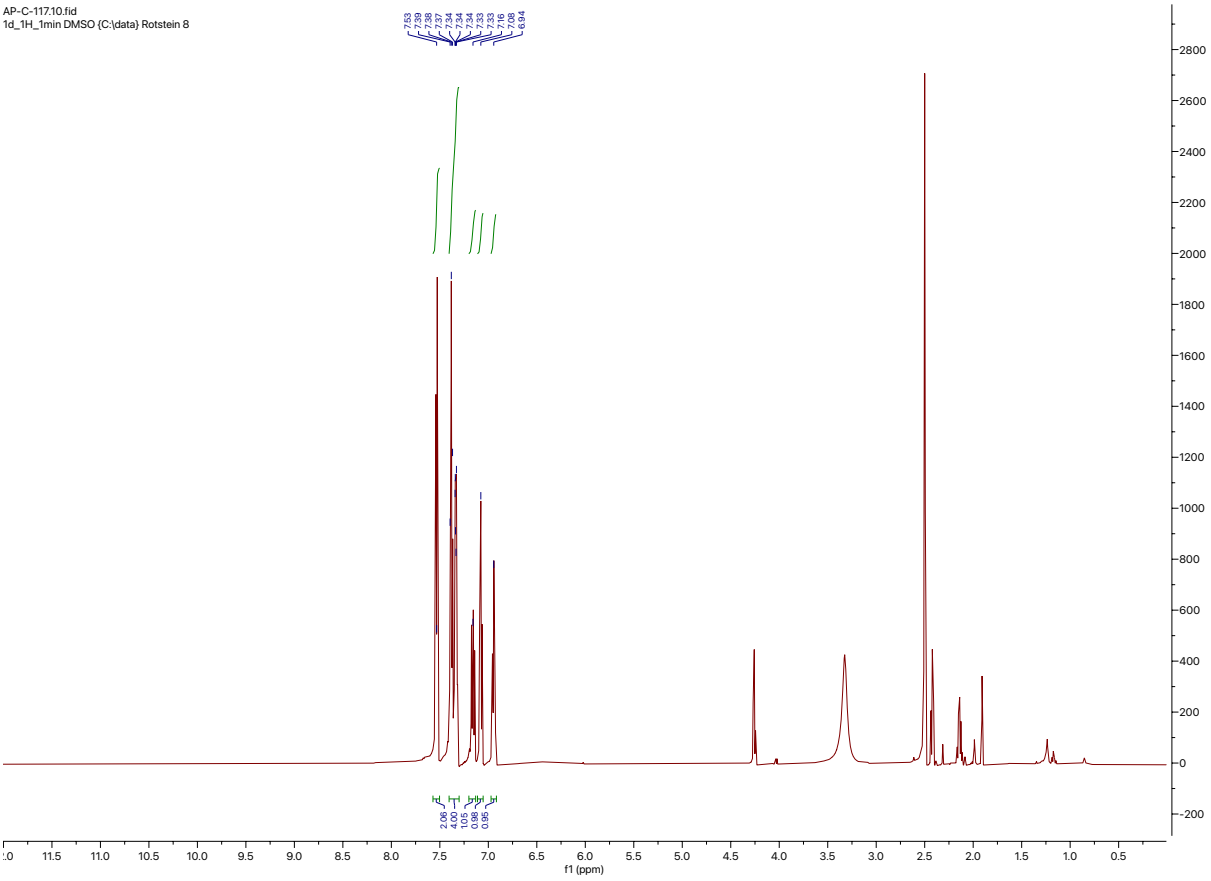

^{13}C NMR (151 MHz, DMSO)

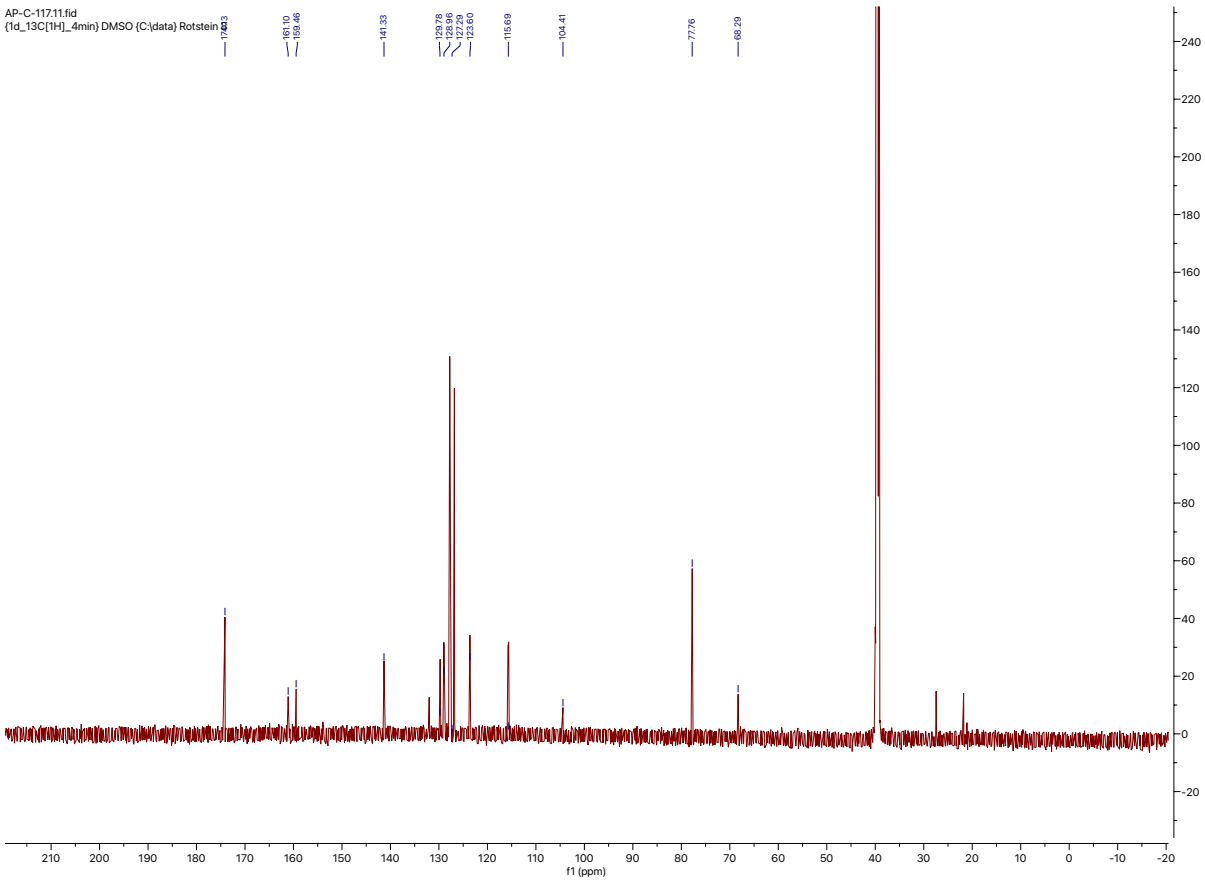

2-(2-(trifluoromethyl)phenyl)-2-hydroxy-2-phenylacetic acid (4.m)

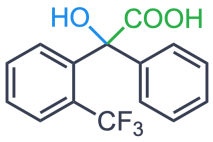

^{1}H NMR (600 MHz, DMSO)

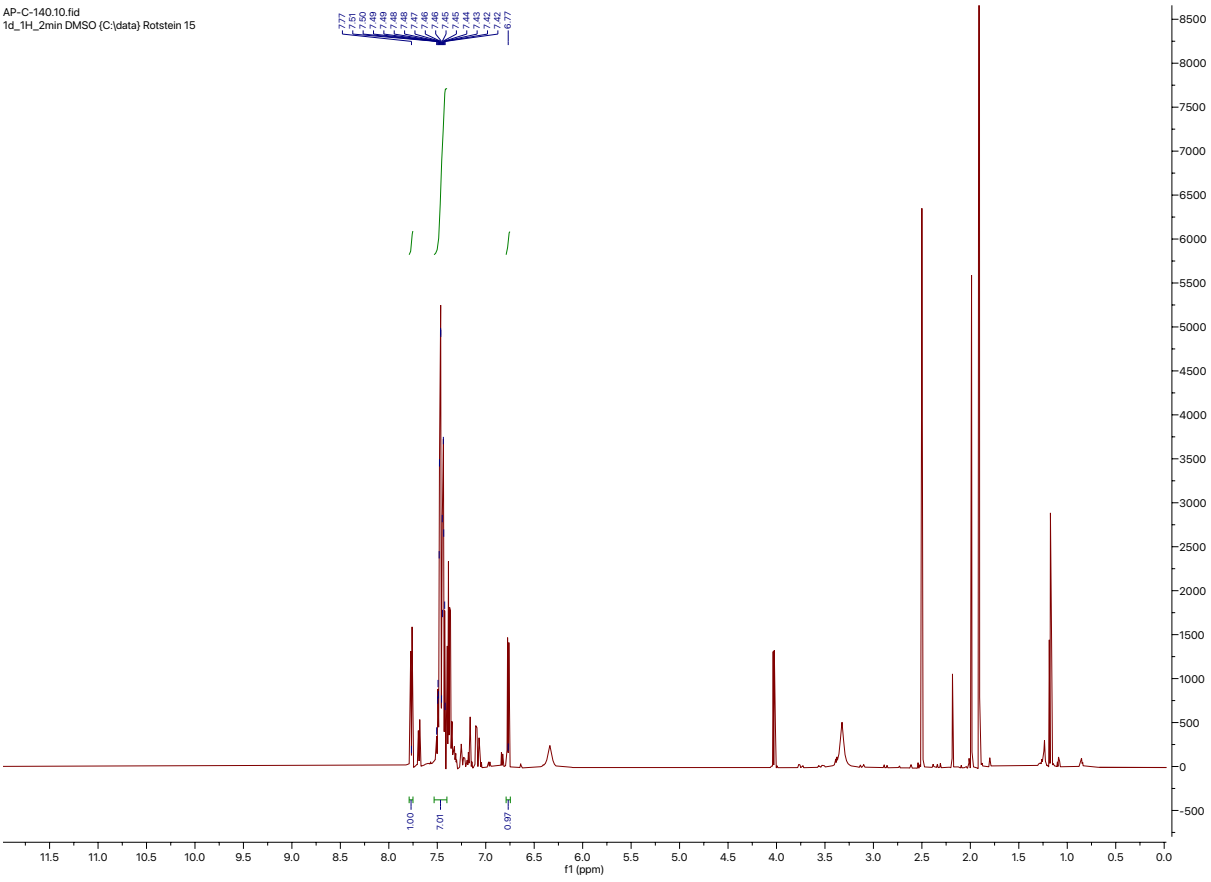

Note: The compound is unstable in solution and attempts to obtain an NMR results in degradation of the compound back to the starting ketone **3.m**, which is observed in the aromatic region.

^{13}C NMR (151 MHz, DMSO)

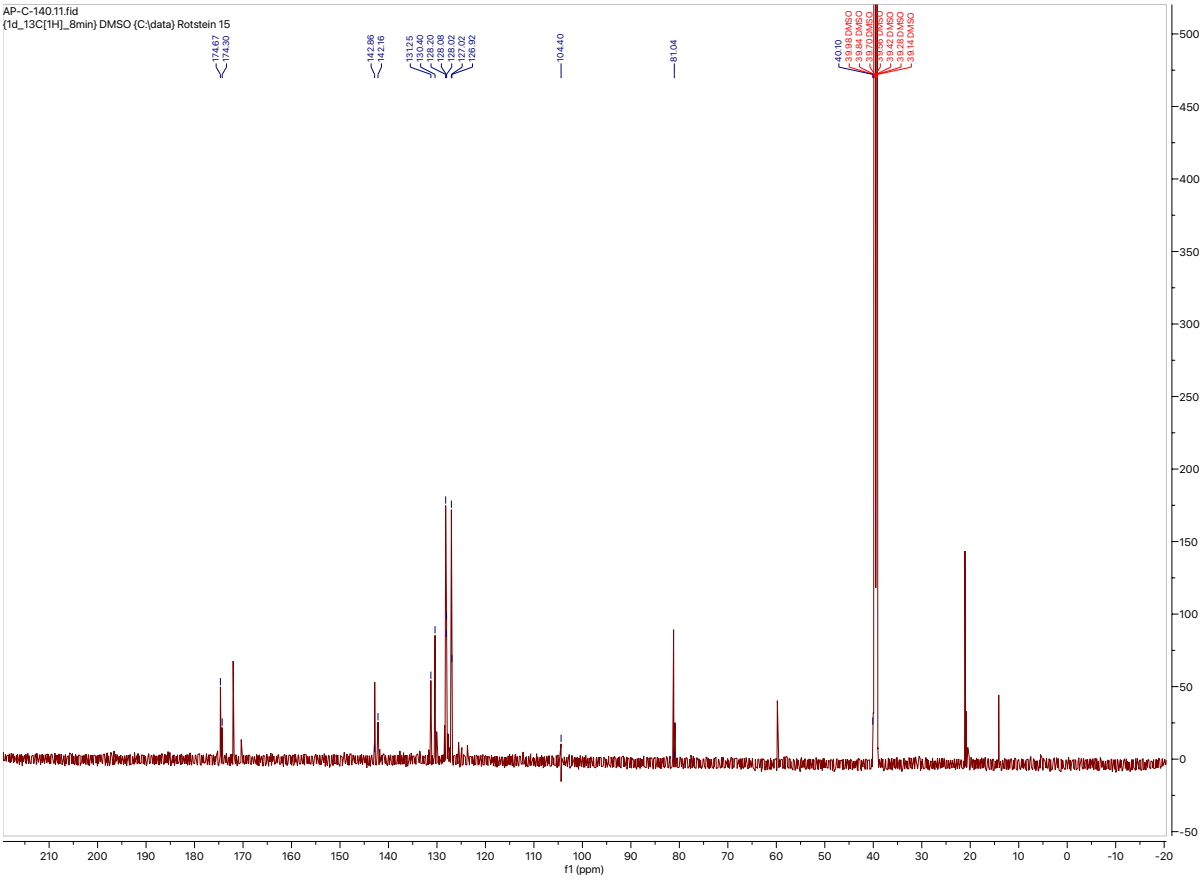

2-hydroxytricyclo[9.4.0.03,8]pentadeca-1(15),3,5,7,11,13-hexaene-2-carboxylic acid (4.o)

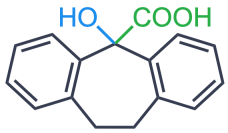

^{1}H NMR (600 MHz, DMSO)

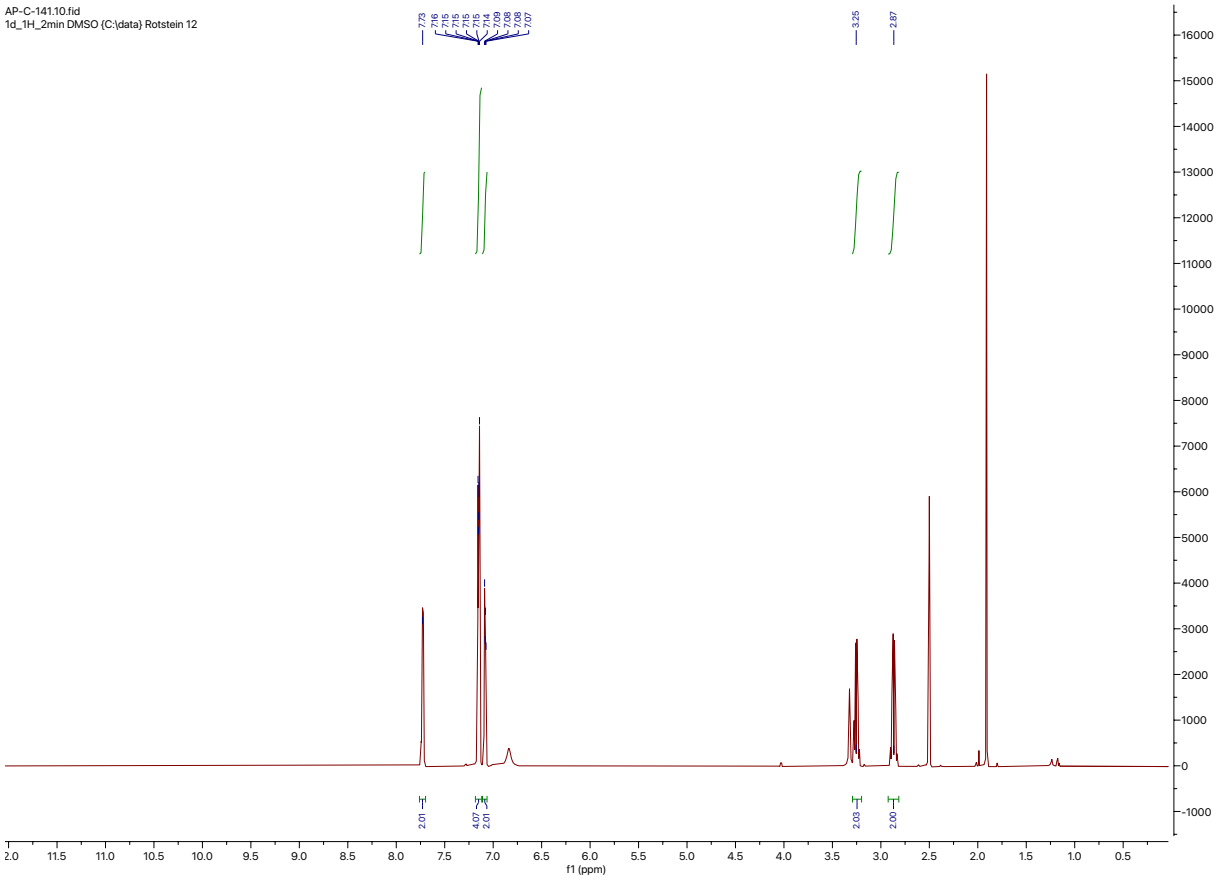

^{13}C NMR (151 MHz, DMSO)

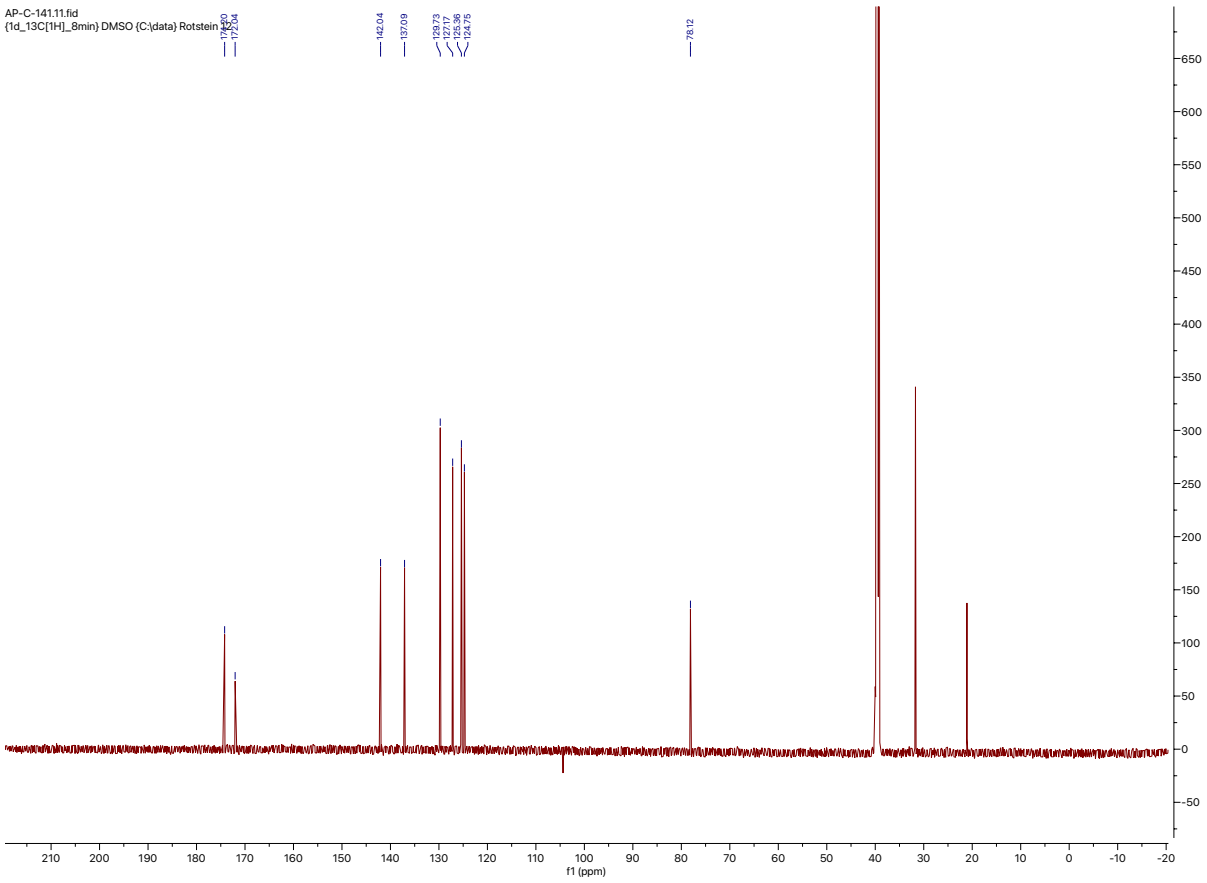

2-hydroxy-2-phenyl-2-(thiophen-2-yl)acetic acid (4.p)

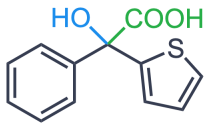

^{1}H NMR (600 MHz, DMSO)

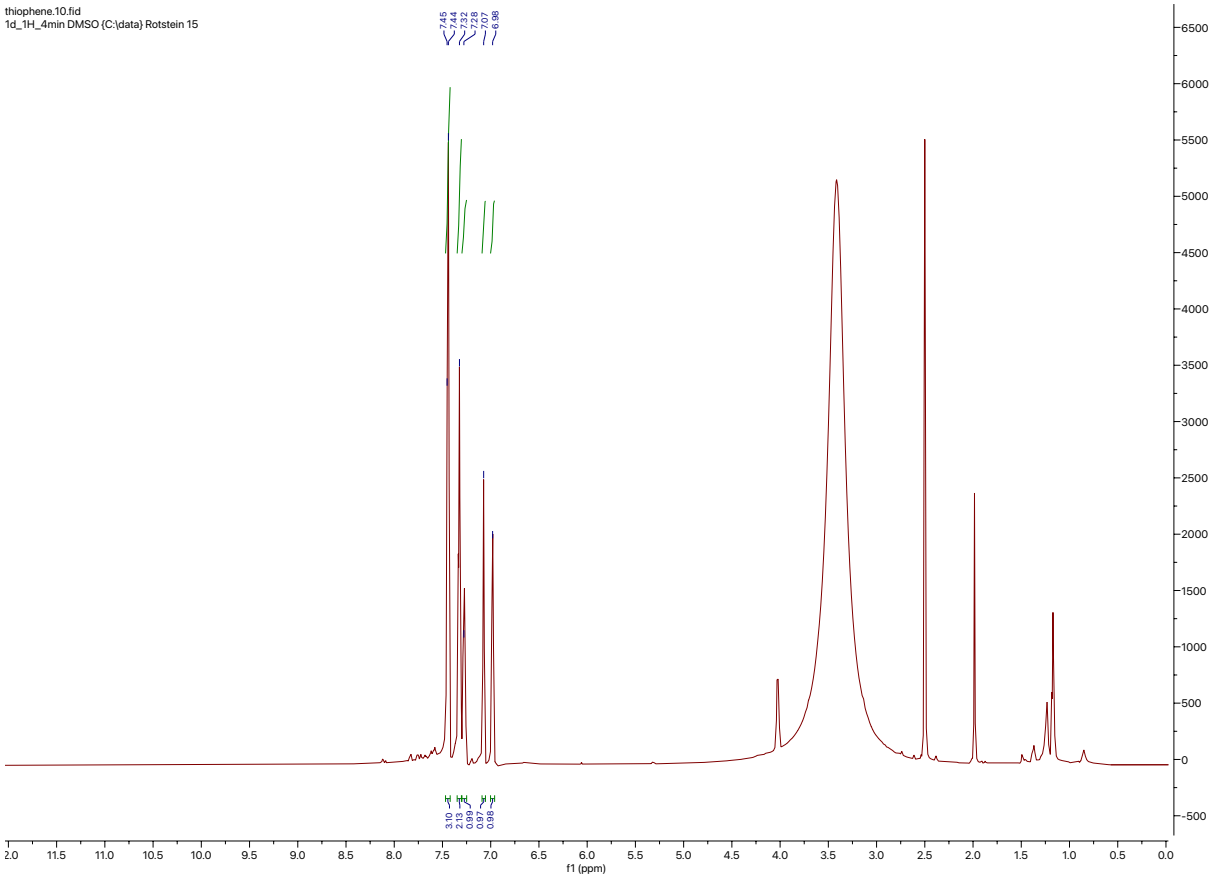

^{13}C NMR (151 MHz, DMSO)